Stability Analysis of Geotextile Encased Sand Columns

By
Shaymaa Kadhim

B.S., the University of Technology, Baghdad – Iraq, 2004

M.Sc., the University of Technology, Baghdad – Iraq, 2007

Submitted to the Department of Civil, Environmental, and Architectural Engineering and the Graduate Faculty of the University of Kansas in partial fulfillment of the requirements for the degree of Doctor of Philosophy

_____
Chairperson Dr. Robert L. Parsons

_____
Co-chairperson Dr. Jie Han

Committee members

_____
Dr. Anil Misra

_____
Dr. Steven D. Schrock

_____
Prof. Chad R. Kraus

Date Defended: May 20th, 2016

The Dissertation Committee for Shaymaa Kadhim certifies that this is the approved version of the following dissertation:

Stability Analysis of Geotextile Encased Sand Columns

_____

Chairperson Dr. Robert L. Parsons

_____

Co-chairperson Dr. Jie Han

Date Approved: 5/23/2016

ABSTRACT

Global instability or deep-seated failure of roadway embankments constructed on soft soils is a serious concern in the field of geotechnical engineering. Different ground improvement techniques, such as stone columns, have been widely implemented to avoid deep-seated failure. Stone columns derive their bearing capacity from the passive resistance provided by the native surrounding soil, therefore, inclusion of stone columns in very soft soils may not be sufficient to yield the desired level of improvement. As a result, geosynthetic encased stone columns (GESC) have been introduced to improve soft soils with low undrained shear strengths. The objective of this study is to quantify the contribution of GESC to vertical and global stability.

In this study, model GESC with geotextile sleeves with three different diameters: 10, 15, and 30 cm, were tested as part of the experimental program. Kansas River Sand of 70% relative density was used as the infill material of GESC. CD triaxial compression tests were conducted on both ordinary sand and geotextile encased sand columns. The results showed that using geotextile encasement increased the strength of column by providing an apparent cohesion and increasing the friction angle beyond the peak friction angle of the ordinary sand column.

The vertical stability of GESC was investigated through a series of loading tests. The loading tests were conducted on columns having various diameters and lengths, installed both in air and in very weak surrounding soil (i.e. loose sand with 30% relative density). The performance of GESC in air and with loose sand surrounding soil was studied with regard to bearing capacity, radial strain, and axial strain relationships. The results of both cases showed that columns of smaller diameters and shorter lengths exhibited higher bearing capacities compared with those of larger diameters and longer lengths. GESC with surrounding loose sand exhibited lower radial and axial strains compared with those in air at the same applied pressure. In addition, GESC with soil

confinement had higher bearing capacities than those in air at the same diameters and length to diameter ratios.

The experimental findings were verified using the finite difference method within the software program FLAC3D 5.01. The numerical results matched well with the experimental data. A parametric study was conducted to assess the factors that may have an impact on the performance of GESC, such as column diameter and length, soil thickness, geotextile encasement length, geotextile stiffness, and friction angle of infill material. The results showed that increasing the size and length of end-bearing GESC reduced its bearing capacity and increased its lateral deformation, while shorter, partially penetrating GESC had lower bearing capacities as compared with longer ones. The effective geotextile encasement length was found to be approximately five times the column diameter. Geotextile stiffness had a substantial influence on the performance of GESC, and the friction angle of infill sand had a less significant effect on the behavior of the GESC.

Finally, a two dimensional finite difference method using FLAC2D 6.0 was used to investigate the effect of ordinary stone columns and GESC on the short-term stability of an embankment constructed over soft soil. Two different models were adopted in this study: column walls and an equivalent improved area. A parametric study was conducted by varying some parameters such as the spacing and size of stone columns, cohesion of the soil deposit, and stiffness of the geosynthetic. The results showed that the equivalent area method yielded higher factors of safety than the column wall method. The stability factor of safety decreased when the center-to-center spacing between columns was increased, and increased when the soil cohesion was less than 25 kPa. Increasing the stiffness of geosynthetic encasement up to 2000 kN/m significantly increased the stability factor of safety.

ACKNOWLEDGEMENTS

I would like to express my sincere gratitude to my advisors, Prof. Robert L. Parsons and Prof. Jie Han, for providing invaluable guidance and support throughout my experience as a graduate student. Under their guidance, I was motivated to improve my knowledge and skills in geotechnical engineering field.

I also want to thank my committee members Profs. Anil Misra, Steven D. Schrock, and Chad R. Kraus for their valuable suggestions and comments in my Ph.D. dissertation work and for serving as members of my examining committee.

Also, I would like to thank my sponsor, The Higher Committee for Education Development in Iraq, HCED, for funding me throughout my Ph.D. study. I would like to acknowledge Itasca group for accepting me in Itasca Education Partnership (IEP) program and providing a one-year loan of the latest version of FLAC3D. I would like to appreciate Zorica Radakovic-Guzina in Itasca Education for serving as my mentor and for the guidance and valuable information that helped me a lot to proceed with modeling using FLAC3D 5.01.

Also, special thanks to Dr. Dimiter Alexiew at Huesker Inc. for providing geotextile tubes and technical guidance in the dissertation work.

Since a lot of people have helped me throughout my research work, I would like to thank the members of KU geotechnical society for their help during the experimental work. Special thanks to Jun Guo, Xaiohui Sun, Lee, Gaith Abdulrasool, Saif Jawad, Mahdi Al-Naddaf, Osama Al-Qassag, Fei Wang, Maryam Al-Taweel. Special thanks to Dr. Ryan Corey and Dr. Xiaoming Yang for their help with FLAC3D work.

Finally, I would like to thank my family, especially my precious mother, for their endless love and support.

Table of Contents

LISTS OF TABLES

LISTS OF FIGURES

CHAPTER 1

INTRODUCTION

1.1 Background

Large areas of the world are covered with soft clay deposits, especially coastal regions. As a result of economic growth, many infrastructure projects, such as roadway embankments, are being constructed in areas with weak soil deposits. Many challenging problems have been encountered with regard to construction on soft soil deposits including bearing capacity issues, excessive deformation, and slope instability. Global instability or deep-seated failure of a roadway embankment constructed on a soft foundation has become a serious issue for geotechnical engineers. Several ground improvement techniques have been widely implemented to avoid deep-seated failures in weak soils including sand compaction columns, stone columns, and deep mixed columns. The stone column, or granular pile technique, has been widely adopted to improve the soft soils through the inclusion of granular columns which have a stiffness and drainage capability that is far higher than those of the surrounding weak soil. In addition to the above benefits, this technique is characterized by the ease of construction.

The development of the stone column technique occurred in Europe. Hughes and Withers (1974) stated that stone columns were common in France as early as the 1830s to strengthen a foundation soil carrying heavy ironworks. Stone columns have been widely used in Europe since the 1950s and in North America since 1970s.

Since a stone column (see Fig. 1.1 (a)) derives its bearing capacity from the passive resistance offered by the native surrounding soil, the inclusion of stone columns in very soft soils may not be sufficient to the desired level of improvement. Therefore, geosynthetic encased stone

columns (as shown in Fig. 1.1 (b)) are introduced as a convenient technique for improving soft soils that have undrained shear strengths lower than 15 kPa (Han, 2015) . Encasing the stone column within geosynthetic increases the stiffness of the column and thereby increases its load capacity when compared with the ordinary stone columns.

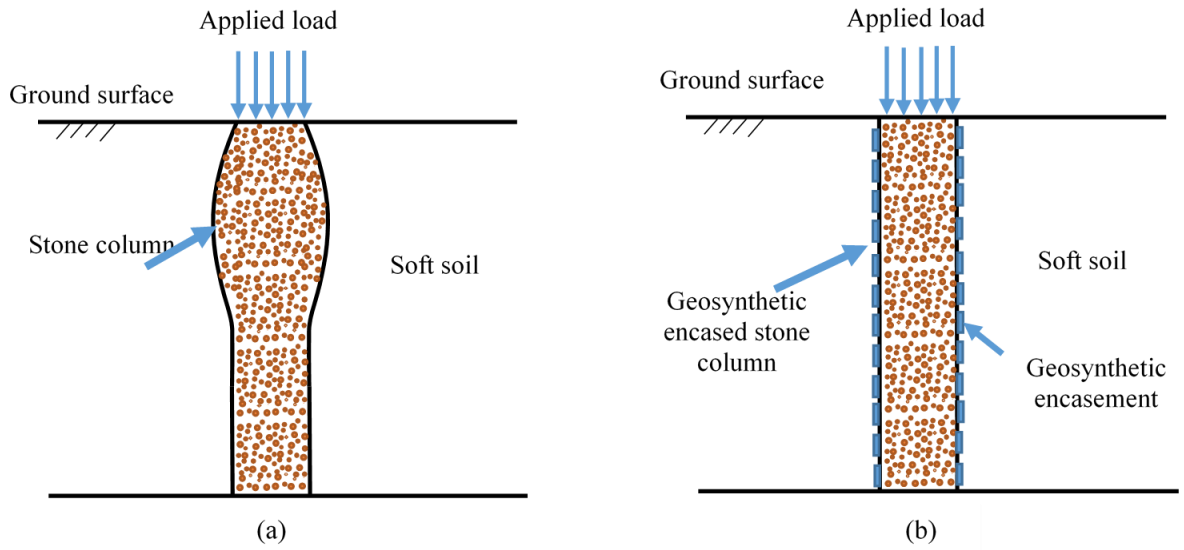

Figure 1.1 Illustration of stone column technique: (a) Ordinary stone column; and (b) Geosynthetic encased stone column

1.2 Problem Statement

Over the last two decades, much research has been conducted to assess the degree of improvement achieved by the inclusion of ordinary stone columns and encased stone columns in soft foundation soils. Experimental data, theoretical solutions, and numerical analyses were employed to investigate the role of stone columns in improving the bearing capacity of improved ground and the lateral deformation patterns of embankments supported by columns at different depths. Researchers have put a great deal of effort into comparing the performance of geosynthetic encased stone columns to that of ordinary stone columns installed in soft soil foundations.

In addition to bearing capacity issues, deep-seated failure, or embankment instability, is one of the major problems that may be encountered when constructing road embankments on soft foundation soils. A few studies have been conducted to assess the global stability of embankments constructed on ground improved through the use of ordinary stone columns (OSC). However, the stability of embankments supported by geosynthetic encased stone columns (GESC) has not been thoroughly investigated yet. This research focuses on the vertical stability of geotextile encased single sand columns (GESC) of various diameters and lengths, installed in both air, which demonstrates performance in the extreme case that the surrounding soil offers no confinement, and in very weak surrounding soil which simulates the more likely case. In reality, soil conditions may lie in between these two cases. The experimental data was verified through numerical analysis using FLAC3D, and a parametric study was conducted to assess factors that may have an impact on the performance of GESC. Finally, the stability of an embankment founded on treated ground with a group of GESC was also investigated using plane strain modeling with FLAC2D under short-term conditions.

1.3 Objectives

The main objectives of this research are:

- To evaluate the vertical stability of geosynthetic encased granular columns.
- To quantify the contribution of geosynthetic encased granular columns to global stability.
- To recommend design methods for vertical and global stability analysis.

1.4 Research Methodology

The research methodology included a literature review, laboratory testing, and numerical analysis. (1) The literature review covers relevant studies related to the installation, load transfer

mechanisms for both ordinary and geosynthetic encased stone columns, and stability analyses for stone column-supported embankments. (2) Laboratory tests were conducted on the infill material (i.e., Kansas River Sand), ordinary sand columns, and geotextile encased sand columns to define the strength properties. (3) Laboratory tests were performed on geotextile encased sand columns in air and with weak surrounding soil to investigate the bearing capacity, radial and axial deformations. (4) Numerical modeling using FLAC3D was conducted to verify and validate the experimental data and to perform a parametric study to investigate the performance of geotextile encased sand columns under different parameters. (5) Numerical modeling was conducted with FLAC2D to evaluate the stability issues of geosynthetic encased stone column-supported embankments.

1.5 Organization of Dissertation

This dissertation comprises six chapters. Chapter One presents an introduction to the background, problem statement, and objectives of this research. Chapter Two contains a literature review of the published work on the installation, functions and load transfer mechanism of ordinary stone columns, applications of geosynthetic encased stone columns, and stability issues. Chapter Three discusses the strength parameters of both ordinary and geotextile encased sand columns as determined through a series of triaxial compression tests. Chapter Four deals with the vertical stability of encased sand columns both in air and in weak surrounding soil. Chapter Five shows results from the numerical analyses implemented on the experimental model and discusses the calibration and validation of the research model and parametric study. Chapter Six presents the numerical study of the stability of an embankment supported by geosynthetic encased stone columns. Chapter Seven presents the conclusions and recommendations for future work.

CHAPTER 2

LITERATURE REVIEW

2.1 Introduction

This chapter contains a summary of selected published research on the inclusion of stone columns in soft soils to improve the performance of foundation soil. The installation process, functions and load transfer mechanism are also covered in this chapter. The applications of geosynthetic encased stone columns are extensively addressed. Lastly, previous numerical and experimental research on the stability of stone column supported embankments is also discussed.

2.2 Ordinary Stone Columns

Stone columns, also known as granular piles, are one of the most popular and widely used ground improvement techniques throughout the world. This section presents a summary of published information concerning the installation, functions and load transfer between stone columns and the surrounding soil.

2.2.1 Installation Process

Stone columns are often installed by either water jetting (replacement or wet method) or air jetting (displacement method). For the wet method, water is injected into the ground producing soil slurry that is flushed out from the hole as shown in figure 2.1(a). For the displacement method (figure 2.1(b)), air is injected into the ground with the use of a vibrating probe to form a hole. The hole is then backfilled with gravel or crushed stone or sand which is densified using the vibratory probe as it is withdrawn from the ground (Zhang et al., 2014; Han, 2015).

Raithel et al. (2005) reported the effect of the selected installation method on the shear strength of soft soil. A comparison was made between the shear strength of soft soil before and

after the vibro-displacement installation process. The measurements showed the undrained shear strength of the soil approximately doubled when compared with pre-installation values.

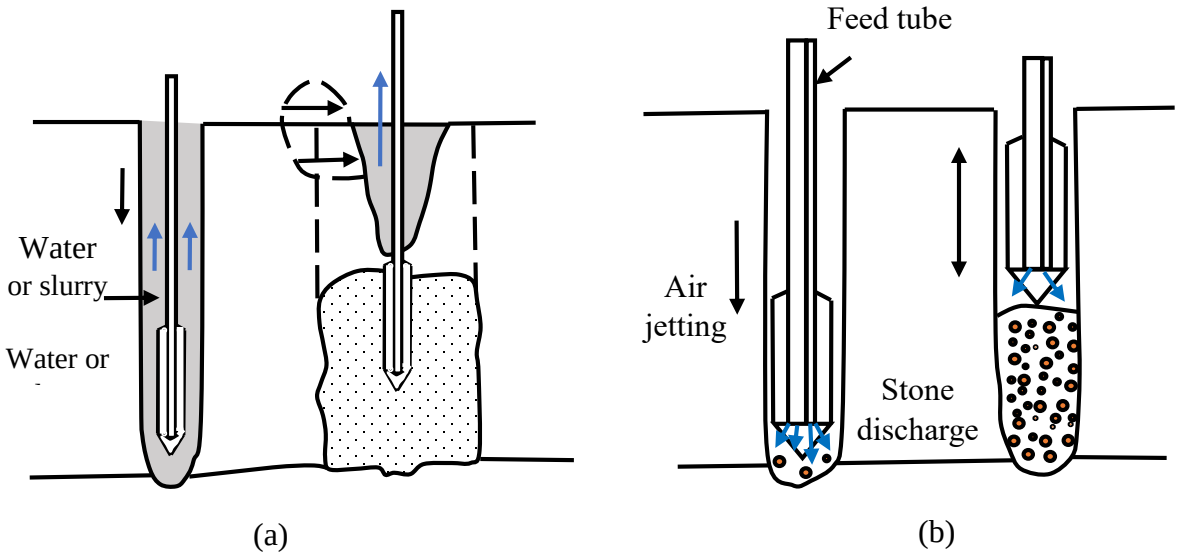

Figure 2.1 Stone column installation: (a) Replacement method; and (b) Displacement method

2.2.2 Functions

Stone columns can serve multiple functions when installed in foundation soils. The primary purposes for using this technique are to improve bearing capacity, reduce settlement, and enhance drainage and stability (Ambily and Gandhi, 2007; Lo et al., 2010; Han, 2012; Zhang et al., 2014).

Since stone columns have a higher stiffness and strength compared with the weak surrounding soil, they can be considered load bearing elements which carry a large portion of the superstructure and/or earth structure load and transmit it to the underlying layers in a way similar to piles (Lo et al., 2010). In addition, stone columns can serve as reinforcing units which act like a steel-reinforced concrete; the soil and the column share the applied load and prevent sliding failure (Han, 2012).

Granular columns can also provide drainage paths for soft soils (Han, 2012). The granular backfill is more permeable than the surrounding soft soil. Thus, the presence of granular columns will accelerate the dissipation of the excess pore water pressure in soft soils which in turn accelerates the consolidation process and reduces both the total and post-construction settlements (Lo et al., 2010).

2.2.3 Load Transfer Mechanism

In a column-reinforced soil, columns carry higher stresses than the surrounding weak soft soils under the same strain (i.e. settlement) because of the differences in stiffness between columns and surrounding soil.

The ratio of the stress on the column (σ_c) to the stress on the soil (σ_s) is referred to as the stress concentration ratio (n). Since the columns and the soft soil have different properties, the stress concentration ratio is not necessarily constant but its value varies according to the properties of columns and soft soils and strain and/or stress level (Han, 2012). Figure 2.2 depicts the stress-strain relationship for both the column and the soil. The stress concentration ratio first increased with strain up to a point where the column had mobilized its maximum strength and then decreased as the stress was transferred back from the column to the soil due to column yield (Han, 2015). Abusharar and Han (2011) made the (conservative) assumption that the stress concentration ratio of 1 for soil column supported embankments because soil columns usually behave in a manner that is similar to a flexible foundation.

Figure 2.3 depicts the load transfer mechanism. Two equal settlement planes are developed; one in the fill zone (when the fill height is greater than critical height h_c) and the other in the soft soil. The critical height was estimated to be 1 to 1.5 times of the clear spacing between columns (Chen et al. 2010). Since the column settlement (S_c) and soil settlement (S_s) are different,

a negative shear stress develops in the column between the upper and lower equal settlement planes. However, the positive shear stress develops below the lower equal settlement planes. Meanwhile, the average vertical column stress (σ_c) increases and the average vertical soil stress (σ_s) decreases due to the negative shear or skin friction. The average vertical soil stress (σ_s) is found to be higher than the initial overburden stress (σ_o) and lower than the average vertical stress for the fill (σ_f).

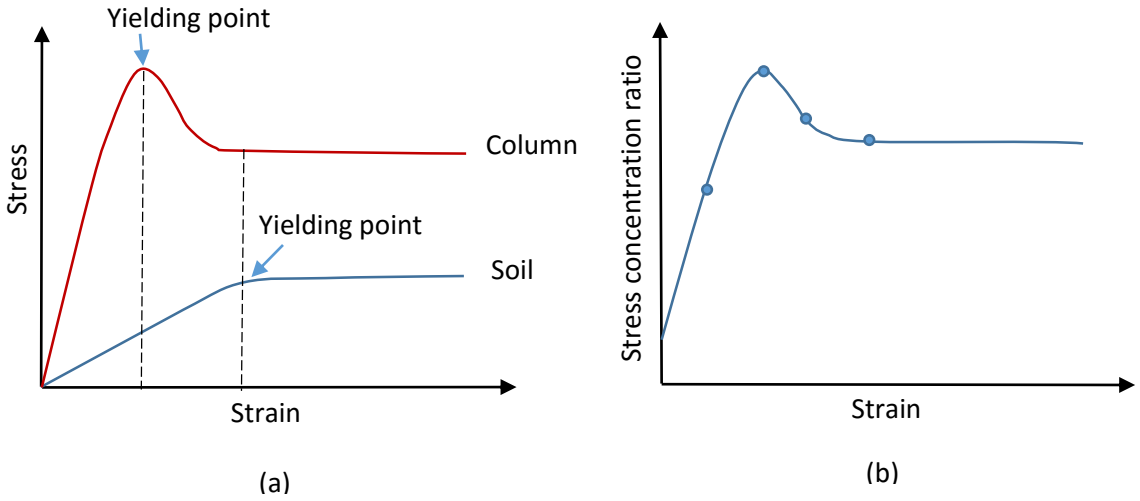

Figure 2.2 Stress concentration ratio: (a) stress-strain curves of the soil and the column and (b) stress concentration ratio versus strain (after Han, 2015)

2.2.4 Unit Cell Concept

In order to simplify the idealization of composite foundations, the unit cell concept has been introduced (Murugesan and Rajagopal 2006; Ambily and Gandhi 2007; Gniel and Bouazza 2009; Lo et. al. 2010; Zhang et al. 2010; Tallapragada et al. 2011, Han 2012). This concept (see figure 2.4) is based on the assumption that the column and the surrounding soil are going to deform together at the same strain. Correspondingly, in order to accomplish the equal strain, two conditions should be met: rigid loading and a loading area larger than the thickness of the

reinforced zone (Han, 2012). It was hypothesized that there was no lateral deformation of the soil at the edge of the unit cell (Ambily and Gandhi, 2007). The stress concentration ratio of a unit cell is thereby the ratio of constrained modulus of the column to that of the surrounding soil at an equal strain condition (Han, 2015). The most common term used in unit cell concept is the area replacement ratio (a_s), that is, the cross sectional area of the column divided by the total cross sectional area of the unit cell.

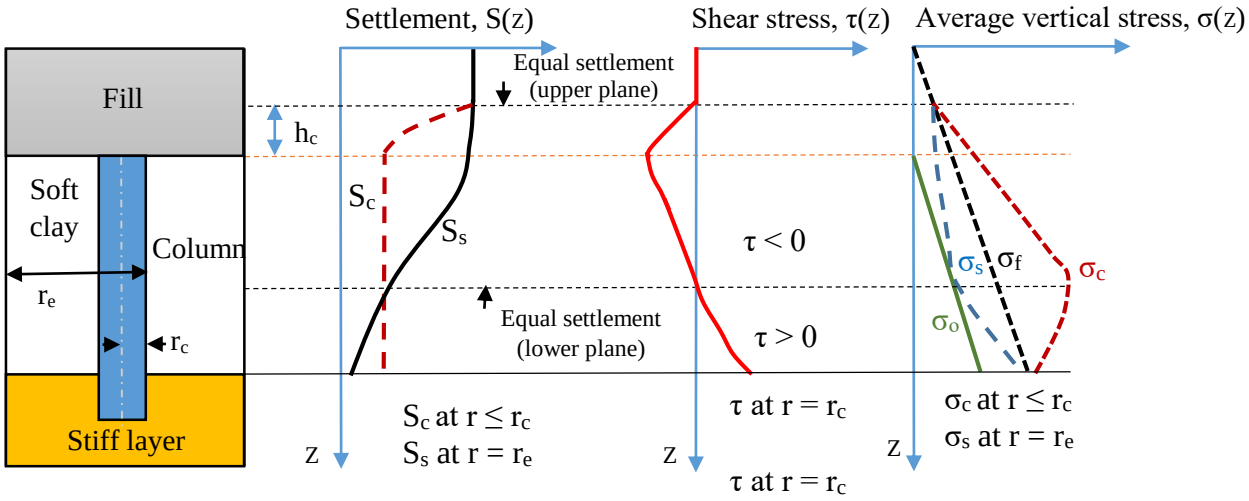

Figure 2.3 Load transfer mechanism (after Han, 2012)

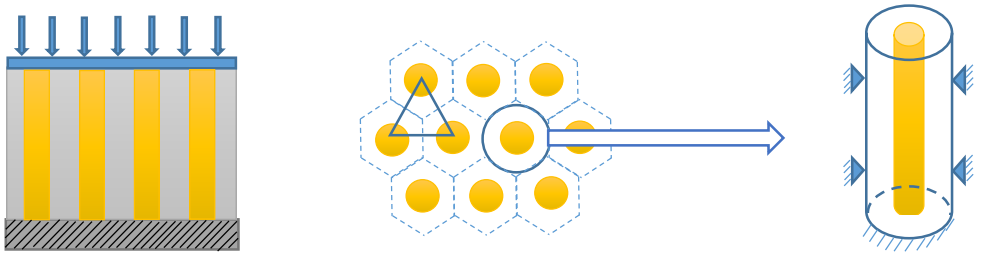

A uniform load is applied to a composite ground

The influence zone of column is assumed to be circular which represents a unit cell

A unit cell fixed at bottom, no radial deformation is allowed at edge

Figure 2.4 Unit cell concept (after Gniel and Bouazza, 2009)

2.3 Geosynthetic Encased Stone Columns (GESC)

Ordinary stone columns (OSC) usually derive their bearing capacity from passive resistance provided by the surrounding foundation soil pressing against the lateral bulging of stone columns as a result of axial load application. When embedded in soft clay, stone columns may bulge due to lack of confinement offered by the surrounding soft soil. Furthermore, the soft clay may enter the voids between granular material of column to cause clogging and reduce the permeability of granular columns for drainage. In order to avoid these consequences, additional confinement can be provided by using geosynthetic encasement. This will help to isolate the granular soil inside the column so that it does not mix with the surrounding soil and increase the stiffness of the columns (Arvizhi and Amparuthi 2007; Murugesan and Rajagopal 2006, 2009). Figure 2.5 demonstrates the geosynthetic encased stone column (GESC). The installation of geosynthetic encased stone columns involves driving a steel casing with a closed end tip into the ground to create a hole. A geosynthetic tube is then inserted inside the steel casing and the granular material is then backfilled. The tip of the casing is opened as the steel casing is withdrawn from the soil with vibration to densify the infill material as shown in figure 2.6.

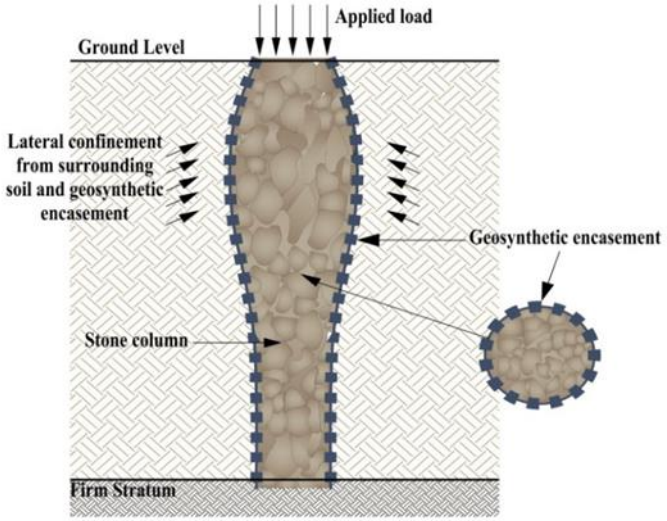

Figure 2.5 Geosynthetic encased stone column (after Murugesan & Rajagopal, 2009)

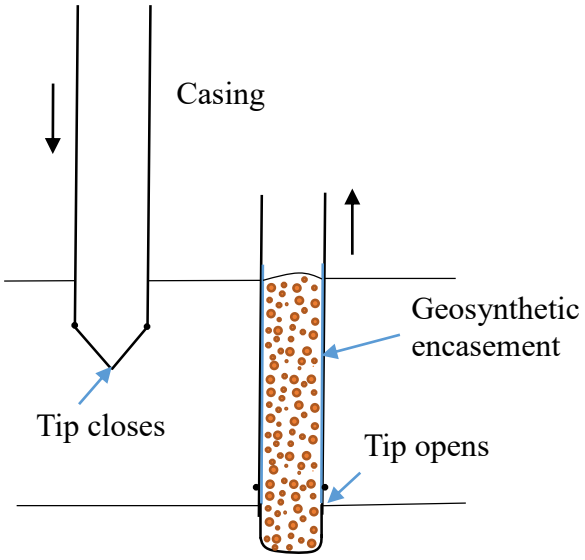

Figure 2.6 The installation procedure of geosynthetic encased stone columns

The radial stress acting on the stone columns $\sigma_{r,s}$ is the sum of the contributions of both the radial stress of the surrounding clay soil ($\sigma_{r,c}$) and the hoop tension (T) from geosynthetic encasement as shown in figure 2.7:

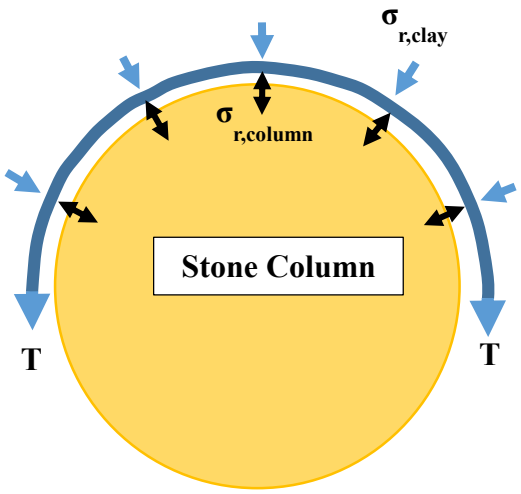

Figure 2.7 Radial stress of surrounding soil and hoop tension of geosynthetic encasement (after Lo et al., 2010)

$$\sigma_{r,s} = \sigma_{r,c} + \frac{T}{R} \quad 2.1$$

Where R= radius of stone column. $\sigma_{r,c}$ and T are each composed of two parts: the initial value time (i.e. $\Delta\sigma_{r,c}$ and ΔT)(Lo et al., 2010):

$$\sigma_{r,s} = \sigma_{r,c}(i) + \Delta\sigma_{r,c} + \frac{T(i)}{R} + \frac{\Delta T}{R} \quad 2.2$$

$$= \sigma_{r,c}(i) + \Delta\sigma_{r,c} + \sigma_{rp} + \frac{\Delta T}{R} \quad 2.3$$

$$\sigma_{r,s} = \sigma_{r,c}(i) + \sigma_{r,p} + \Delta\sigma_{r,s} \quad 2.4$$

$$\Delta\sigma_{r,s} = \Delta\sigma_{r,c} + \frac{\Delta T}{R} \quad 2.5$$

The hoop tension force (T) is influenced by the lateral strain of column material under the superimposed load.

2.4 Design Considerations of Ordinary Stone Columns (OSC) and Geosynthetic Encased Stone Columns (GESC):

2.4.1 Bearing Capacity and Lateral Bulging of Granular Columns

Columns have been designed to carry not only vertical loads but they can also transfer horizontal loads. When subjected to vertical compressive loads, columns transfer the load to the adjacent soil via the side friction generated between the soil and the column (Han, 2012). Han and Ye (1991) summarized the potential modes of failure for an individual column subjected to axial compressive load: punching failure, crushing failure, shear failure, and bulging failure. However, bulging failure is considered the most common mode of failure for granular columns (stone columns) when they are embedded in soft soil deposits.

The inclusion of stone columns enhanced the bearing capacity of improved ground when compared with that of the weak native soil (Ambily and Gandhi, 2007; Arvizhi and Amparuthi, 2007; Murugesan and Rajagopal, 2009). Ambily and Gandhi (2007) investigated the performance

of a single stone column and a group of stone columns constructed in soft soils through small scale laboratory tests and numerical analysis. They found that when only the top area of the column was loaded, the maximum bulging failure occurred at a depth of approximately one half of the diameter of the stone column. In addition, loading tests were also performed through loading the whole area of the unit cell to simulate an internal column in a grid of many columns loaded at the same time. They concluded that when the ratio of the spacing from center to center of columns to the diameter of column (s/d) is 3 or greater, no remarkable improvement in axial loading capacity can be achieved. Furthermore, the ratio of the modulus of column material to the surrounding soft clay modulus is essentially a function of the friction angle of the column material and spacing between columns.

Arvizhi and Amparuthi (2007) observed that the effective bulging of the column was extended to a depth of four times of column's diameter. OSC may suffer larger lateral expansion close to the surface. In contrast, GESC can have considerably higher lateral expansion at deeper depths. This may be attributed to the fact that the superimposed load is transferred to deeper depths because of the presence of the encasement (Murugesan and Rajagopal 2006).

The hoop tension force of geosynthetic encasement (T) has a significant effect on the degree of improvement regarding the bulging failure extended to a depth of twice the diameter of the column (Murugesan and Rajagopal, 2006). Since hoop tension is mainly related to the stiffness of geosynthetic encasement, increases in bulging can be reduced when the hoop tension is mobilized in the encasement. As a result, developing a greater hoop tension leads to a stiffer geogrid (Arvizhi and Amparuthi, 2007). Unlike OSC, GESC possess considerably higher stress concentration ratios (n) due to the additional confinement resulting from the increased modulus of GESC. Therefore, Murugesan and Rajagopal (2009) concluded that GESC behavior is similar to semi-rigid piles.

The effect of partial encasement for isolated and group columns was reported by different researchers (Gniel and Bouazza, 2009; Khabbazian et al., 2010). It was observed that the radial expansion failure happened just beneath the level of the encasement. Therefore, a partially encased column would be a feasible and economic solution over the OSC for soil profiles where soft clay is underlain by firm strata. Another study was conducted by Gu et al. (2015) to investigate the effect of the encasement length on load capacity and lateral bulging of GESC. They concluded that the effective length for the column's encasement was three to four times the column's diameter, and any further increase in encasement length did not give an additional improvement to the load capacity of encased stone columns. This may be attributed to the mobilization of the confining stress of the encasement in the upper portion of the column and the depth of bulging failure was limited to twice of the diameter of column. In contrast to the individual column's loading, Yoo (2010) recommended use of full length encasement for GESC under embankments to obtain optimum reduction in settlement of improved ground.

A comprehensive study of the load transfer mechanism of a single column using a 3D finite element program (ABAQUS) was performed by Khabbazian et al. (2010). It was hypothesized that the load transferred to the tip was much greater for GESC as compared to OSC due to the increased stiffness of encased columns. They calculated that both the skin friction and end bearing resistance of the column were increased by 35% and 65%, respectively.

With regard to the impact of a column's size on the degree of the improvement, small diameter columns will have a higher hoop tension (T) in geosynthetic encasement and thus higher confinement, which will lead to higher stiffness in the GESC and higher load bearing capacity (Murugesan and Rajagopal, 2009; Castro and Sagaseta, 2011).

Tallapragada et al. (2011) proposed a new approach to stone column design in order to improve the bearing capacity of soft clay for two cases; with and without geosynthetic-encasement

under a superimposed axial load. A small percentage of sand, stone dust, lime and filler material were added to the ordinary granular material with the presence of geosynthetic encasement to enhance its bearing capacity due to the provided adhesion and cohesion between particles. Further enhancement in bearing capacity was achieved when using geosynthetic encasement.

Hong et al. (2016) addressed the effect of the mechanical properties of geotextile encasement (i.e. strength and stiffness) on the behavior of geotextile encased stone columns constructed in a soft clay deposit. They reported that weaker geotextiles exhibited bulging at a depth of 2.5 times the diameter of column, whereas for geotextiles of higher stiffness, the lateral displacements were distributed uniformly along the entire length of the column. Moreover, they concluded that a higher geotextile stiffness resulted in an increase in the amount of load transferred to the bottom of the column.

Encasing stone columns in geosythetic encasement has proven to be an ideal solution to improve the performance of columns not only in soft clay but also in expansive soil (Kumar and Jain, 2013). The encased granular pile performs better since the ultimate bearing capacity of ground improved with encased columns was found to be 4.5 to 4.8 greater than that of untreated expansive clay.

2.4.2 Settlement of Granular Columns

While the installation of stone columns improved the bearing capacity of the treated ground, a significant settlement reduction is also achieved as compared to untreated soft ground. Tallapragada et al. (2011) reported a considerable reduction in the settlement of encased stone columns compared with ordinary stone columns. This reduction was even greater for larger diameters and longer lengths of columns.

The impact of the length of stone columns on settlement was investigated by Arvizhi and Amparuthi (2007). They reported that no significant reduction in settlement was recorded when the ratio of column length to diameter (L/d) is greater than 10.

Another factor that may affect the settlement reduction is the area replacement ratio. Madhyannapu et al. (2006) stated that settlement was reduced significantly as the area replacement ratio increased.

Lo et al. (2010) investigated the impact of lowering the stiffness of stone and locked-in stress (preloading stress, Tpre) resulting from pre-straining the geosynthetic encasement on the settlement values and forces of stone columns. They demonstrated that locked-in geosynthetic tension is the dominant factor controlling the performance of stone columns with regard to stiffness, while the stiffness of compacted stones is found to have an insignificant effect on the degree of improvement.

The effect of encased stone columns on settlement and consolidation time was reported by Castro and Sagaseta (2011). They concluded that the efficiency of using GESC was dominated by the encasement stiffness relative to that of the surrounding soft soil and the diameter of columns. In addition, the applied load must not exceed the tensile strength of the encasement.

Geosynthetic encased stone columns has been found to shorten the time required for consolidation settlement. Furthermore, the stress concentration will contribute considerably to the acceleration of excess pore water pressure dissipation for GESC compared with OSC (Elsawy, 2013).

2.5 Stability Issues

Instability of an embankment over soft soil may result from local failure, surficial failure, toe slope failure or deep-seated slope failure as shown in figure 2.8. The problem of column

supported embankments constructed on soft foundations has been significantly addressed by several researchers using numerical methods (Madhyannapu et al. 2006; Abusharar and Han 2011; Zhang et al. 2014). Han et al. (2004) stated that the deep seated slope (global slope failure) problem is considered the major concern when constructing embankments over soft soils. Thus, one of the ground improvement techniques that has proven to be effective for solving deep seated slope stability problems is the inclusion of stone columns to support embankments over soft soils (Zhang et al., 2014). Han (2012) summarized the potential modes of failure of columns under embankments into six major types: sliding, rotation, bending, horizontal shear, circular shear and combined failure. He observed that these failure modes are basically dependent on the column's strength, rigidity, length, diameter, location and end bearing, the strength and stiffness of soft soil, and the slope angle and height of the embankment.

For slope stability analysis, Bishop's modified method can be considered the most commonly used limit equilibrium method (LEM) for analysis of the stability of embankments over soft soils. A numerical analysis to investigate the stability of an embankment supported with deep mixed columns proposed by Han et al. (2004) showed that the critical slip surface was not circular as Bishop's modified method assumes. Also, they concluded that Bishop's modified method overestimated the stability factor of safety for embankments supported by deep mixed columns over soft soil.

When compared with numerical methods, the limit equilibrium method would overestimate the factor of safety if the columns failed due to tension, bending or rotation (Han et al., 2005). This was primarily a function of the assumption of a circular slip surface, which resulted in an overestimation of factor of safety.

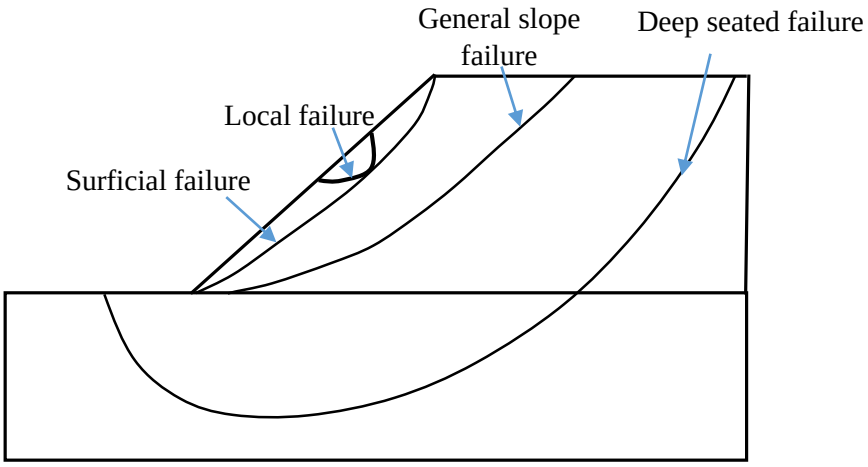

Figure 2.8 Potential slope stability failures (after Han et al., 2004)

Mohapatra et al. (2014) compared the shear resistance of a composite foundation of ordinary stone columns to that of geotextile encased stone columns when subjected to lateral loading with a series of large shear box tests. They found that OSC were sheared together with the soil at the shear plane while GESC did not have a shear plane that was as well defined due to the presence of geotextile encasement (see Fig. 2.9). In addition, OSC showed constant post peak shear strengths because of the shear failure of columns while GESC exhibited higher post shear strengths at larger horizontal displacements due to the mobilization of hoop tension. Stone columns with larger diameters showed higher shear resistance because they possessed higher area replacement ratios.

2.6 Numerical Analysis of Column Supported Embankments

Numerical methods, represented by finite difference (FDM) and finite element (FEM), have proven to be powerful tools for estimating the stability of embankments and slopes through the computation of the factor of safety (Cala and Flisiak, 2001; Han et al., 2004; Han et al., 2010; Abusharar and Han, 2011; Zhang et al., 2014).

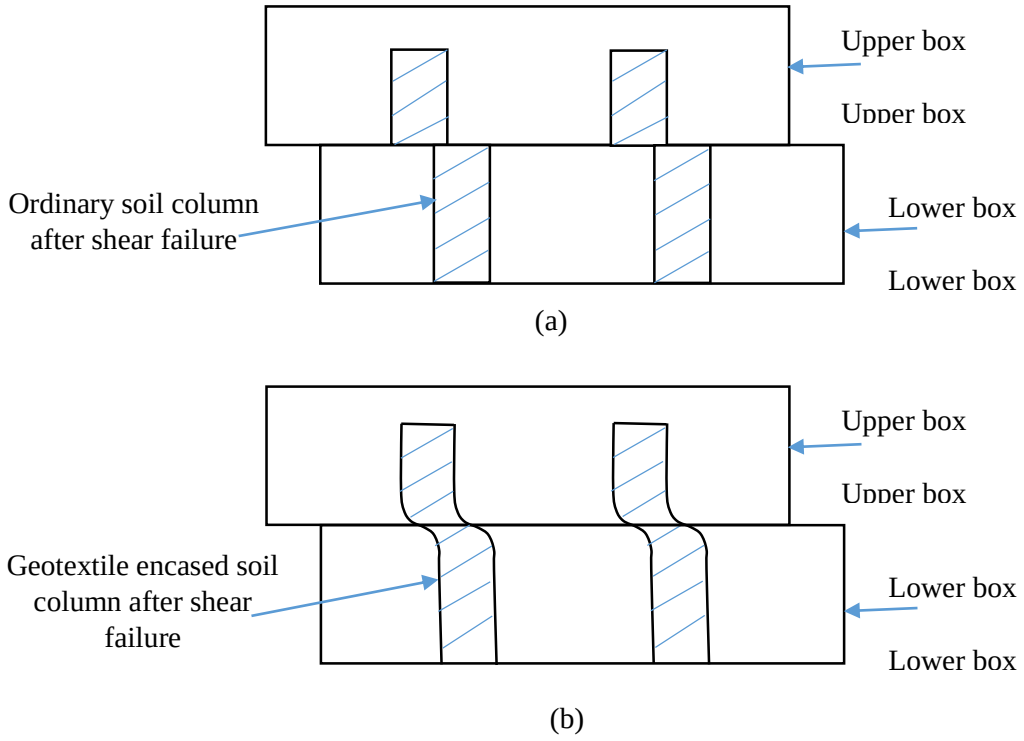

Figure 2.9 Failure modes of (a) Ordinary soil column; and (b) Encased soil column (after Mohapatra et al., 2014)

The finite difference software FLAC (Fast Lagrangian Analysis of Continua), developed by Itasca Consulting Group, is widely utilized for the analysis of the stability of embankments supported by deep mixed columns (Han et al., 2004). When compared with limit equilibrium methods (LEM), the estimation of the stability factor of safety using the finite difference method (FDM) can be characterized by (1) no pre-defined slip surface is needed; (2) the potential exists for the slip surface to be any shape; (3) no assumptions are made for the functions of inter-slice forces; (4) multiple failure surfaces may exist; (5) the capability exists to include different structural components, like tunnels, footings and structural elements using beams, cables and interfaces; (6) kinematics are satisfied (FLAC ITASCA, 2008).

In order to compute the factor of safety for slope stability problems, the finite difference approach (FLAC) applies a shear strength reduction (SSR) using series of trial factors of safety for both cohesion (c) and friction angle (φ) to cause the model slope to be on the verge of failure (FLAC ITASCA, 2008):

$$c_{trial} = \frac{c}{FS_{trial}} \quad 2.6$$

$$\phi_{trial} = tan^{-1}\left(\frac{tan\phi}{FS_{trial}}\right) \quad 2.7$$

Cala and Flisiak (2001) investigated the effect of complex slope geology on the computation of the factor of safety using SSR and LEM. It was found that the factor of safety computed from SSR was 20% lower than that for LEM due to the fact that the slip surface for SSR penetrated deeper than the slip surface of LEM. Furthermore, they recommended using FLAC with the SSR method to analyze large scale slopes that are characterized by complex geometry. LEM overestimates the stability factor of safety compared to SSR (Han et al., 2004; Han et al., 2010).

Due to the complexity of three dimensional (3D) column problems, there are several methods used to simplify these problems into two dimensional (2D) problems by adopting equivalent properties and dimensions. Converting a 3D problem into a plane strain problem involves two common methods: the column wall method and the equivalent area method as shown in figure 2.10.

Since the task of modeling a large number of columns beneath the embankment is complex, modeling an equivalent area is utilized more commonly in practice, although the latter method yields a higher factor of safety when compared with the column wall method. Abusharar and Han (2011) suggested for the short term condition a reduction factor of 0.9 for the value of the factor of safety computed by the equivalent method if a water table is not present and 0.92 if there is a

water table. No reduction factor was recommended for the factor of safety for the long term condition (Zhang et al., 2014).

Zhang et al. (2014) performed numerical analysis using FLAC2D 5.0 software to investigate the stability of an embankment supported by stone columns in soft soil under short and long term conditions. A parametric study was conducted using two methods (column wall method and equivalent area method) by varying factors like stress concentration, area replacement ratio and soil properties under short and long term conditions. They found that stress concentration was an insignificant factor for the stability of stone column supported embankments since this ratio was close to 1 when the slope approached the limit equilibrium condition.

Zhang et al. (2014) also reported that equivalent area method yielded higher factors of safety compared to the column wall method under the short-term condition, while the computed safety factors of the two methods matched well for the long-term condition. For a stress concentration equal to 1, higher area replacement ratios increased the computed factors of safety for both of the aforementioned methods. They also observed that some individual columns did not yield and remained in an elastic condition under the short-term condition, whereas all points in composite ground (equivalent area) mobilized their shear strength. For the long-term condition, both columns and soil mobilized their shear strengths.

Elsawy (2010) performed a parametric study using the finite element program PLAXIS to investigate the behavior of a highway embankment supported by geosynthetic encased stone columns embedded in soft clay for both short and long term conditions. He concluded that smaller diameters of stone columns, narrower spacing between columns and higher stiffness of geosynthetic encasement will enhance the degree of improvement. This was found to be true for both short and long term conditions and strongly supported the literature documenting previous findings.

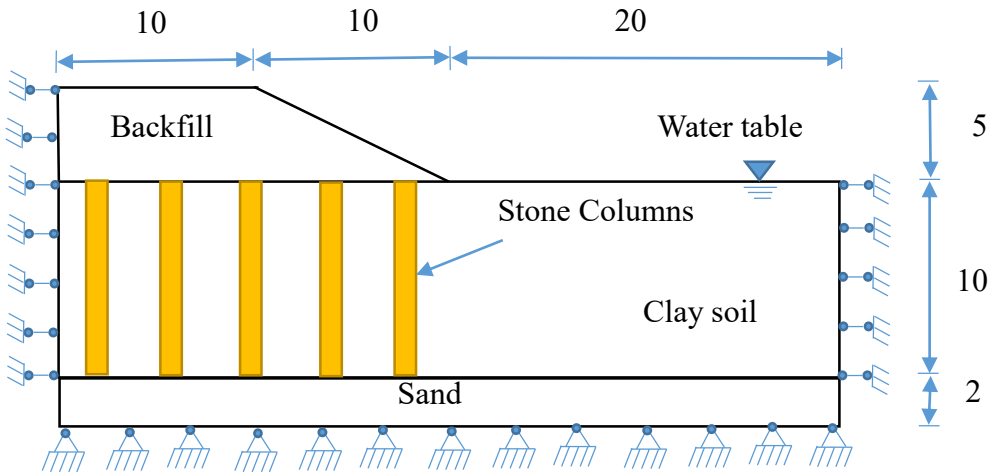

(a)

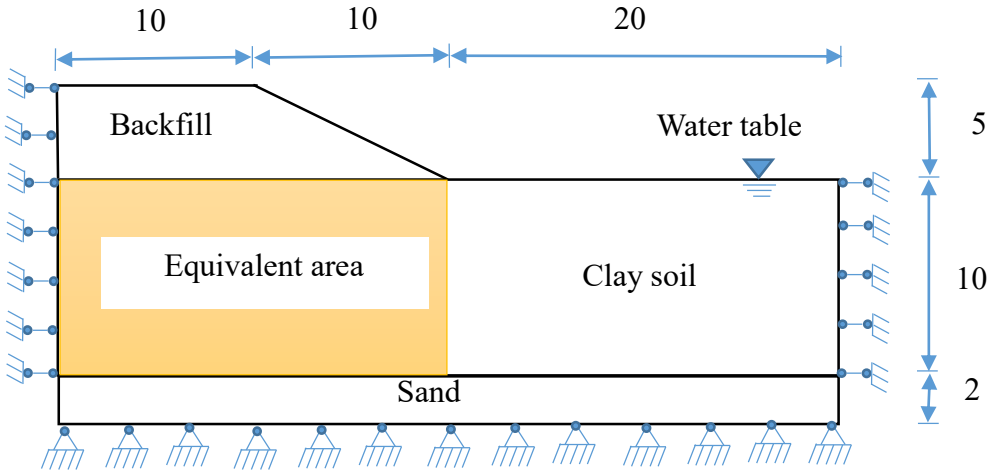

(b)

Figure 2.10 Plane strain model of stone column supported embankments: (a) Column wall method; and (b) Equivalent area method (after Abusharar and Han, 2011)

Previous studies demonstrated the role of horizontal geosynthetic reinforcement in stabilizing the riverside of a levee against any surficial, local and deep-seated failure. Han et al. (2010) investigated the degree of improvement in the stability of the levee by treating the foundation soft soil with deep mixed columns and reinforcing the riverside of the levee with

geosynthetic in order to mitigate the potential for seepage failure and rapid drawdown problems. They concluded that deep mixed columns improved the resistance to the shear/moment failure mode.

CHAPTER 3

MATERIAL PROPERTIES AND SHEAR STRENGTH PARAMETERS OF ORDINARY AND GEOTEXTILE ENCASED SAND COLUMNS: EXPERIMENTAL WORK

3.1 Introduction

This chapter presents the properties of the materials used in the experimental work (i.e. sand and geotextile encasement). The procedure and the results of a series of triaxial compression tests conducted on ordinary and encased sand columns to obtain the shear strength parameters are also described.

3.2 Material Properties

This section describes the properties of Kansas River Sand and geotextile encasement material used in the experimental work.

3.2.1 Kansas River Sand

In this study, Kansas River Sand was used as infill granular material placed inside the geotextile encasement to form the GESC and as the surrounding soil around the GESC. It was classified as a poorly graded sand (SP) according to Unified Soil Classification System with a D_{10} of 0.28 mm. The particle size distribution is shown in figure 3.1. The coefficients of uniformity (C_u) and curvature (C_c) of this soil were 1.62 and 0.99, respectively. The minimum and maximum density tests of this sand were performed in accordance with ASTM D4254-00 and ASTM D4253-00 and the minimum and maximum densities were 1.63 and 1.92 gm/cm^3, respectively. The relative density of sand (D_r) can be determined from the following equation:

$$D_r = \frac{\rho_{d\,max}\,(\rho_d - \rho_{d\,min})}{\rho_d\,(\rho_{d\,max} - \rho_{d\,min})} \qquad 3.1$$

Where ρ_{dmin} and ρ_{dmax} = minimum and maximum dry densities (gm/cm^3), ρ_d = dry density that corresponds to a specified relative density (gm/cm^3). The dry density of sand compacted to D_r = 70% was 1.82 gm/cm^3, which is the same density that was adopted to prepare the sand (infill soil) inside the geotextile encasement.

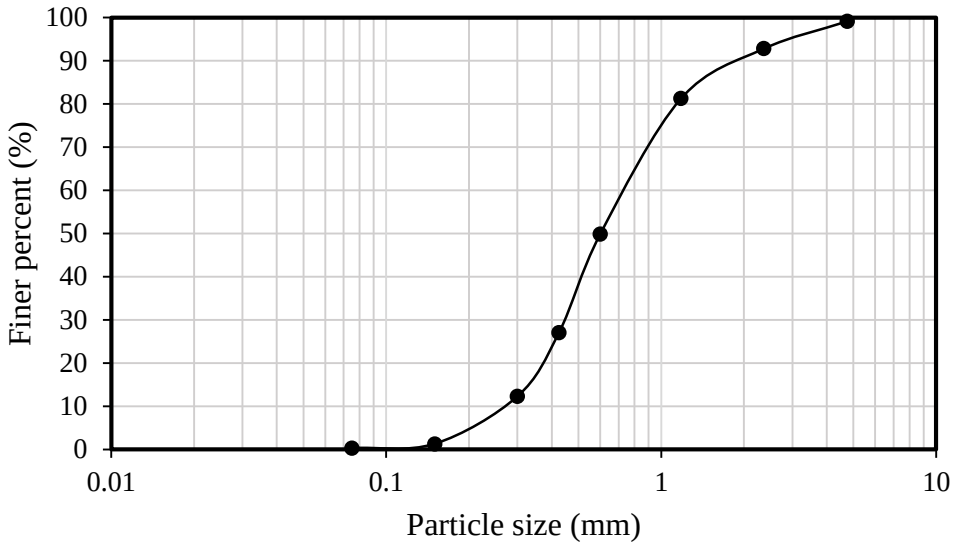

Figure 3.1 Grain size distribution of Kansas River Sand

3.2.2 Geotextile Encasement

Woven geotextile sleeves were fabricated and stitched by Huesker Inc. in Germany with three various diameters: 10, 15, and 30 cm. Stripe-tensile tests on a woven geotextile sheet, the material used to fabricate the geotextile sleeves, were conducted by Huesker on five samples for both machine (MD) and cross machine (CMD) directions to determine the mechanical properties of the geotextile material provided for this research. Table 3.1 and figure 3.2 show the results of the stripe-tensile test. The stiffness of geotextile (kN/m) in a specific direction can be computed as the ratio of the tensile force (kN/m) to the tensile strain in that direction. For instance, the tensile

strength and stiffness of geotextile corresponding to 2% axial strain were 7.06 kN/m and 353 kN/m in the machine direction and 17.22 kN/m and 861 kN/m in cross machine direction, respectively.

Table 3.1 Mechanical properties of geotextile material from stripe-tensile test

Direction	Tensile strength (kN/m)			Maximum tensile strength T_{max} (kN/m)	Strain at max. tensile strength ε_{max} %
	2% axial strain	3% axial strain	6% axial strain		
Machine direction MD	7.06	11.96	26.28	51.12	12.14
Cross machine direction CMD	17.22	24.68	44.34	53.86	8.18

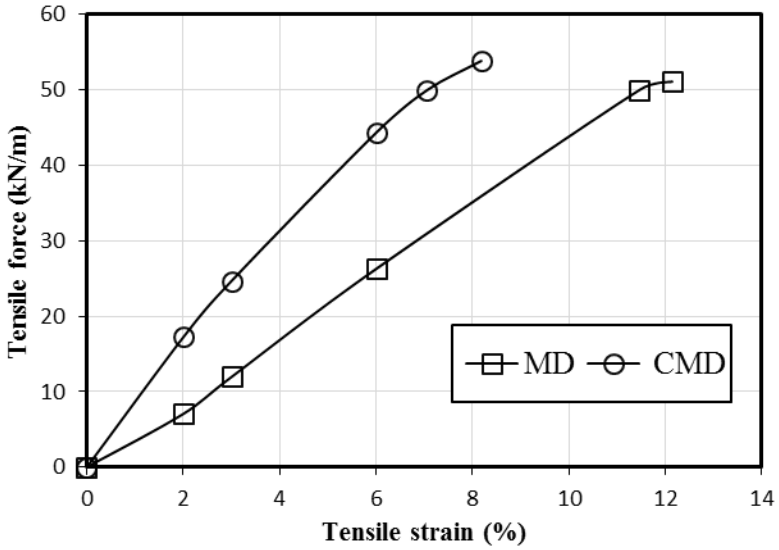

Figure 3.2 The results of stripe-tensile test conducted by Huesker

3.3 Shear Strength Parameters of Ordinary and Geotextile Encased Sand Columns

Six Consolidated Drained triaxial compression tests were performed on both ordinary and encased sand columns with woven geotextile sleeves. Testing procedure and results are discussed in the following sections.

3.3.1 Triaxial Compression Test Procedure for OSC and GESC

Geotextile sleeves with a diameter of 10 cm (4 inch) were chosen to perform all triaxial compression tests because the available apparatus in the KU laboratory is able to accommodate this size. Consolidated Drained triaxial tests (CD) for ordinary and encased sand columns were performed for three different confining stresses: 34.5 kPa (5 psi), 69 kPa (10 psi), and 103.4 kPa (15 psi). All samples (OSC and GESC) were prepared inside a split cylinder mold and had a relative density in a range of 60% to 70% and a length to diameter ratio of 2. In order to apply the chamber pressure, a rubber membrane of 0.635 mm (0.025 inches) thickness was used throughout these tests. For the encased column, the geotextile sleeve was placed inside the rubber membrane and then they were both inserted into a split mold which had an inner diameter of 10 cm (4 inch). The rubber membrane was held against the bottom platen by O-rings to prevent water from getting into the sample and to prevent sand from escaping. Then, dry sand with a known mass was poured into the geotextile sleeve and compacted to (60%-70%) relative density. A single rubber membrane was considered too likely to break due to the compaction of the sample or contact with sharp edges on the geotextile tubes. Therefore, two rubber membranes were used to cover each geotextile encased sample to guard against any possible leakage. The axial load was applied by means of a load cell at a strain rate of 0.5%/min. The volume change readings were recorded by the amount of water squeezed out of the sample. Figure 3.3 depicts the prepared samples for triaxial compression tests of ordinary sand columns (OSC) and geotextile encased sand columns (GESC).

(a) (b)

Figure 3.3 Triaxial test samples: (a) sand column; and (b) geotextile encased sand column

3.3.2 Test Results and Discussions

The results of triaxial tests conducted on both ordinary and encased sand samples are illustrated in figures 3.4 (a) and (b). The deviatoric stresses increased with increasing axial strain for both OSC and GESC and were higher for higher confining stresses. Ordinary sand samples exhibited lower shear strengths compared with encased sand samples and started to yield after 1% axial strain. The residual shear strength of OSC was not much less than the peak shear strength, as shown in figure 3.4(a). For woven geotextile encased sand columns (see figure 3.4(b)), the deviatoric stresses continued to increase with the increase of the axial strains. The granular infill material of the column pressed laterally against the geotextile sleeve as the axial loading increased. The geotextile tube was therefore stretched and the hoop tension force mobilized to provide

additional confinement to the column, which significantly enhances its bearing capacity (Wu et al., 2009).

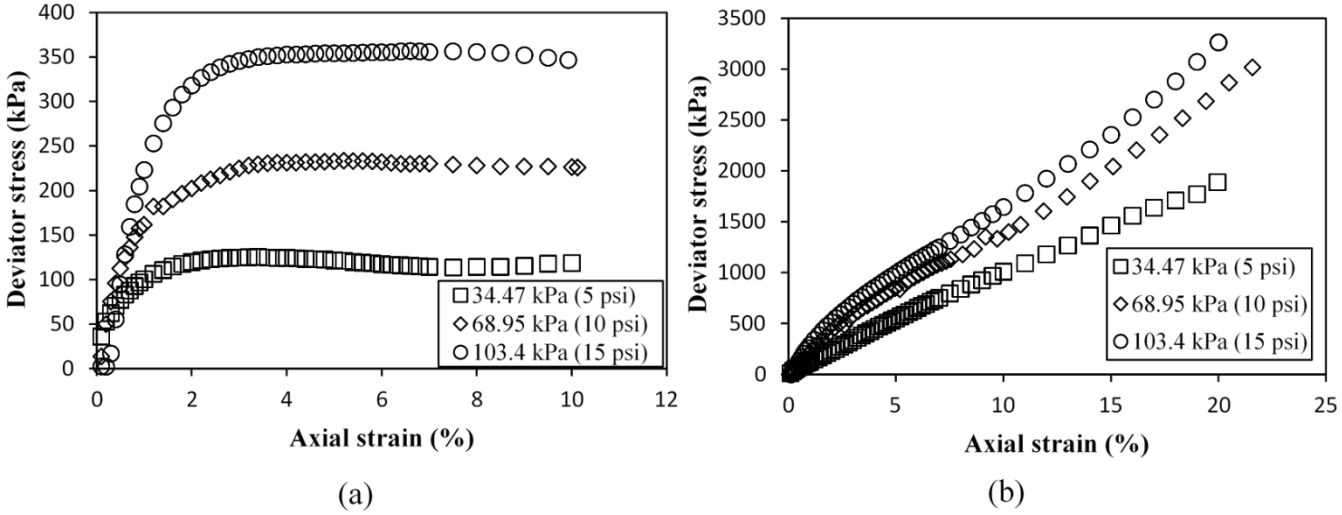

Figure 3.4 Triaxial compression results of: (a) ordinary sand column; and (b) geotextile encased sand column

The volumetric strain-axial strain relationships for geotextile encased columns are illustrated in figure 3.5. Samples subjected to higher confining stresses exhibited lower volumetric strain. In order to investigate the volumetric strain-axial strain relations of both OSC and GESC, a comparison was made between them at the same confining stress as illustrated in figures 3.6 and 3.7. As shown in figure 3.6, for the low confining stress of 34.4 kPa (5 psi), the GESC exhibited less volumetric strain than the OSC for axial strains below 8%. For axial strains above 8% the OSC had less volume change. As shown in Figure 3.7, the same relationship was observed for the somewhat higher confining stress of 103.4 kPa (15 psi), with the volumetric strain plots crossing at 6%. This could be related to the fact that geotextile encased sand columns continued to support higher shear stresses as the axial strains increased without failing, unlike the ordinary sand columns which approached the steady state at lower axial strains.

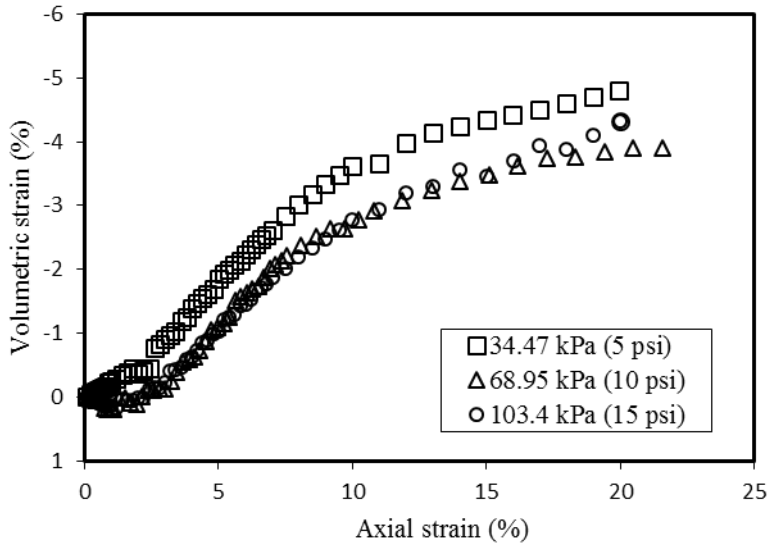

Figure 3.5 Volumetric strain vs. axial strain for geotextile encased sand column

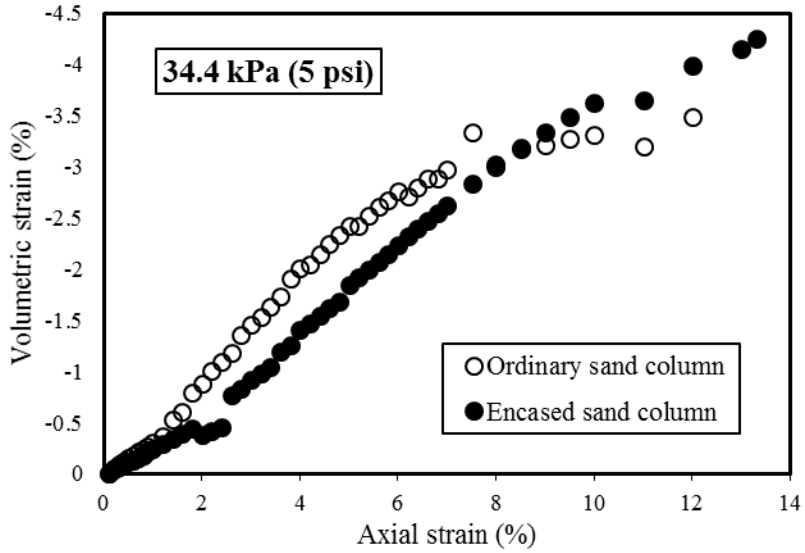

Figure 3.6 Volumetric strain vs. axial strain for both OSC and GESC at 34.4 kPa confining stress

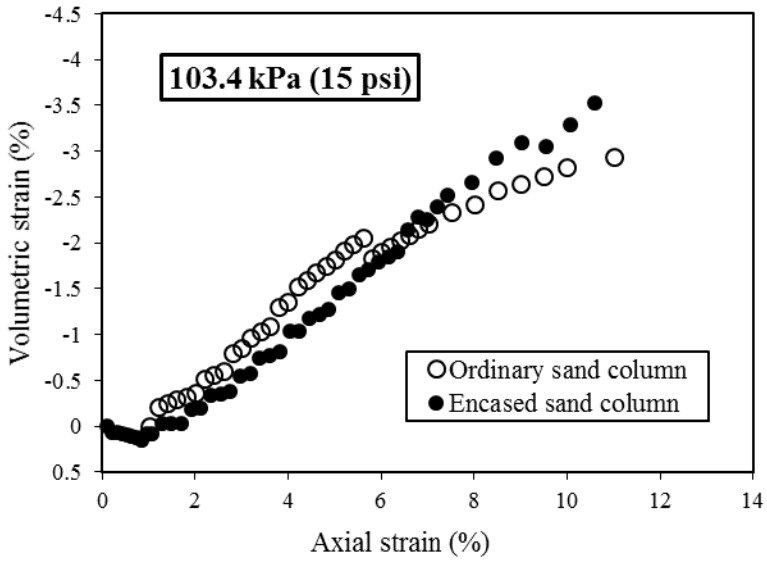

Figure 3.7 Volumetric strain vs. axial strain for both OSC and GESC at 103.4 kPa confining stress

Figures 3.8 (a) and (b) show lateral bulging of both ordinary and encased sand columns. The maximum bulging was located at the mid-height of the columns. Geotextile encased sand samples exhibited reduced lateral bulging as compared with ordinary sand samples, and these lateral deformations continued to develop for larger axial strains. It was a difficult task to take a photo of the OSC sample after the completion of the test because it was about to collapse, therefore the image provided in figure 3.8(a) was for the sample still inside the triaxial chamber.

Figures 3.9 and 3.10 depict the shear strength parameters of ordinary sand columns; cohesion and friction angle, as illustrated by Mohr's circles. Since sand does not have cohesion, the slope of the line drawn from the origin of the shear stress-normal stress graph and tangent to the Mohr's circles represents the friction angle of sand. Peak and residual angles of internal friction from consolidated drained tests were found to be 38.6^{o} and 37.4^{o}, respectively at 70% relative density.

(a) (b)

Figure 3.8 Lateral bulging: (a) Ordinary sand column; and (b) Geotextile encased sand column

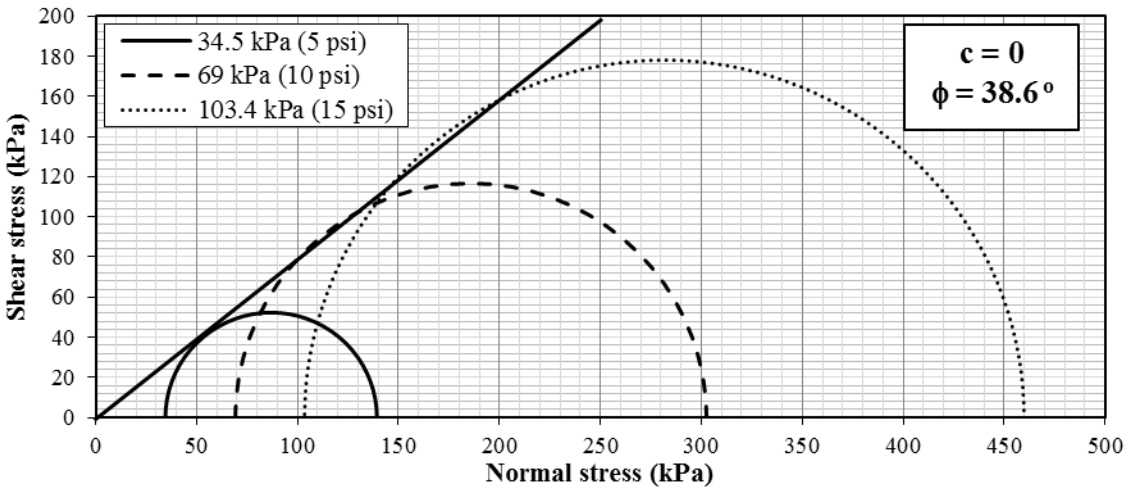

Figure 3.9 Peak strength parameters of ordinary sand columns

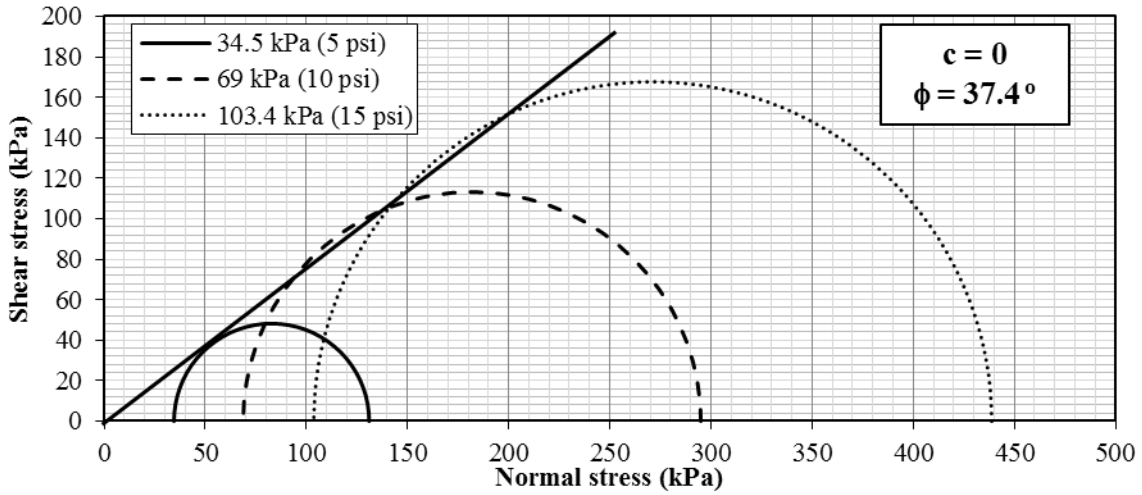

Figure 3.10 Residual strength parameters of ordinary sand columns

The shear stress-normal stress relationship for geotextile encased sand columns showed that the inclusion of geotextile encasement not only introduced an intercept, or an apparent cohesion, to the shear strength parameters, but it also caused the friction angle of the column to increase to a value greater than even the peak friction angle of ordinary sand columns, as shown in figures 3.11, 3.12, and 3.13. Bathurst and Karpurapu (1993) pointed out that the contribution to the shear strength due to the inclusion of geocell, which is simlar to geosynthetic encasement, can be expressed as equivalent or apparent cohesion.

Shear strength parameters for the GESC increased as the axial strains became higher. For instance, the angles of internal friction and apparent cohesions corresponding to 2%, 5%, and 10% axial strains were 39.2^{o} and 20 kPa, 47^{o} and 80 kPa, and 53.5^{o} and 120 kPa, respectively. Since there were no definite peak strengths for the encased sand columns and they supported higher deviatoric stresses as the axial strains increased, it is convenient to define the shear strength parameters in accordance with the level of axial strain used in design.

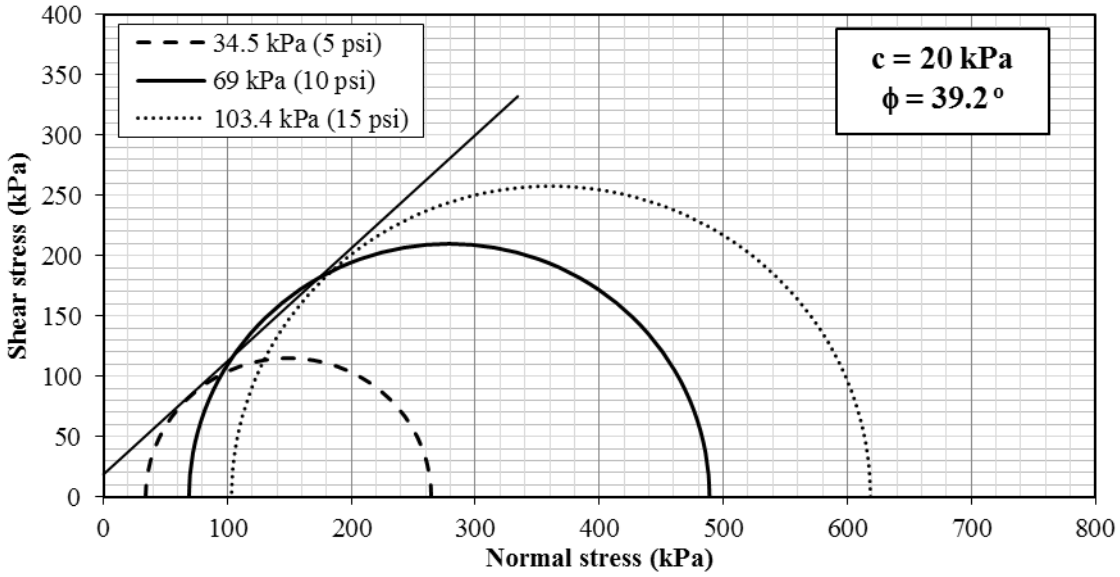

Figure 3.11 Strength parameters of geotextile encased sand column at 2% axial strain

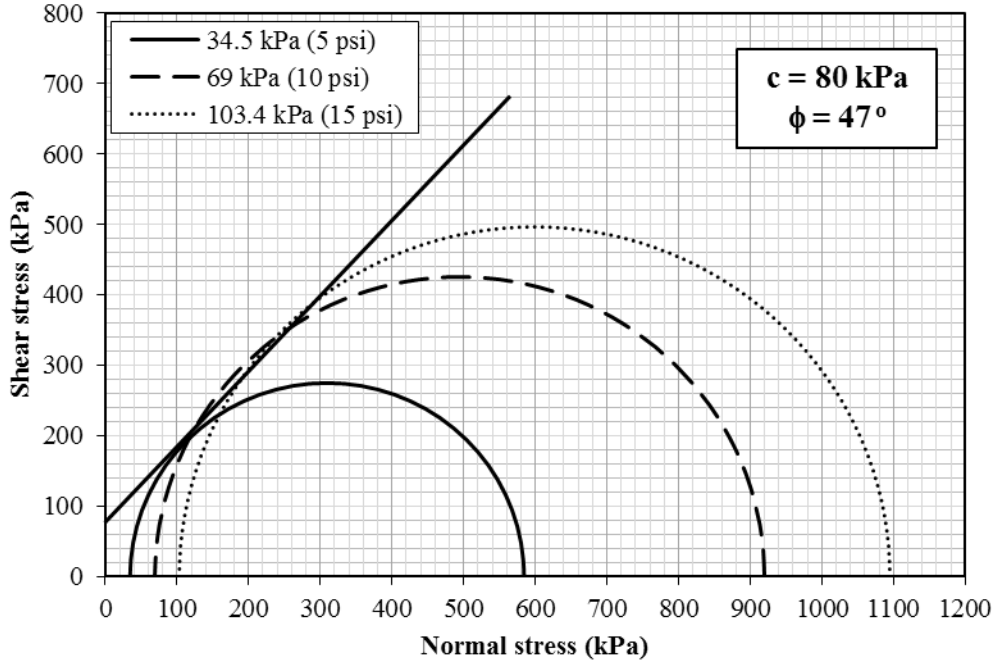

Figure 3.12 Strength parameters of geotextile encased sand column at 5% axial strain

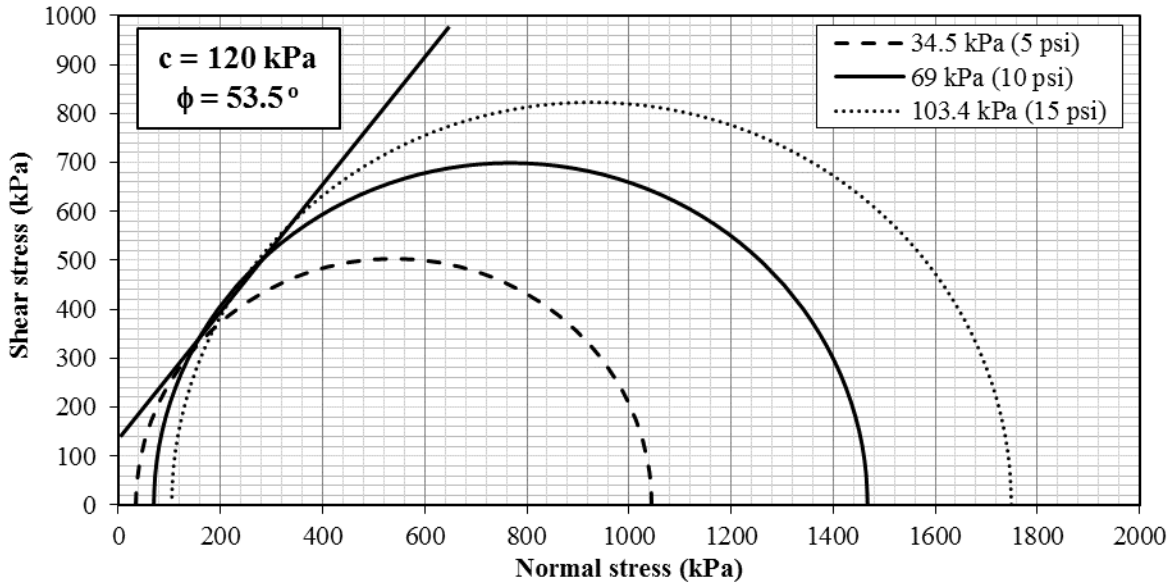

Figure 3.13 Strength parameters of geotextile encased sand column at 10% axial strain

3.3 The Influence of Geotextile Encasement on Shear Strength

A great deal of effort has been expended by previous researchers to simulate the effect of the geosynthetic encasement on the shear strength of GESC. The effect of the additional confinement provided by geocell due to the membrane action in the conventional triaxial test was adopted by Henkel and Gilbert (1952). It was hypothesized that the additional confining pressure of geosynthetic encasement can be expressed as follows:

$$\Delta\sigma_3 = \frac{2\,J\,\varepsilon_c}{d\,(1-\varepsilon_a)} \tag{3.2}$$

$$\varepsilon_c = \frac{\left(1-\sqrt{1-\varepsilon_a}\right)}{1-\varepsilon_a} \tag{3.3}$$

where $\Delta\sigma_3$= the additional confinement pressure due to encasement, (kPa), J = geosynthetic stiffness, (kN/m), ε_c = circumferential strain, d= geosynthetic encased column diameter, and ε_a = axial strain. Bathurst and Karpurapu (1993) pointed out that the enhanced strength due to the inclusion of geocell can be expressed as equivalent or apparent cohesion:

$$c_r = \frac{\Delta\sigma_3}{2} \tan\left(\frac{\pi}{4} + \frac{\phi}{2}\right) \quad (3.4)$$

where: c_r = apparent cohesion, kPa and ϕ = the friction angle of stone column.

Due to the presence of a seam in geotextile tubes, the tensile strength of the geotextile sleeve with a seam would be lower than that of without a seam. Therefore, in order to account for the seam effect, the tensile strength was reduced by 50% to that of the geotextile without a seam. Han (2015) stated that the ratio of the tensile strength of the geotextile with a seam to that without a seam is within a range of 50-70%.

A comparison was made between the computed apparent cohesion from the equation proposed by Bathurst and Karpurapu (1993) and the triaxial test results of this study as shown in Fig. 3.14. The apparent cohesion was determined from the results of this study by fitting a failure envelope with a slope equals to 38.6^o (i.e. the peak friction angle of sand) to Mohr circles drawn for each axial strain value. The intersection of the failure envelope with the y-axis represented the apparent cohesion. This procedure was performed to obtain the apparent cohesions for three different axial strains: 2, 5, and 10%. The apparent cohesions were 50, 160, and 300 kPa corresponding to 2, 5, and 10%, respectively. The apparent cohesions corresponding to three different axial strains (i.e. 2, 5, and 10%) were calculated using Bathurst and Karpurapu (1993) equation. As mentioned previously in this section, the values of tensile strength were reduced to half of that provided from the manufacturer stripe-tensile test due to the seam effect. The calculated apparent cohesions were 94, 224, and 398 corresponding to 2, 5, and 10%, respectively. Therefore, the results of triaxial compression tests performed on GESC are in a good agreement with the results computed from Bathurst and Karpurapu (1993) study as shown in Fig. 3.14.

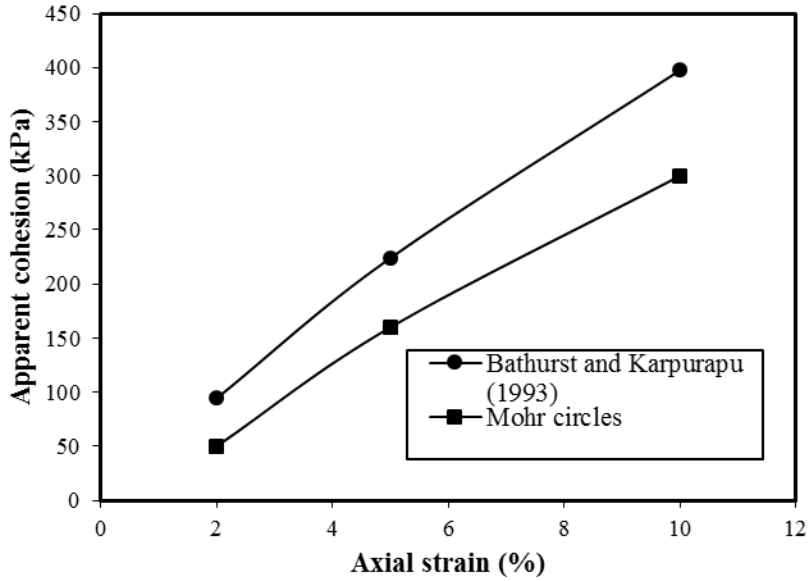

Figure 3.14 Apparent cohesion versus axial strain

3.3 Summary

Laboratory tests were conducted on the sand column material as well as the geotextile material used to form the geotextile sleeves. Consolidated drained triaxial tests were performed on both OSC and GESC to obtain the shear strength parameters of columns and to quantify the contribution of geotextile encasement to the performance of sand column. The results showed that geotextile encasement enhanced the shear strength of the sand column through providing an apparent cohesion and increasing the friction angle even beyond the peak friction angle of OSC.

CHAPTER 4

VERTICAL STABILITY OF GEOTEXTILE ENCASED SAND COLUMNS: EXPERIMENTAL WORK

4.1 Background

Regardless of the material used to construct a column, there are two main instances in which a column may buckle: when the column penetrates a soft soil deposit and for the case of long and slender columns (Han and Frost, 1999). For these circumstances, the column bends and deforms laterally under axial compressive load to the point at which an excessive lateral deformation happens for a small additional load increment. Buckling failure of a column occurs suddenly when the applied load reaches the critical load, and for this reason this type of failure is considered catastrophic. This chapter addresses the vertical stability of encapsulated sand columns. Individual geotextile encased sand columns were tested first with no confinement (in air) to simulate the worst case scenario of a very soft clay deposit. They were then tested with low confinement provided by loose sand surrounding the column, because in reality soil conditions may lie in between those two cases.

4.2 Buckling Tests in Air

The following section presents the testing procedure and results for woven geotextile encased columns with no confinement (in air):

4.2.1 Preparation of Geotextile Sleeve

As mentioned in the previous chapter, prefabricated woven geotextile tubes were used throughout this research. Those geotextile tubes were stitched into three different diameters: 10, 15, and 30 cm, in order to conduct a parametric study by varying the size of geotextile tubes and the length to diameter ratios for each specific size of encased sand column. Length to diameter

ratios (L/D) of 2, 4, and 6 were used for all three diameters, except for the 30 cm geotextile sleeve size which was limited to L/D ratios of 2 and 4 due to testing device height limitations for a L/D ratio of 6. The geotextile sleeves were marked at a specified spacing to measure the diameter change (i.e. radial strain) and axial strain.

4.2.2 Sample Preparation

After cutting the geotextile tube to the desired length, its edges were sealed by placing the ends on a heater to prevent the unraveling of the geotextile. A margin of extra geotextile material was retained to account for fixing the bottom of the sample. A circular plate of the same diameter or slightly smaller than the size of the geotextile tube was inserted inside the geotextile tube in the bottom. Several rubber bands were placed around the bottom of the sample to secure the geotextile to the plate to prevent any gaps that might cause sand leakage. A hollow, relatively rigid plastic pipe was employed as a mold by cutting it into two halves and connecting one side with clasps; it was installed outside the geotextile tube. This mold was tightened around the geotextile tube with several hose clamps along its entire height to keep the sample vertical and straight. The weight of the mold along with the geotextile tube and base plate was recorded. Sand was then poured through a truncated cone into the geotextile tube in four layers, each compacted with an application of 40 blows using a steel rod. The height and weight of each layer was verified to achieve the targeted relative density of Dr = 70%. After the completion of sample preparation, the sample and mold were weighed together to verify the density of the sample.

4.2.3 Testing Procedure

Buckling tests were conducted by applying load increments to the loading plate through a 15 cm (6 inch) air cylinder with a pressure capacity of 900 kPa (130 psi) against a reaction frame for two GESC diameters: 10 and 15 cm. Meanwhile, short encased sand columns of L/D=2 for

both the 10 and 15 cm diameter columns were tested using the triaxial loading frame in the main laboratory at the University of Kansas. Because of the limited pressure capacity of the aforementioned air cylinder, buckling tests relevant to 30 cm GESC diameter were performed in the large box frame in the west campus soil laboratory at the University of Kansas. The sample inside the mold was mounted on the center point of the platform of the loading frame to avoid any loading eccentricity as shown in figure 4.1.

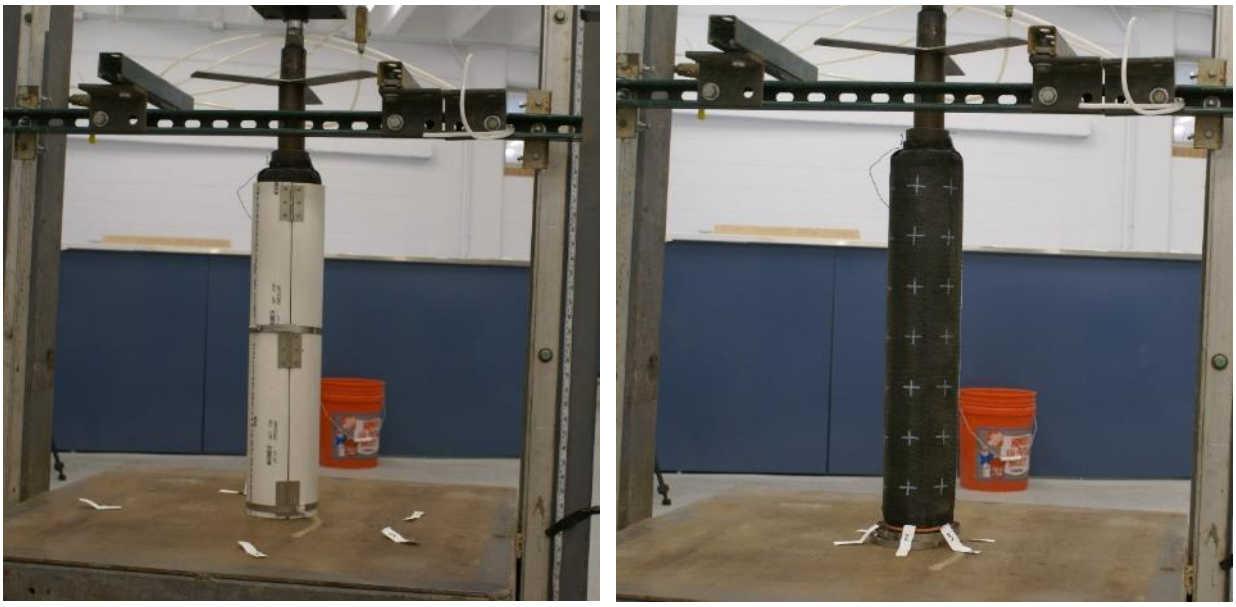

(a) (b)

Figure 4.1 Geotextile encased sand column: (a) inside the mold; and (b) After mold removal

Another circular plate designed to be equal in size to the diameter of the column (i.e. plate sizes: 10, 15, and 30 cm), was positioned at the top of the sample to distribute the load uniformly. The sample was pre-stressed to a relatively small pressure of around 20.7 kPa (3 psi) to hold the column after the removal of the mold. After fixing both ends, the mold was removed and cameras were fixed 2 m away from the sample to take photos of the sample at each loading increment. The photos were analyzed later using ImageJ software to determine the axial strains at the highlighted

markers along the height of the column. Three dial gauges were mounted at angles of 120º to measure the average settlement of the column's head at each loading increment. Before starting the test, initial perimeter readings were measured with a fabric tape for each location highlighted by cross marks along the column height. The test was conducted with equal pressure increments of 34.5 kPa (5 psi) or 69 kPa (10 psi) depending on sample capacity. The pressure was applied and maintained for 10 minutes before increasing to the next pressure increment. Perimeter measurements were taken along the height of the column after 7 minutes of load application. Photos and the average of the settlement readings was recorded from the dial gauges after maintaining the load increment for 10 minutes. The test was terminated and the sample was unloaded after failure of the column due to buckling, geotextile burst failure, or both. Figures 4.2 (a) and (b) show the GESC after failure and the burst failure at the seam for columns with L/D of 4 for columns with sizes of 10 and 15 cm, respectively.

4.2.4 Test Results and Discussion

Loading tests were conducted on three different groups of encased sand columns. The groups were labeled as groups A, B, and C corresponding to GESC diameters of 10, 15, and 30 cm. The same installation and preparation procedure was adopted as described previously. Length to diameter ratios of 2, 4 and 6 were tested within each group to investigate the buckling behavior.

4.2.4.1 Loading Test on Geotextile Encased Sand Columns

The settlement readings from three dial gauges were recorded for each loading increment. The averages of the settlement readings were plotted against the applied vertical pressure at the column head. Figure 4.3 depicts the results of loading tests conducted on groups A, B, and C with L/D ratios of 2, 4 and 6. Because of the high bearing capacities of short columns with a L/D of 2 for all groups, the loading tests were stopped after the settlements exceeded 10% of the column

length. However, for the columns with L/D=4 and 6 in groups A and B, loading tests were terminated after the columns experienced vertical stability failure due to excessive lateral deformations and geotextile failure of the seam by either bursting or stretching at that location. For L/D=4 of group C, the loading test was stopped after the sample reached a settlement at the column's head of close to 90 mm settlement.

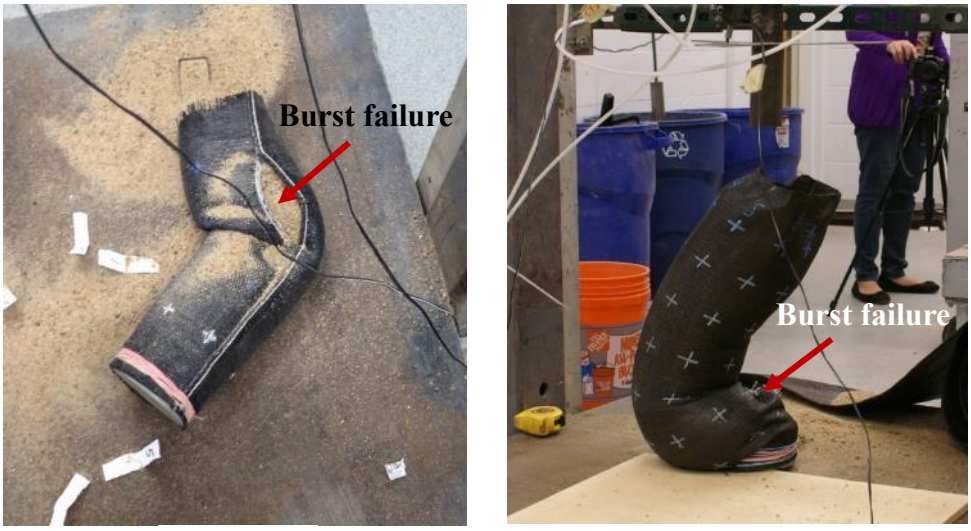

(a) (b)

Figure 4.2 GESC failure due to buckling and geotextile burst failure at seam for L/D=4: (a) 10 cm diameter; and (b) 15 cm diameter

Figure 4.3 (a) shows that the ultimate bearing capacities of geotextile encased sand columns corresponding to group A for a settlement of 10 mm (i.e. 10% of plate diameter) were 674 kPa, 407 kPa and 252 kPa for L/D = 2, 4 and 6, respectively. Therefore, the pressure on the top of the column for this amount of settlement with L/D =2 was 1.5 times that on the column of L/D=4, and 2.5 times that on the column of L/D=6.

Meanwhile, the bearing capacities for the geotextile encased sand columns of group B (see figure 4.3 (b)) were lower than those of group A, since increasing the size of the encased column

decreases the hoop tension force mobilized in the geotextile encasement and thus decreases the stiffness of the column and its bearing capacity. The ultimate bearing capacities for encased columns in group B at 15 mm (i.e. 10% of plate diameter) were 428 kPa, 264 kPa and 186 kPa for L/D ratios equal to 2, 4 and 6, respectively. The pressure applied on the top of the short column with a L/D=2 was 1.6 times that carried by the encased column with L/D=4, and 2.3 times the pressure on the column with L/D=6.

For the largest column diameter, Group C, as shown in figure 4.3 (c), the bearing capacities were even lower than those of group A and B for the same L/D ratio. The ultimate bearing capacities, taken at 30 mm (i.e. 10% of plate diameter), were 210 kPa and 124 kPa for L/D ratios equal to 2 and 4, respectively. The pressure on the encased column of this group with L/D=2 was 1.7 times greater than that carried by the column with L/D=4. The GESC of a L/D of 4 exhibited larger vertical settlements as the applied pressure increased on the top of the column.

With regard to encased sand columns of the same group (i.e. same size), shorter columns exhibited higher bearing capacities compared with longer ones because the vertical instability and excessive lateral deformation were more pronounced as the column length increased. Columns with larger diameters showed lower bearing capacities compared to those of smaller diameters since the geotextile hoop tension is inversely proportional to the column's diameter. In general, geotextile encasement typically failed at a seam.

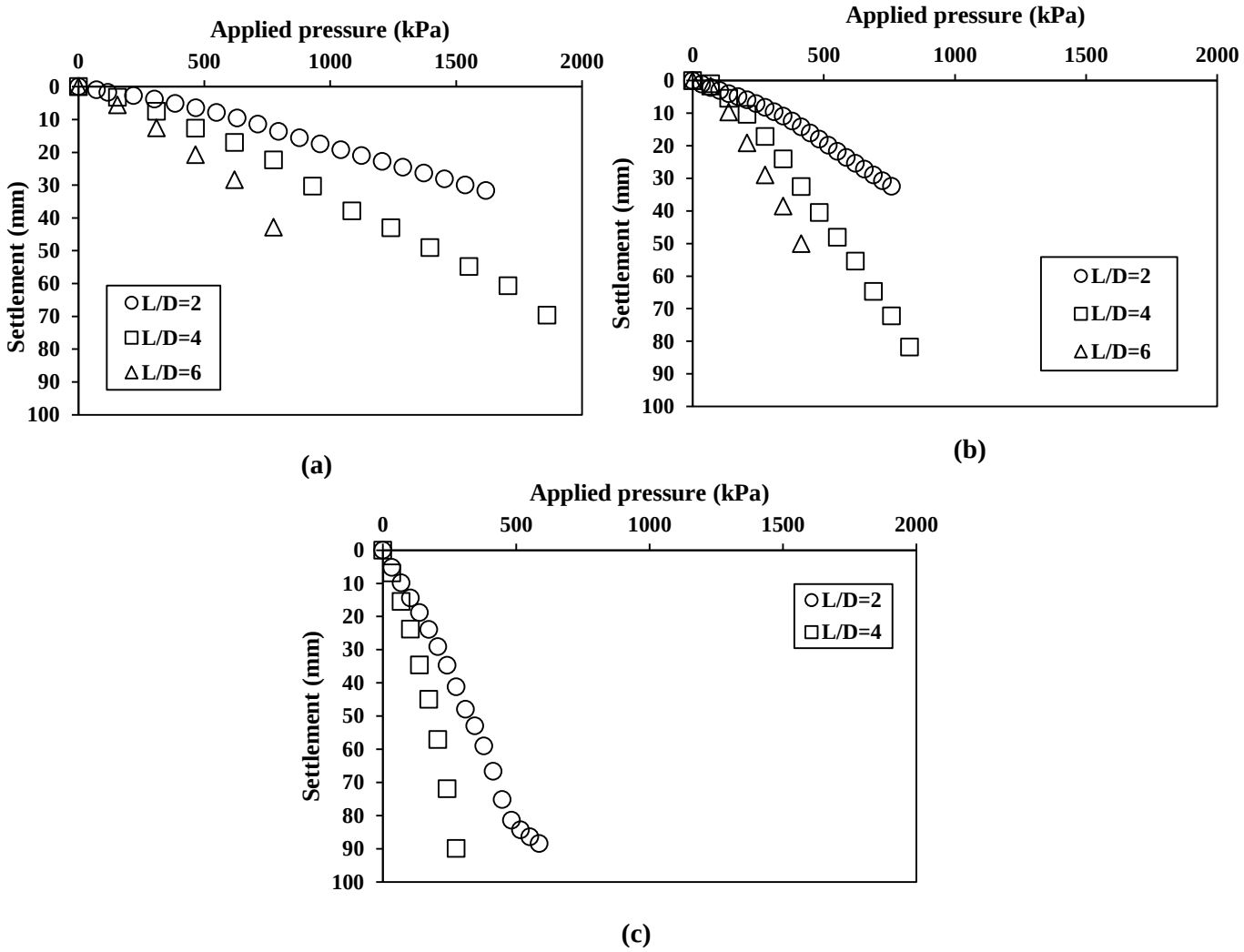

Figure 4.3 Vertical pressure-settlement curves of encased sand columns: (a) Group A; (b) Group B; and (c) Group C

4.2.4.2 Radial Strain Measurements

Because of the axial symmetry of the cylindrically-shaped encased sand columns, the circumferential strains of GESC were assumed to be the same as their radial strains (i.e. $\varepsilon_\phi = \varepsilon_r$). The lateral deformations of GESC (i.e. bulging) were measured as the perimeter change taken after seven minutes at each load increment application along the column's height. Radial strain was calculated as the ratio of the difference in perimeter at each loading increment corresponding to

the reference perimeter (at zero pressure) to the reference perimeter. Figures 4.4, 4.5 and 4.6 depict the lateral deformations of GESC at the locations of the highlighted markers. The measured diameter after each load increment was labelled as D1, D2, ...etc for columns of group A, B, and C respectively.

Figures 4.7, 4.8 and 4.9 show the radial strains of GESC versus the ratio of the height measured from the top of the column to the diameter of column (Z/D) for column groups A, B, and C respectively. All groups of GESC showed an increase in the radial strain values with the increase of the applied pressure increments. The trend of the radial strains was relatively symmetrical for all encased sand columns installed in air.

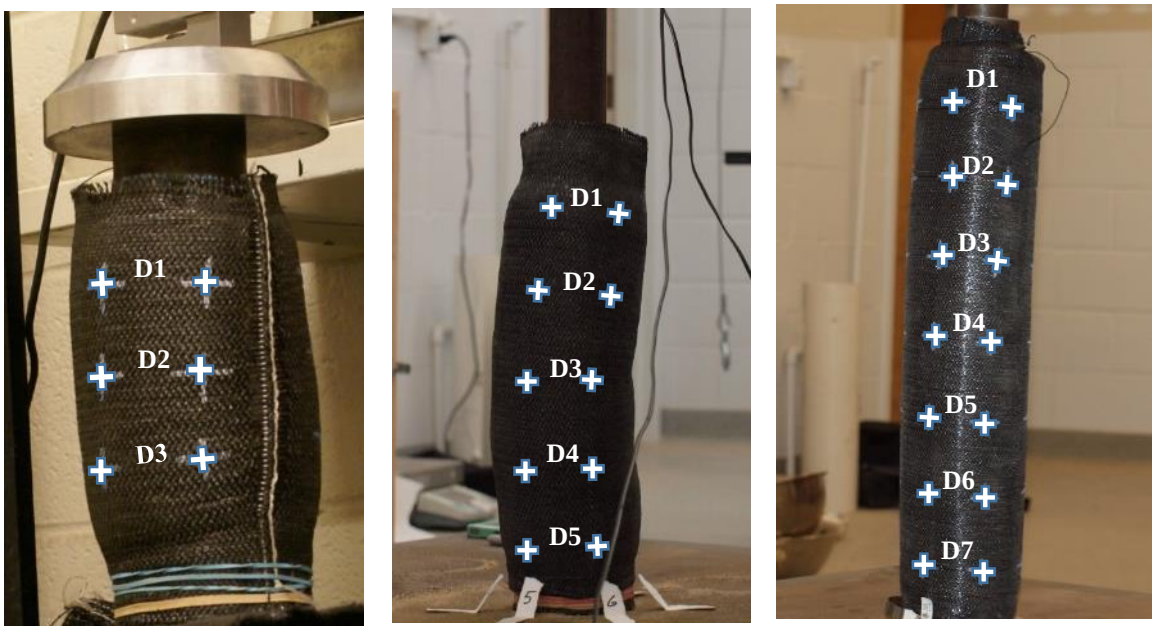

(a) (b) (c)

Figure 4.4 Lateral deformations along the column's length for group A: (a) L/D=2; (b) L/D=4; and (c) L/D=6

(a) (b) (c)

Figure 4.5 Lateral deformations along the column's length for group B: (a) L/D=2; (b) L/D=4; and (c) L/D=6

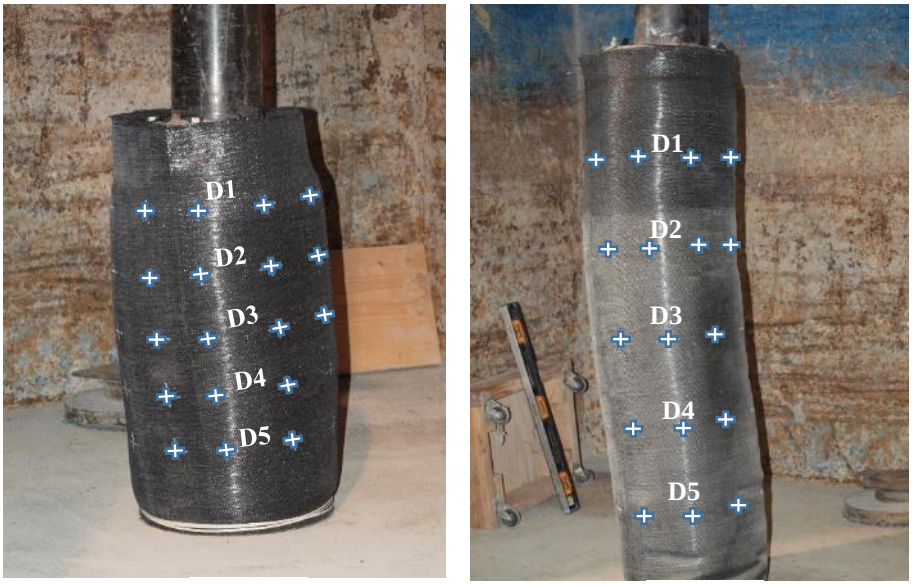

(a) (b)

Figure 4.6 Lateral deformations along the column's length for group C: (a) L/D=2; (b) L/D=4; and (c) L/D=6

For the shorter columns shown in figures 4.7 (a), 4.8 (a), and 4.9 (a) with L/D=2, it is apparent that the maximum values of lateral deformation (i.e. bulging) happened at a Z/D of 1 (Z/L = 0.5), and lower radial strains were observed at the top and the bottom of the column due to the friction effect between the soil and the base plates. The lateral deformations of columns with L/D=2 increased with the increase of the size of the column for the same applied pressure due to the lack of the confinement provided by the geotextile encasement for columns of larger diameters. For instance, at an applied pressure equal to 569 kPa, the radial strains for columns of group A, B, and C were 4.1%, 6.4%, and 12% respectively.

In contrast, for columns with L/D of 4, the effect of buckling was more pronounced throughout the entire height of the columns due to the columns' increased length. A repeated pattern of radial strain curves was apparent in figures 4.7 (b) and 4.8 (b) for the upper and lower halves of the column, similar to that for the columns with a L/D = 2, where for this case each half had a L/D of 2. The friction between the soil and the top and bottom plates decreased the radial strains at those locations. Columns in three groups (figures 4.7 (b), 4.8 (b), and 4.9 (b)) which have an L/D of 4, showed a necking shape close to their mid-height (Z/D=2) at which the lateral strain was less. Two peaks of radial strains were also observed: one in the upper portion of GESC and the other in the bottom. Geotextile burst failure at the seam occurred at the location of high radial strain, which corresponded to Z/D of 1.2 and 3.6 for columns in groups A and B. At 285 kPa applied pressure, the maximum radial strains occurred in the bottom part of the columns, 1.76% and 5% for columns having a L/D of 4 of groups B and C respectively. While for GESC of group C as shown in figure 4.9 (b), the maximum radial strain for L/D of 4 occurred close to the surface at Z/D = 0.67, which caused stretching signs to appear in the geotextile seam.

Longer columns had lower bearing capacities and mostly failed due to vertical instability and excessive lateral deformations before showing a definite sign of geotextile rupture at the seam. For longer columns with L/D=6, the maximum radial strain occurred at a Z/D of 4.6 and 2 for encased columns of group A and B, respectively.

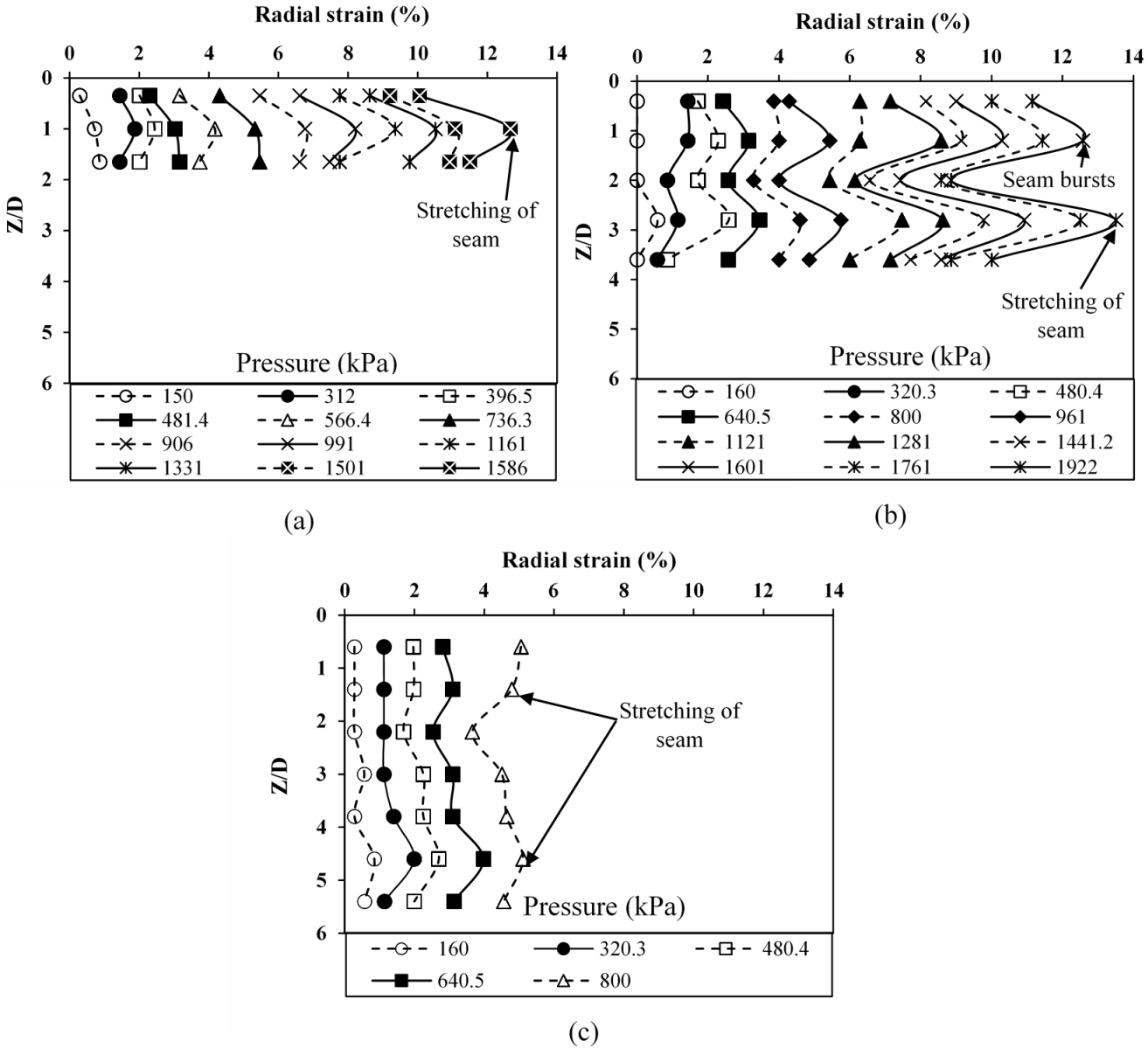

Figure 4.7 Radial strain versus Z/D for encased column of group A (a) L/D = 2; (b) L/D = 4; and (c) L/D = 6

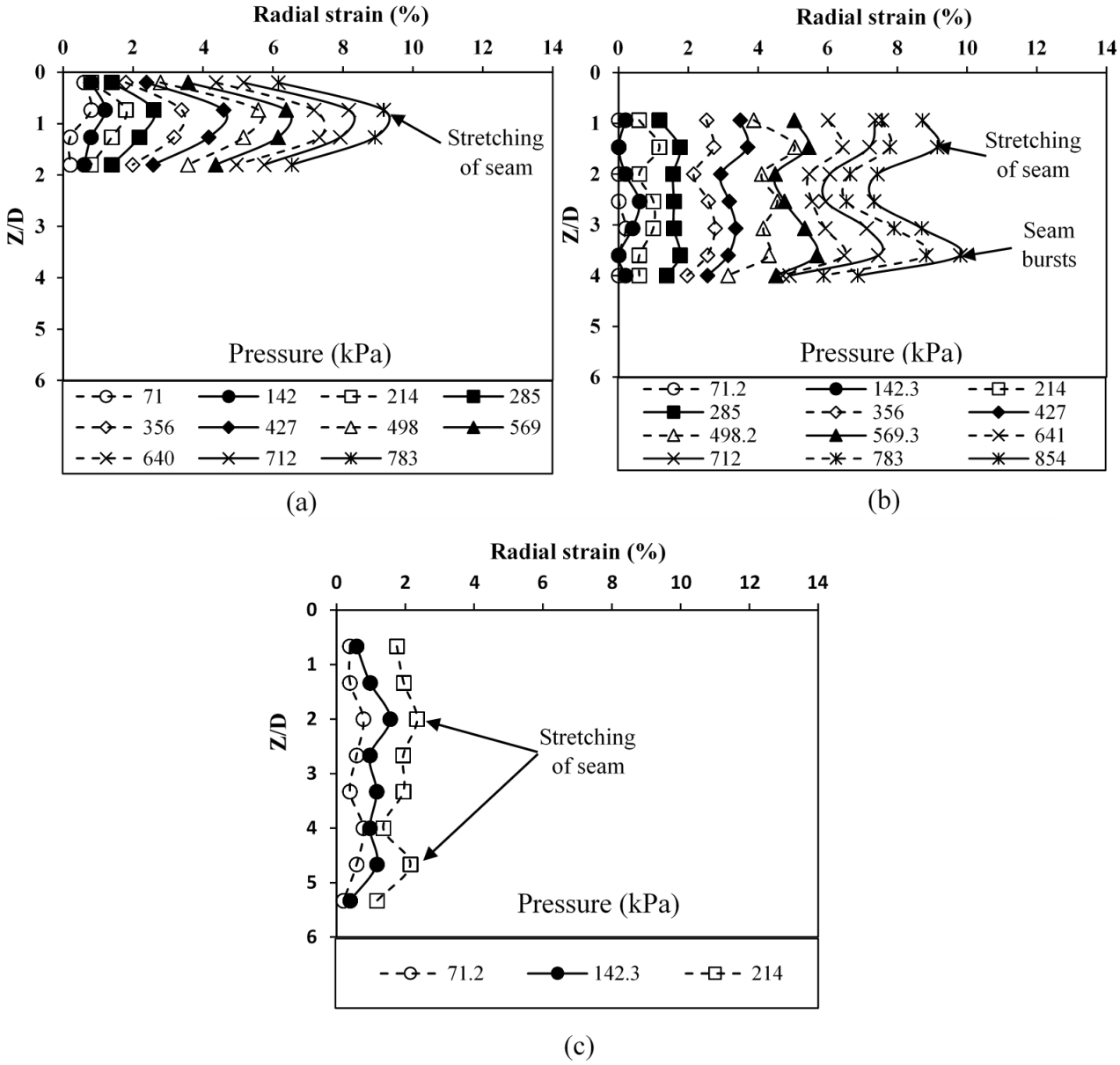

Figure 4.8 Radial strain versus Z/D for encased column of group B (a) L/D = 2; (b) L/D = 4; and (c) L/D = 6

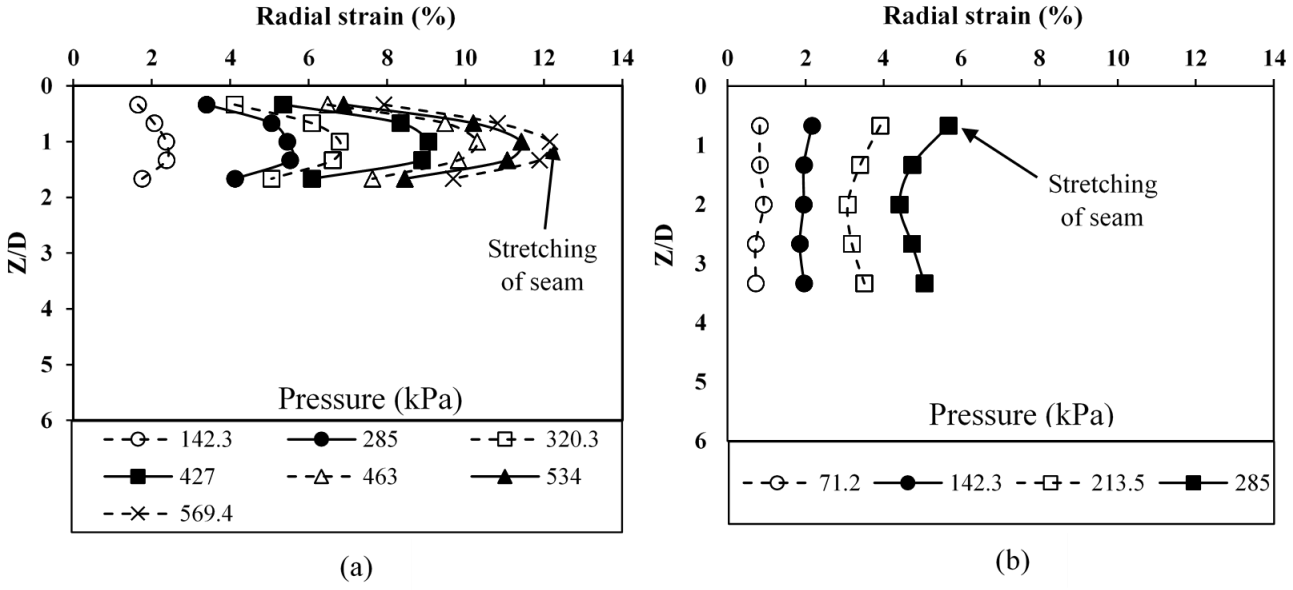

Figure 4.9 Radial strain versus Z/D for encased column of group C (a) L/D = 2; and (b) L/D = 4

4.2.4.3 Axial Strain Measurements

In addition to radial strain measurements, the axial strains (i.e. vertical strain) were also computed along the entire height of the columns at vertical zones located between two vertical grids marked on the geotextile sleeves. The axial strain at each loading stage was defined as the ratio of the change in length between the two vertical grids divided by the reference length. Images, taken after 10 minutes of each loading increment, were analyzed by ImageJ software to compute the axial strains of each column. Figures 4.10, 4.11 and 4.12 show the distribution of axial strains versus the ratio of the height measured from the top of column to the diameter of the column (Z/D) for groups A, B, and C. The calculated axial strains were found to increase along the entire column depth as the load increased, although to different extents.

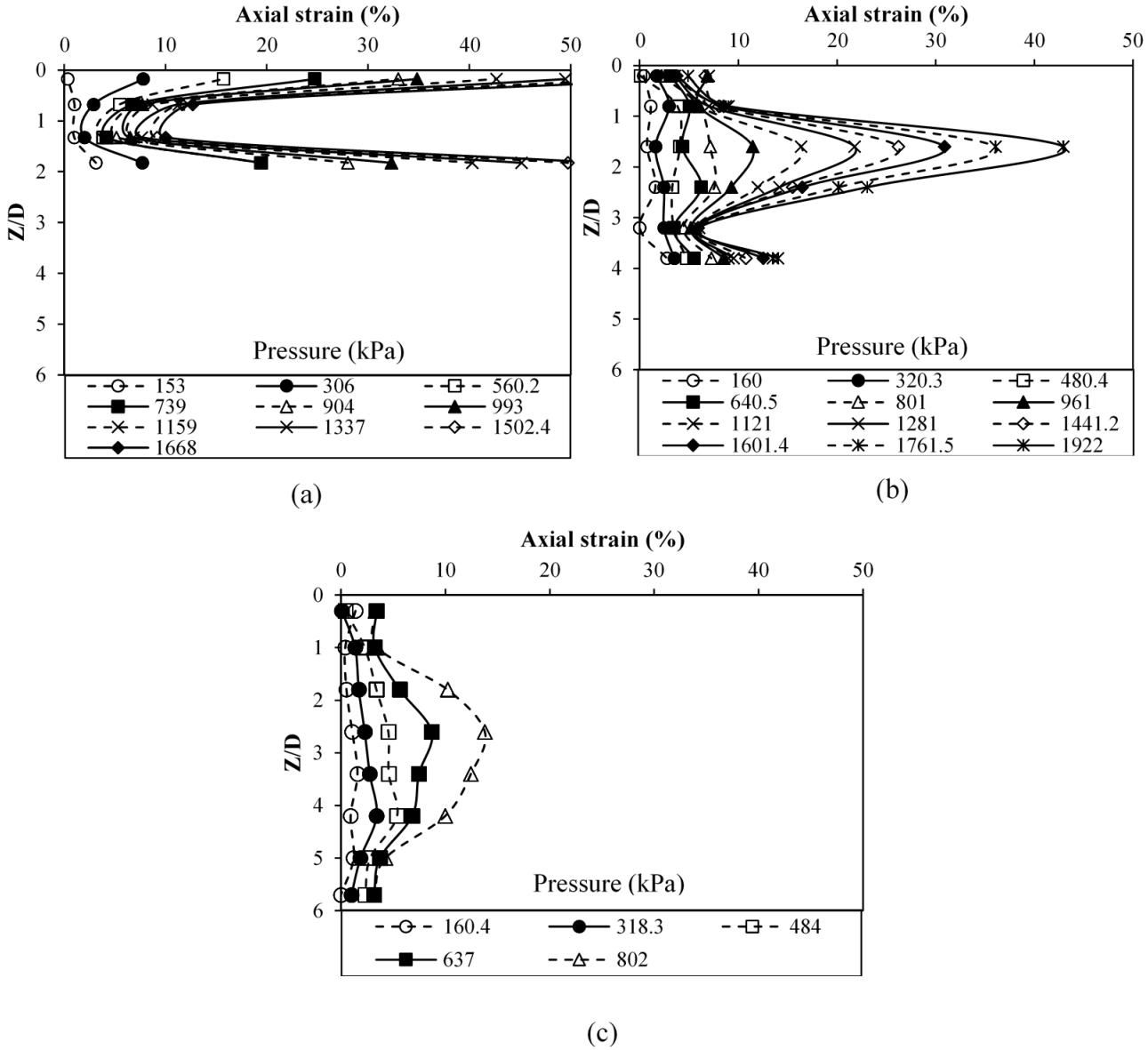

Figure 4.10 Axial strain versus Z/D for encased sand columns of group A: (a) L/D=2; (b) L/D=4; and (c) L/D=6

For shorter columns with a L/D of 2, columns appeared to exhibit higher axial strains in both the top and bottom portions and lower axial strains in the middle, as shown in Figs. 4.10 (a), 4.11 (a), and 4.12 (a). This was because the images were taken from the outside of the GESC and did not capture the vertical settlement of sand inside the geotextile encasement as there was some

slippage between the geotextile sleeve and infill soil. For GESCs of group A, the maximum axial strain happened at Z/D of 1.6 for L/D=4 as shown in Fig. 4.10 (b) due to excessive lateral deformation of the column (i.e. buckling), which influenced the pattern of vertical settlements at this location. However, the maximum axial strain occurred at a Z/D of 2.6 for the L/D=6, which corresponded to a higher vertical settlement observed at this location (Fig. 4.10 (c))

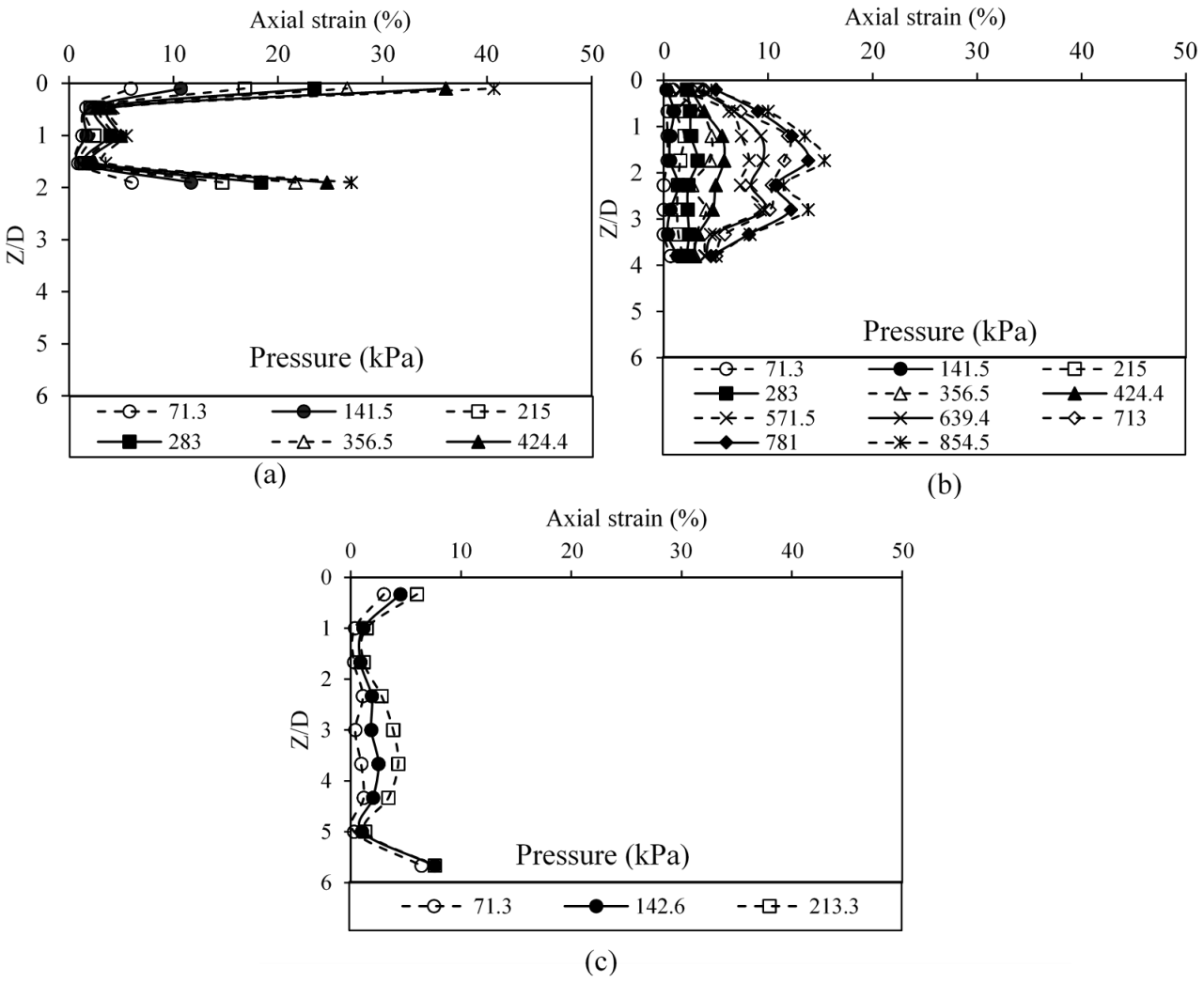

Figure 4.11 Axial strain versus Z/D for encased columns of group B: (a) L/D=2; (b) L/D=4; and (c) L/D=6

The shape of column buckling affected the trend of axial strain curves for columns of group B. It was observed that the maximum buckling happened at Z/D of 1.7 and 2.8 for a L/D of 4 as shown in Fig. 4.11 (b), and this resulted in higher axial strains at those two locations. Symmetric relationships were observed for columns with a L/D of 6 but the behavior still is not clear since this column's L/D ratio cannot support higher loads due to buckling failure (i.e. vertical instability) at early loading stages.

The trend of axial strain curves for GESC of group C with L/D ratios of 2 and 4 were similar to Groups A and B. Higher axial strains were observed at the top and bottom of the column and lower axial strains in the middle due to the shape of the lateral deformations (i.e. buckling) along the column's length that made some locations settle vertically more than other zones. For instance, at an applied pressure of 284 kPa on the GESC of group C, the column with a L/D=4 delivered higher axial strain (i.e. 28%) compared to the shorter column of L/D=2 (i.e. 19.4%) since the latter is more susceptible to buckling failure (see Fig. 4.12 (a) and (b)).

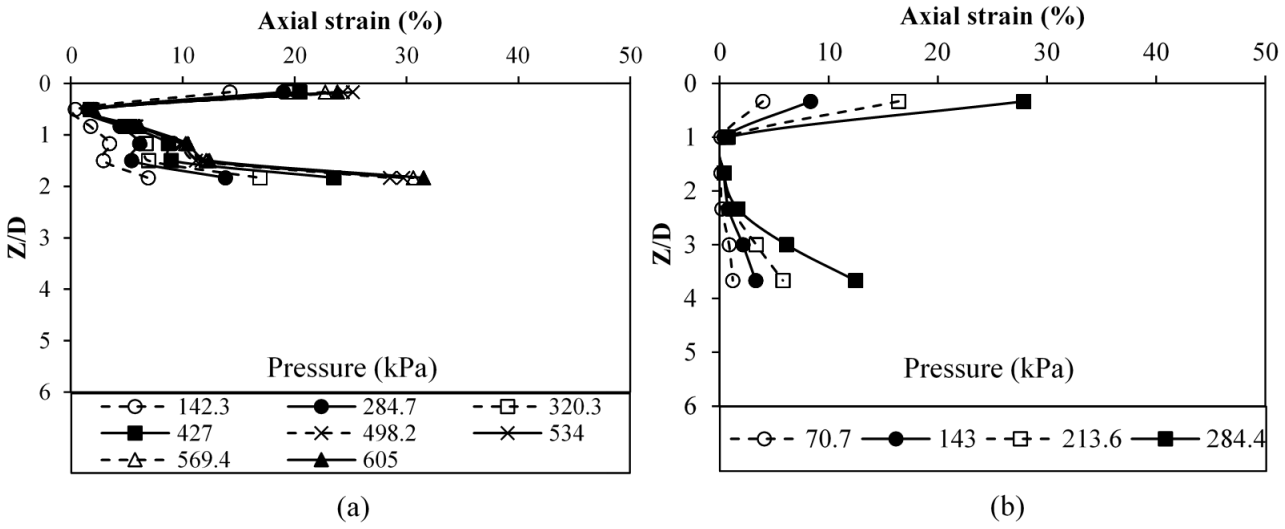

Figure 4.12 Axial strain versus Z/D for encased columns of group C: (a) L/D=2; and (b) L/D=4

4.3 Loading Test with Surrounding Soil

To evaluate the performance of geotextile encased sand columns, another series of loading tests was conducted to account for the effect of soil confinement on the capacity, radial strain, and axial strain of the encased sand columns as compared to those installed in air. Before starting the loading tests of encased sand columns surrounded by sand, a loading test was conducted on the loose sand bed used as a surrounding soil so the degree of improvement achieved on the bearing capacity of the foundation soil after the inclusion of geotextile encased sand columns could be evaluated.

4.3.1 Loading Test Procedure for Loose Sand Bed

To assess the degree of improvement in bearing capacity obtained after the inclusion of geotextile encased sand columns, a loading test on a loose sand bed was performed in the main soil laboratory at the University of Kansas using a 15 cm (6 inch) air cylinder. A cylindrical, Steel-Reinforced High Density Polyethylene (SRHDPE) pipe, the inner diameter and height of which were both 60 cm (24 inch), was first placed around the center point of the loading frame platform as a rigid boundary. The inner surface of the SRHDPE pipe was considered smooth enough to minimize any potential friction created between the surrounding soil and the inner surface of this pipe. Dry Kansas River sand was poured into the pipe from a low height using a scoop to obtain a loose sand with a relative density of 30%, and sand was added up to the height of 60 cm (24 inches). A 15 cm (6 inch) loading plate was chosen to perform the test so that the size of the rigid boundary was four times the plate size (see figure 4.13 (a)). The settlement readings were recorded from three dial gauges mounted at a spacing angle of 120^{o}. Figure 4.13 (b) shows the excessive settlement that occurred at the loading plate location.

(a) (b)

Figure 4.13 Loading test for loose sand: (a) Test set up; and (b) Sand displacement at surface

4.3.2 Material and Sample Preparations for Geotextile Encased Column Samples

The preparation of the geotextile tube followed the same procedure used for encased sand columns in air. To determine the radial strain at various depths, steel wires were mounted around the perimeter of the woven geotextile tube and stitched loosely at certain locations to keep the steel wires from moving away from their positions. From the same selected depths, other steel wires were affixed and extended vertically to measure the axial strains (i.e. vertical strains). To prevent friction between steel wires and loose surrounding soil, the wires were inserted inside a plastic hose that was stitched to the geotextile tube along the vertical direction starting from the desired depth. It had been verified that steel wires moved freely inside the plastic tubes. The same Kansas River sand used for column backfill material was prepared in a dry condition and compacted to

30% relative density to get a loose surrounding soil. While it would have been preferable to use a saturated soft clay bed as a surrounding soil, that would have taken an extensive period of preparation incompatible with the time available for this testing program. Mohapatra et al. (2014) also used dry sand as a surrounding soil instead of soft clay. A SRHDPE pipe of an inner diameter of 60 cm was utilized as an outer boundary.

4.3.3 Loading Test Procedure of Geotextile Encased Sand Columns with Surrounding Soil

All loading tests for this group were conducted in a large geotechnical box with planar dimensions of 2.2 m x 2.0 m x 2.0 m high in the west campus soil laboratory at the University of Kansas. Figure 4.14 shows the loading test set-up with detailed instrumentation. Figure 4.15 depicts the step by step procedure used to prepare the sample with surrounding soil. First, the sample of woven geotextile encased sand column was prepared inside a mold to a targeted relative density of 70% and placed at the center point of the large-scale box, which was determined by a laser tape to avoid any loading eccentricity. A SRHDPE pipe with a 60 cm inner diameter was set around the center of the prepared encased sand column sample to provide a rigid boundary (see Fig. 4.15 (a)). Kansas River sand was backfilled into the SRHDPE pipe around the sample in a loose state to simulate a soft soil condition as shown in Fig. 4.15 (b). To obtain the 30% relative density condition, sand was poured using a scoop from a very low height. Sand was added up to a height of 30 cm (1 ft) from the bottom of the SRHDPE pipe. The mold was raised approximately 23 cm (9 inches) and the process was repeated until the entire pipe was filled (see Fig. 4.15 (c) and (d)). Steel wires were also used for radial strain measurements and were installed around the column and then inserted inside the same type of plastic tubes used for the vertical wires from the periphery of the column sample to the inner boundary of the rigid pipe to minimize the potential friction between the soil and steel wires (see Fig. 4.15 (c)). Radial steel wires penetrated through

holes made at the same depths on the boundary pipe and extended outside the pipe where they were attached to rubber bands that acted as springs to hold the wire tight but still provide free movement. The recorded weight of the buckets of sand poured into the rigid pipe combined with the known volume of the pipe were used to calculate the relative density of the sand bed. The mold then was pulled up to a height of 30 cm (1 ft) and this procedure was repeated until the sand reached the same level of the soil inside the geotextile tube as shown in Fig. 4.15 (d) and (e). This was done to keep the sample vertical and straight. All horizontal and vertical wires were attached to rubber bands, which in turn were fixed into a wooden board (see figure 4.14).

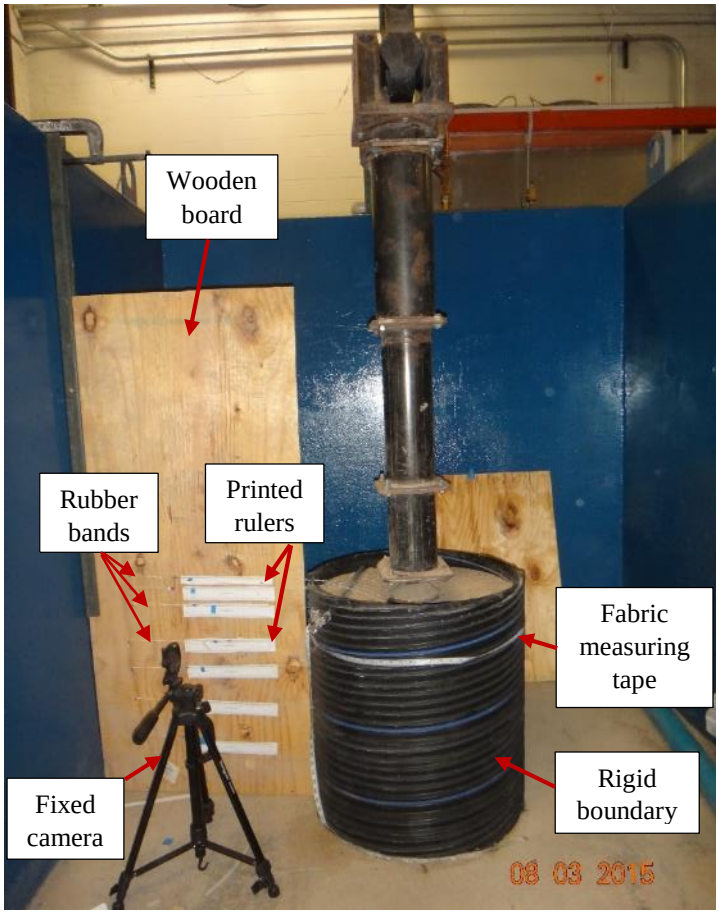

Figure 4.14 Loading test set up with surrounding soil

For vertical wires, a smooth steel rod was mounted on the surface of the surrounding soil away from the loading plate to transfer the direction of the wires towards the wooden board (see Fig. 4.15 (f)).

(a) Placing the sample and SRHDPE pipe at center of testing box

(b) Filling the soil around the sample

(c) Inserting horizontal steel wires inside plastic tubes

(d) Filling the surrounding soil while lifting the mold up

(e) Leveling the surrounding soil with the soil inside geotextile tube

(f) Using a smooth steel rod to transfer the direction of vertical wires

Figure 4.15 Preparation procedure of a geotextile encased sand column with surrounding soil

In order to measure the vertical and lateral deformations at specified depths, printed rulers were glued to the wooden board. A reference point was marked on each steel string to measure the movement that occurred from that point. Two cameras mounted on fixed tripods were used to take photos to capture the vertical and lateral movements after each load increment.

4.3.4 Test Results and Discussions

Two important issues were verified when conducting each test, the relative density of the surrounding soil and the validity of the rigid boundary. The range of the relative density of surrounding soil was found to be 26%-33%, which was consistent with a loose sand condition. The perimeter of the boundary pipe was measured at different loading stages during the test and no perimeter change was observed.

4.3.4.1 Loading Tests on Loose Sand and Geotextile Encased Columns with Surrounding Soil

Woven geotextile tubes with diameters of 15 and 30 cm corresponding to area replacement ratios of 6.25 % and 25%, respectively, were tested in this series. Three different length to diameter ratios; 2, 4, and 6, were adopted for the 15 cm diameter column and a L/D of 2 for the 30 cm diameter column. Figure 4.16 shows the benefit of the inclusion of geotextile encased sand columns in improving the bearing capacity of a loose sand foundation. The ultimate bearing capacity of loose sand based on deformation equal to 10% of the plate diameter (i.e. 15 mm) was 34.5 kPa, while the ultimate bearing capacities for 15 cm encased columns at 15 mm settlement (i.e. 10% of plate diameter) were 515, 346, and 281 kPa for L/D ratios equal to 2, 4 and 6, respectively. Therefore, the inclusion of a 15 cm diameter GESC with a L/D of 4 increased the bearing capacity of the composite foundation by a factor of 10 compared with the unreinforced foundation (i.e. loose sand bed). Whereas for 30 cm encased sand column, the ultimate bearing capacity corresponding to 10% of the plate diameter (i.e. 30 mm) was 830 kPa. Figure 4.16 also

illustrates that shorter columns had higher bearing capacities compared to longer ones. In addition, for the same length of encased columns, for instance L=60 cm, GESC that had a larger size (i.e. D=30 cm) exhibited higher bearing capacities compared with those of smaller size (i.e. D=15 cm), and this may be attributed to the boundary effect of the SRHDPE pipe on the 30 cm column. A comparison between bearing capacities of GESC with and without surrounding soil is illustrated in figure 4.17. Encased columns with soil confinement delivered higher bearing capacities than those in air at the same L/D ratios as shown in table 4.1. For instance, the pressures on the top of 15 cm diameter GESC with surrounding soil at settlements corresponding to 10% of plate diameter were 1.2, 1.3 and 1.5 times those on the GESC in air for L/D= 2, 4, and 6 respectively. Meanwhile, the pressure on the top of a 30 cm diameter GESC with L/D=2 installed in loose sand based on 10% of plate size was around 4 times that on the GESC of the same size installed in air. The enhanced bearing capacity of the 30 cm GESC was principally attributed to the boundary effect that contributed to higher confinement for this GESC when installed in a 60 cm diameter of the rigid boundary.

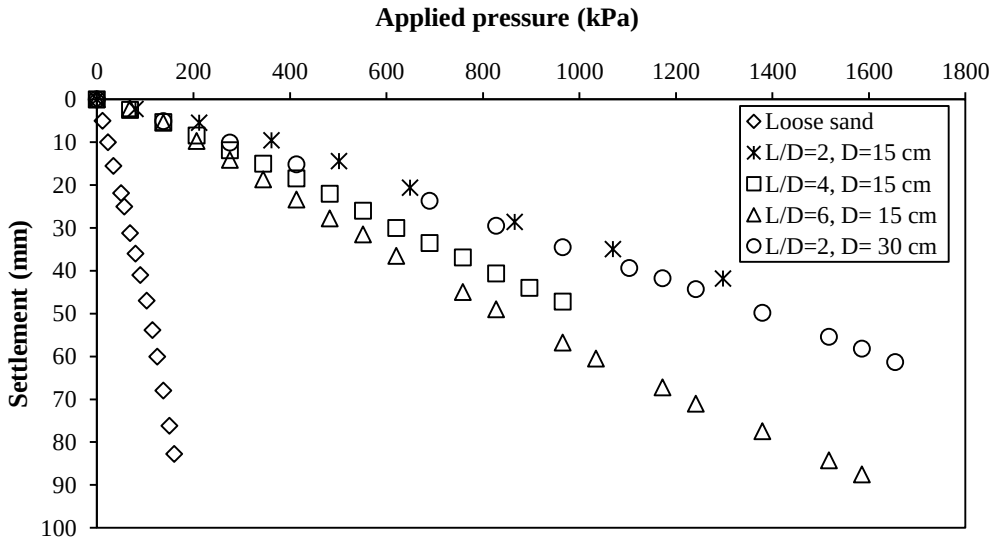

Figure 4.16 Vertical pressure versus settlement of GESCs with surrounding soil

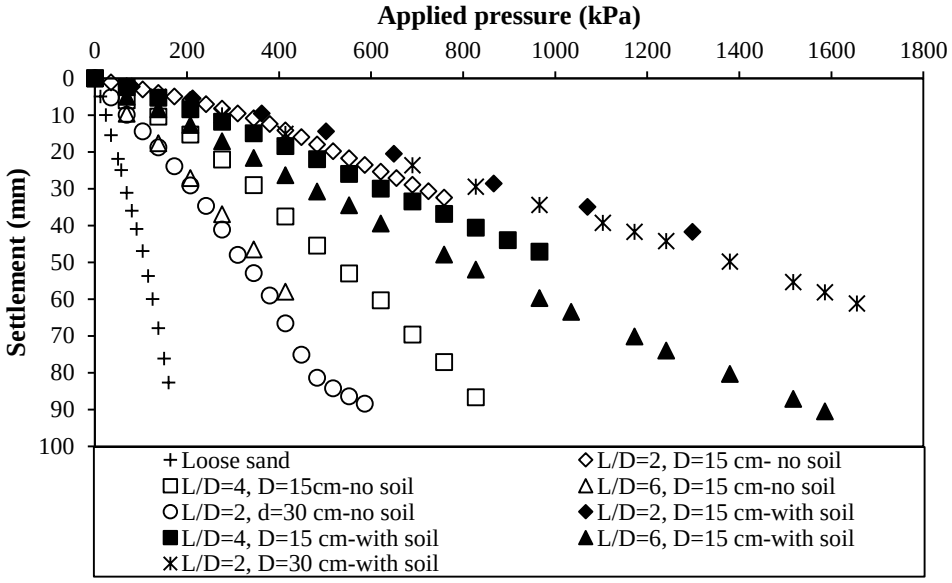

Figure 4.17 A comparison of bearing capacities of GESCs with and without surrounding soil

Table 4.1 Ultimate bearing capacities of GESCs in air and with surrounding soil in (kPa)

Diameter (cm)	GESCs in air			GESCs with surrounding soil		
	L/D=2	L/D=4	L/D=6	L/D=2	L/D=4	L/D=6
10	674	407	252			
15	428	264	186	515	346	281
30	210	124		830		

4.3.4.2 Radial Strain Measurements

Radial strain was measured as the ratio of the distance that the horizontal steel string traveled from a reference point to the perimeter of the column. Figure 4.18 shows the distribution of the radial strain according to the ratio of the height measured from the top of the column to the diameter of the column (Z/D) during different loading increments for a column diameter of 15 cm.

Radial strains of GESC installed in loose sand increased with the increase of the applied pressure on the column head. For different length to diameter ratios, the maximum radial strains

occurred at the top portion of the encased columns at which maximum bulging failure was observed. Lateral deformations decreased gradually with depth until they faded away close to the bottom of the column. The pattern of the radial strain for a L/D=2 (Fig. 4.18 (a)) was similar to that pattern of the encased column in air at the same L/D. For L/D=4 and 6, geotextile rupture happened at the point of maximum radial strain. For the 30 cm columns, the maximum radial strain corresponded to a Z/D of one-third (see figure 4.19).

Fewer lateral deformations were observed for GESC with surrounding soil as compared with GESC in air. For example, the maximum radial strain for a 15 cm diameter GESC having a L/D of 4 installed in air was 9.8%, while the maximum value was 5.7% for GESC installed in a loose sand bed with the same applied pressure (854 kPa) as shown in figure 4.20. Another comparison was made between the lateral bulging profiles of GESC installed in air and loose sand for 15 cm diameter columns with L/D=6 at 214 kPa applied pressure as shown in figure 4.21. It is clear from the data that the GESC in air showed higher radial strains with a maximum value of 2.3% while GESC in loose sand had a maximum lateral strain of 0.1% at the same applied pressure. In addition, the radial strain profile of GESC in air had two peaks whereas the maximum radial strain of GESC installed in loose sand occurred in the upper portion of the column.

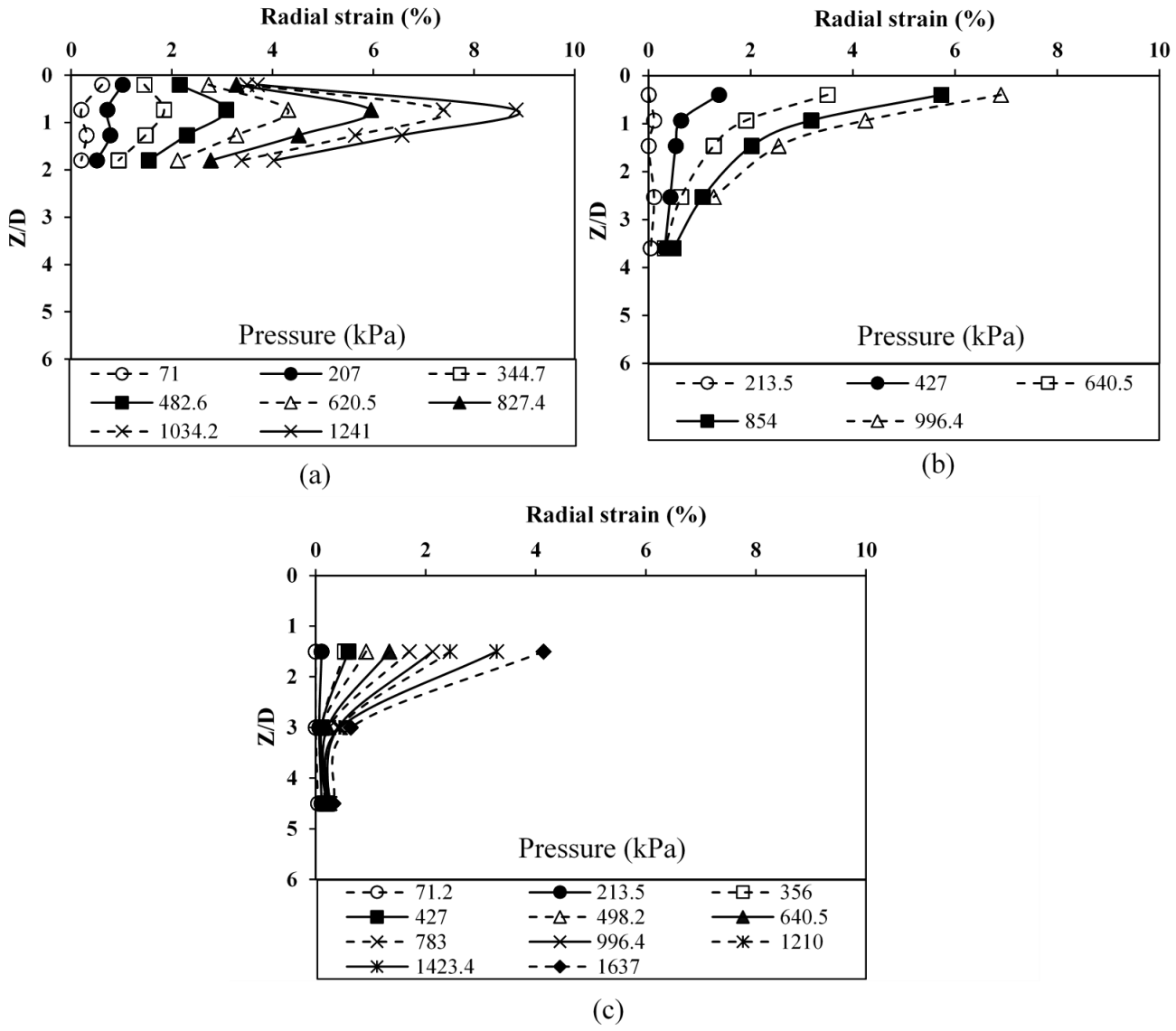

Figure 4.18 Radial strain versus Z/D ratio for 15 cm diameter encased column: (a) L/D = 2; (b) L/D = 4; and (c) L/D = 6

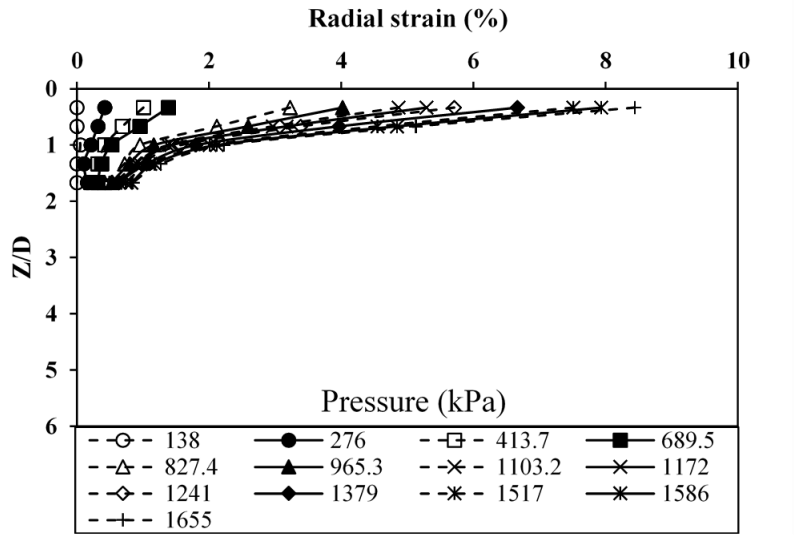

Figure 4.19 Radial strain versus Z/D ratio for 30 cm diameter encased column with surrounding soil (L/D = 2)

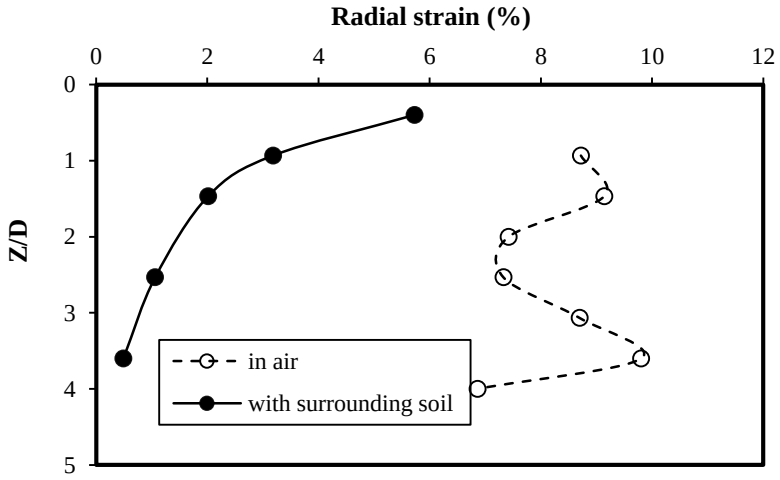

Figure 4.20 A comparison between the radial strains of a 15 cm diameter GESC with L/D=4 installed in air and with surrounding soil at applied pressure = 854 kPa

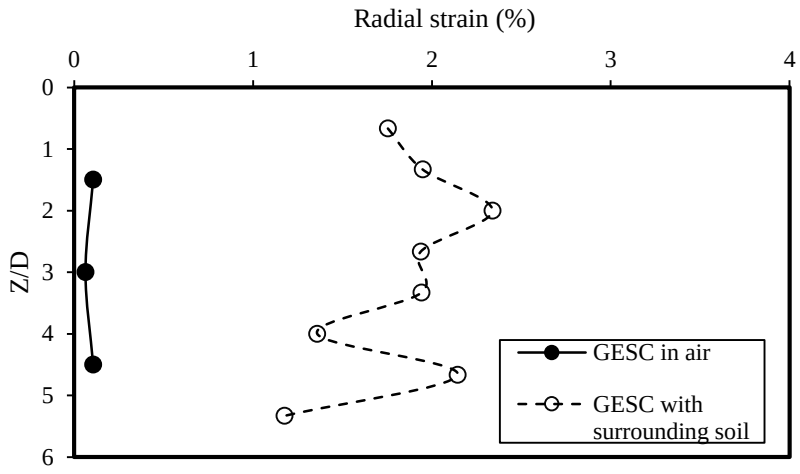

Figure 4.21 A comparison between the radial strains of a 15 cm diameter GESC with L/D=6 installed in air and with surrounding soil at applied pressure = 214 kPa

4.3.4.3 Axial Strain Measurements

As mentioned earlier, the vertical steel wires were extended from different depths to measure the deformations along the length of the column. The axial strain for a zone was calculated as the difference between the vertical settlements of the column at top and bottom of the zone divided by the length between those two points. In general, maximum axial strain was observed to occur in the top portion of the column as shown in figures 4.22 and 4.23. The observed settlement distribution along the length of the column showed a maximum strain in the top zone. Strain generally decreased with depth, although there were somewhat higher strain values in the bottom zones because the settlement of the bottom points of the columns at the base plate location was assumed to be zero, and that made the settlement difference a bit high in this zone. A comparison between the axial strain profiles for GESC installed in both air and in the loose sand bed is depicted in figures 4.24 and 4.25. In general, the axial strain distribution of GESC of 15 cm size in air exhibited two peaks in the middle for a L/D = 4 and a one peak located in the mid-height of GESC,

with relatively higher axial strains at both the top and bottom of the GESC with a L/D of 6, while GESC with surrounding loose sand showed a maximum axial strain close to the top of column. At 854 kPa applied pressure on the top of GESC with L/D of 4, the maximum axial strain for GESC without confinement was 15.4% at Z/D of 1.73, whereas the axial strain of GESC with surrounding soil was 25.4 % close to the surface at Z/D of 0.47, as shown in figure 4.24.

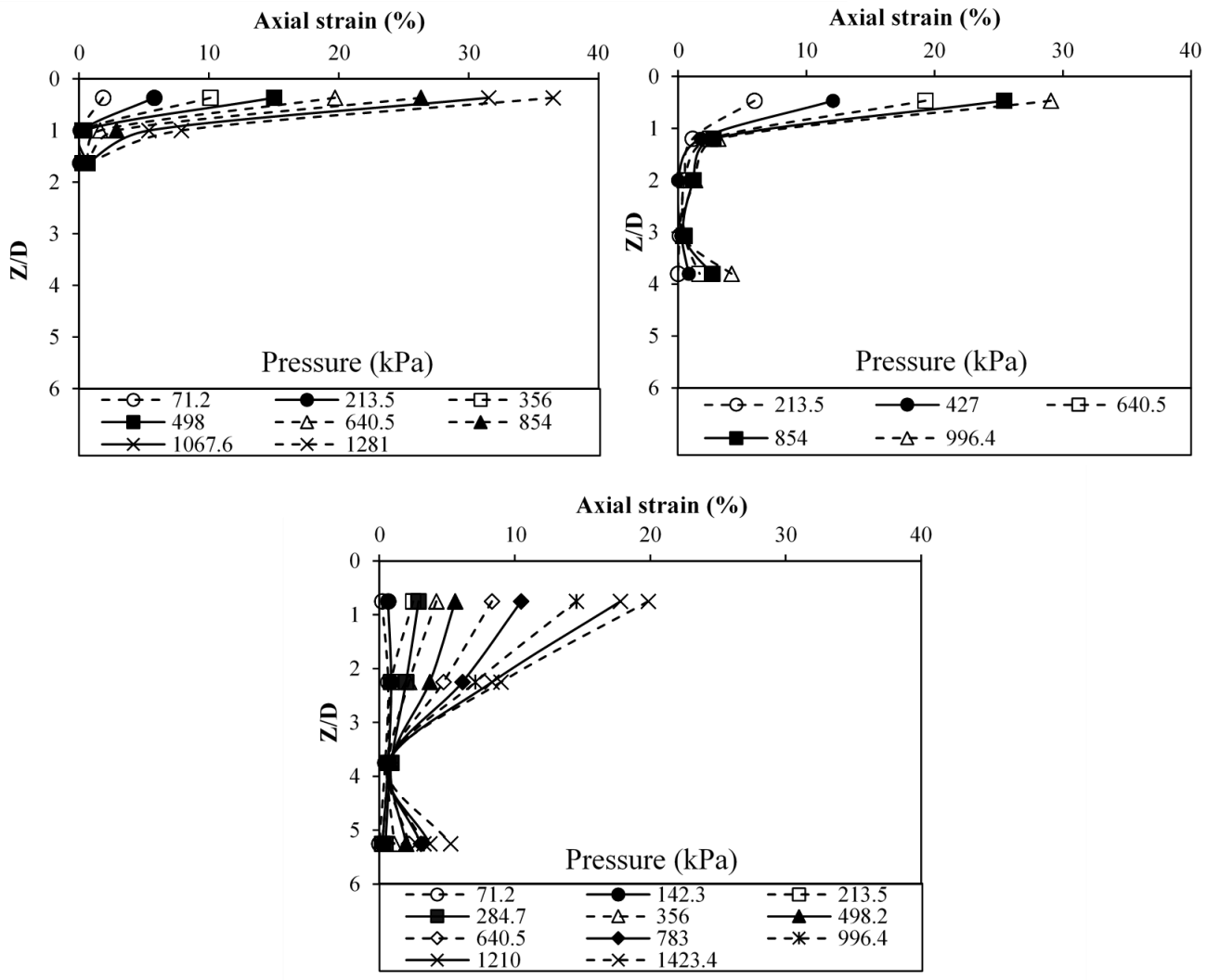

Figure 4.22 Axial strain versus Z/D ratio for 15 cm diameter encased column: (a) L/D = 2; (b) L/D = 4; and (c) L/D = 6

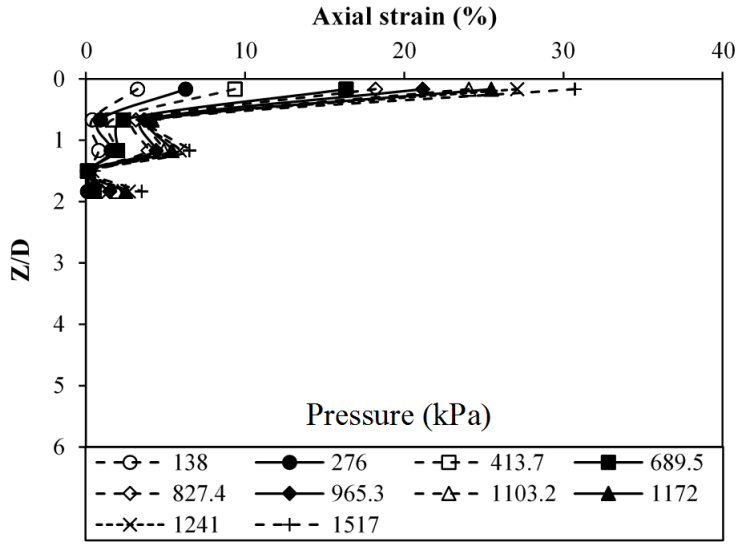

Figure 4.23 Axial strain versus Z/D ratio for 30 cm diameter encased column with surrounding soil (L/D = 2)

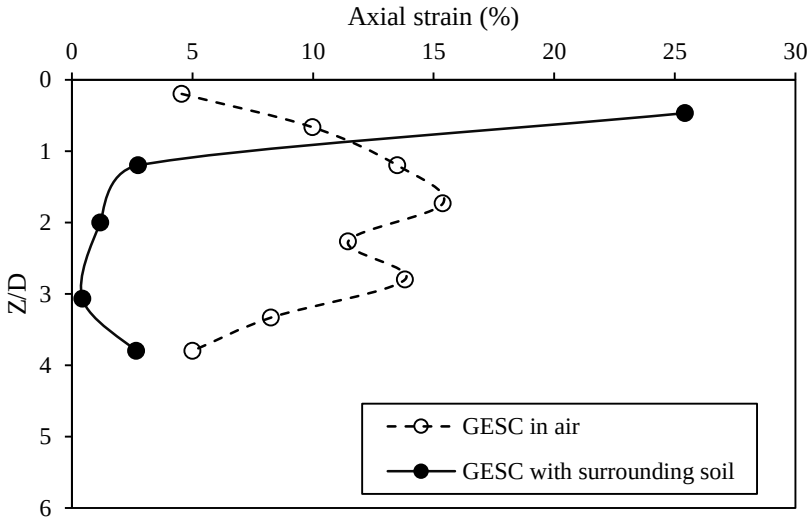

Figure 4.24 A comparison between the axial strains of a 15 cm diameter GESC with L/D=4 installed in air and with surrounding soil at applied pressure = 854 kPa

For GESC with L/D of 6, the maximum axial strain for GESC in air was 7.6% located at Z/D of 5.7 close to the base of the column, while the maximum axial strain of GESC in loose sand was 2.5 % at Z/D of 0.75 close to the surface at 214 kPa applied pressure.

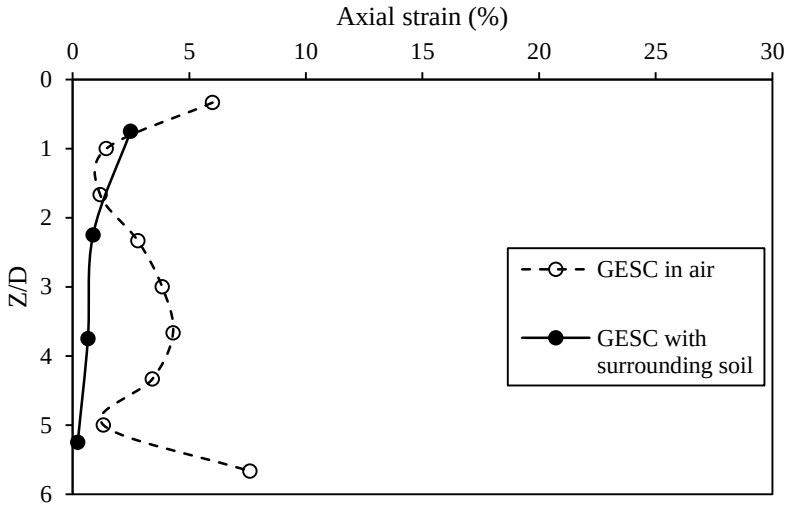

Figure 4.25 A comparison between the axial strains for a 15 cm diameter GESC with L/D=6 installed in air and with surrounding soil at applied pressure = 214 kPa

4.4 Strength Gain

The amount of strength gained by encased sand columns when surrounded by soil confinement is presented in figure 4.26. The strength gain percentage was computed as the ratio of the strength difference of an encased sand column with and without surrounding soil to the strength of the encased column in air. Longer columns benefited more from soil confinement than did shorter columns since longer columns are more susceptible to buckling failure (i.e. vertical instability). Also, columns of larger diameters delivered higher strength gains compared to smaller column sizes.

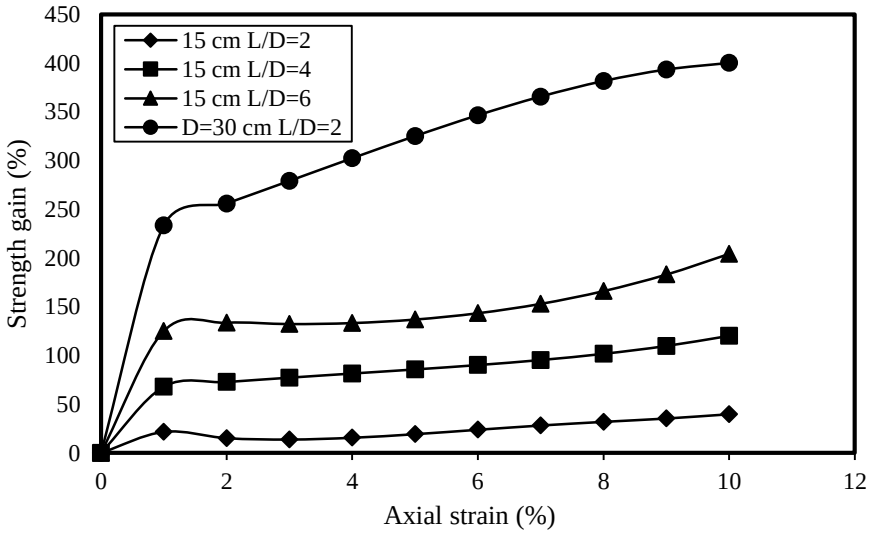

Figure 4.26 Strength gain due to surrounding soil confinement versus axial strain

CHAPTER 5

THREE DIMENSIONAL ANALYSIS OF GEOTEXTILE ENCASED SAND COLUMNS: NUMERICAL ANALYSIS

5.1 Introduction

A finite difference program, FLAC3D 5.01, was employed to perform three dimensional numerical analyses of an individual GESC with surrounding loose sand. First, parameter calibration was performed to obtain estimates of the properties of the infill soil and geotextile sleeve. Then, the numerical model was verified with the results of experimental load tests on the GESC, discussed previously in Chapter 4. For these experiments the individual GESC were surrounded with loose soil and loaded only on their top area. The numerical results matched well with the results of laboratory tests. A parametric study was then conducted using the model to investigate various parameters that may have a significant impact on the performance of GESC.

5.2 Numerical Modeling for GESC with Surrounding Soil

In order to create a three dimensional model of a GESC with surrounding soil, a commercial program, FLAC3D, which stands for Fast Lagrangian Analysis of Continua, was adopted for this study. This program uses an explicit finite difference technique to solve problems with initial and boundary conditions. FLAC3D supports various constitutive models and structural elements that are utilized to model various geotechnical and structural materials, such as soil reinforced with geosynthetic. The following sections explain the constitutive models adopted in this study for GESC materials.

5.2.1 Kansas River Sand

Both the infill material used for the GESC, which was dense Kansas River Sand compacted to 70% relative density, and the weak surrounding soil, which was loose Kansas River Sand

prepared to 30% relative density, were modeled as a linear elastic perfectly plastic material using Mohr-Coulomb criterion. The parameters of the Mohr-Coulomb model are: friction angle of material (ϕ), cohesion (c), dilation angle (ψ), elastic modulus (E), and Poisson's ratio (ν).

5.2.2 Geotextile Encasement

Geotextile encasement was modeled as an orthotropic linear elastic material using the embedded liner structural element. The decision to model the geotextile as an orthotroipc material was based on the results of the stripe-tensile test conducted on a geotextile sheet, which showed that the circumferential stiffness in the cross machine direction was higher than that in the vertical direction (machine direction). This assumption was confirmed by Khabbazian et al. (2009), who proved that modeling the geosynthetic encasement as an isotropic linear material increased the bearing capacity of GESC by 10% and unfavorably influenced the profile of their lateral deformations.

By default, liner elements can resist both bending and membrane forces. However, the membrane loading was only activated in the written code for the embedded liner since geotextiles can only resist membrane forces. In addition, a CST element, which is a three-noded plane-stress triangular element, was utilized to simulate the geotextile material because it can only tolerate membrane loading.

Liner elements interact with FLAC3D grid through two components: the shear component in the direction of the tangent plane to the liner surface and the normal component. The stresses acting on the interface between the liner surface and FLAC3D grid are normal stress (σ_n) and shear stress (τ) that are balanced by the stresses generated in the liner element as shown in Fig. 5.1. Embedded liner elements can be attached to FLAC3D mesh on both its sides in a way that each node has two links connected to two different soils. The interface between the liner element and soil was modeled as a linearly elastic interface using Mohr-Coulomb criterion. The interface in

FLAC3D at each node of the embedded liner element was simulated by two springs, one in the normal direction with a tensile strength and the other in the transverse direction (i.e. tangent plane to the liner surface). The normal component is controlled by normal stiffness per unit area (k_n) and tensile strength as shown in figure 5.2. While, the shear component is based on the shear stiffness per unit area (k_s), cohesion (c), residual cohesion (c_r), and friction angle (ϕ) as shown in figure 5.3. The interface cohesive strength (c) is replaced by residual cohesion (c_r) when the liner element is failed in tension as shown in Fig. 5.3 (b).

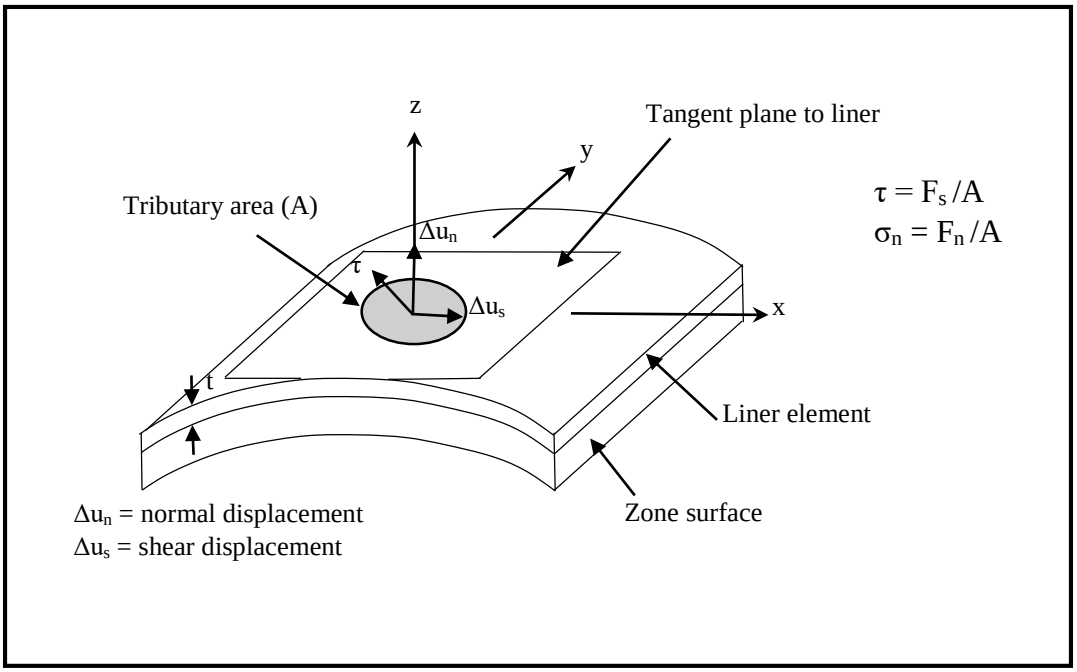

Figure 5.1 Liner-grid interface (Itasca, 2013)

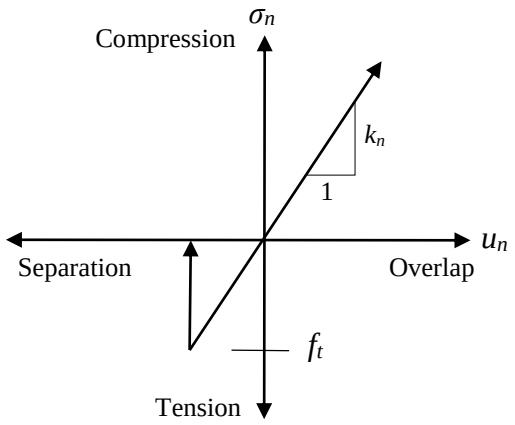

Figure 5.2 Interface in the normal direction for liner element (Itasca, 2013)

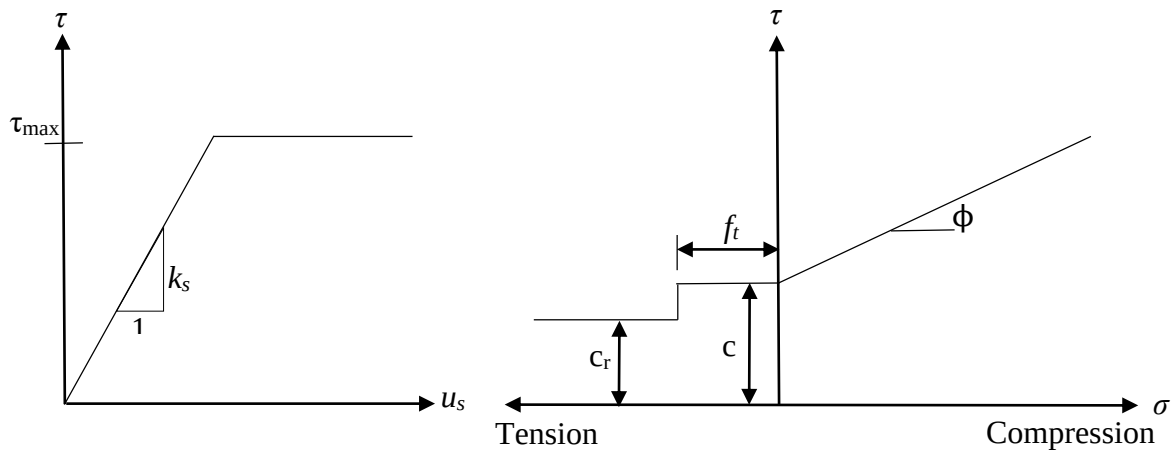

Figure 5.3 Shear interface between the liner element and soil: (a) shear stress versus shear displacement; and (b) shear strength criterion (Itasca, 2013)

The embedded liner-grid interface is required not only to be sufficiently stiff, but it also must be able to slide and separate when a load is applied. To guarantee that the displacements in the interface springs are sufficiently lower than those of the surrounding zone, the apparent

stiffness (k_n and k_s) (stress/unit distance) for a zone perpendicular to the surface can be computed as:

$$k_n = \ k_s = \max\left[\frac{\left(K + \frac{4}{3}G\right)}{\Delta z_{min}}\right] \tag{5.1}$$

Where K = bulk modulus, G= shear modulus, and Δz_{min} = the smallest element size of the adjacent zone perpendicular to the liner element as illustrated in figure 5.4. For the curved surface of embedded liner, the apparent stiffness must be multiplied by 100 to assure small deformations in the interface zone as compared with those in the adjacent zone (Itasca, 2013).

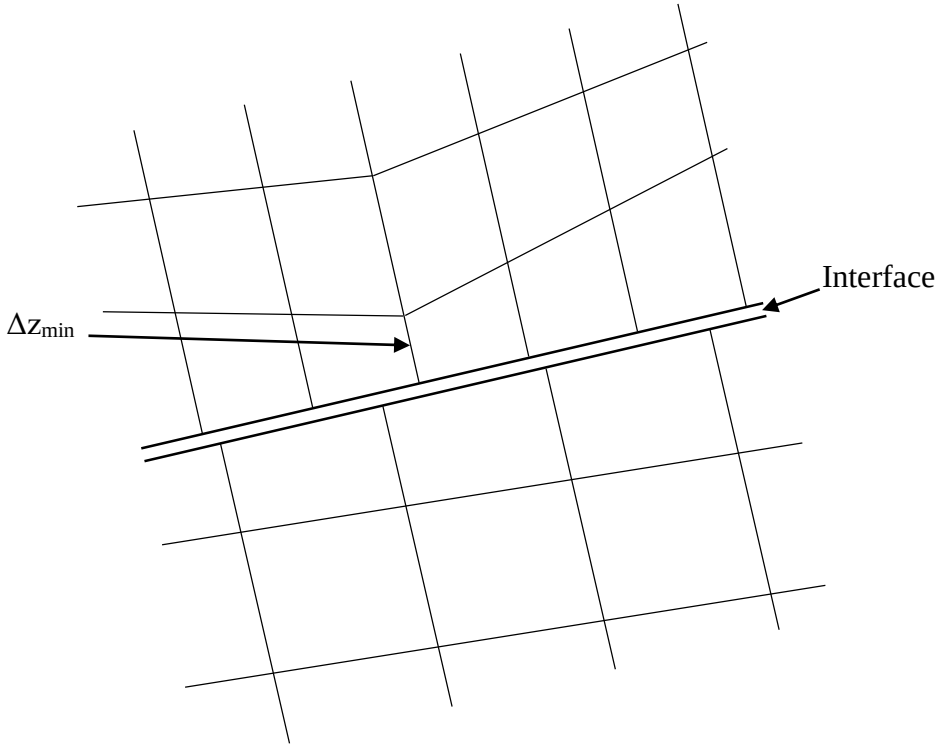

Figure 5.4 Zone size used in apparent stiffness equation (Itasca, 2013)

5.3 Parameter Calibration

Laboratory tests were conducted in order to obtain the soil parameters required for the Mohr-Coulomb model. In addition, laboratory tests were also conducted on GESC to determine the parameters required to model the geotextile sleeve such as the circumferential stiffness (J).

5.3.1 Infill Material

As mentioned in chapter three, the peak angle of internal friction for Kansas River Sand obtained from three CD triaxial compression tests conducted on OSC prepared at 70% relative density was found to be 38.6º. The initial slope of the deviator stress-axial stain curve was used to determine the initial elastic modulus (E) used in the Mohr-Coulomb model. The initial slope of the deviator stress-axial stain curve was found to be 25 MPa. FLAC3D results compared reasonably well with triaxial test results conducted on OSC as shown in figure 5.5. The soil parameters of the infill sand are summarized in table 5.1.

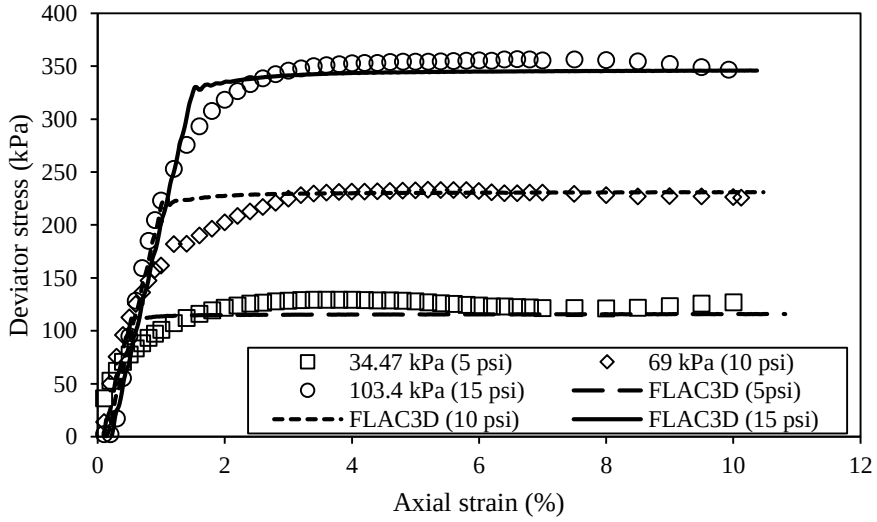

Figure 5.5 Calibration of triaxial tests results of OSC

Table 5.1 Infill dense sand properties used in numerical analysis

Parameters	Value
Peak friction angle (ϕ) (Deg.)	38.6
Elastic modulus (E) (MPa)	25
Poisson's ratio (ν)	0.3
Dilation angle (ψ) (Deg.)	0
Soil cohesion (c) (kPa)	0

5.3.2 Loose Surrounding Soil

A plate load test was conducted on Kansas River Sand prepared at 30% relative density to determine the elastic modulus of the loose soil surrounding the GESC. Numerical results showed a good match with the experimental data at an elastic modulus of 1 MPa, as shown in figure 5.6. Loose sand had a very low elastic modulus since the modulus of sand is mainly dependent on the level of confinement. The normal pressure was applied on the loading plate of a 15 cm diameter. No normal pressure was applied on the top surface of the loose sand, which limited confinement to a very low level.

The friction angle of loose sand was found to be 32^{o} from a CD triaxial compression test conducted on an OSC sample at 30% relative density under confining stress of 20.7 kPa (3 psi) as shown in figure 5.7. Table 5.2 shows the loose sand parameters used in the numerical analyses.

5.3.3 Geotextile Encasement Properties

Geotextile properties were investigated through a series of CD triaxial compression tests conducted on GESC samples prepared at 70% relative density. These properties were calibrated in FLAC using the results of the triaxial tests to determine the circumferential stiffness of the geotextile sleeve, since the provided stiffness from the stripe-tensile test was for a geotextile sheet

and not for a seamed geotextile sleeve. The calibrated circumferential stiffness (J) decreased from 800 kN/m (i.e. the value provided from stripe-tensile test) to 400 kN/m due to the presence of the seam.

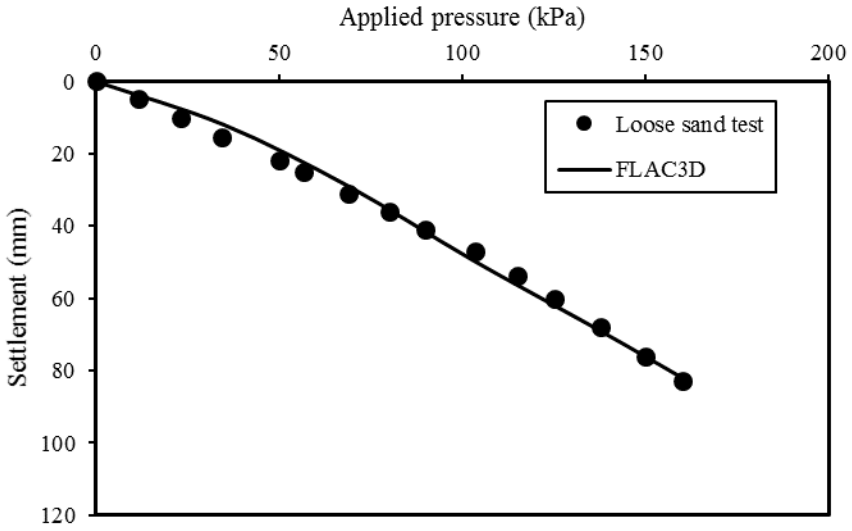

Figure 5.6 Calibration of loose sand plate loading test

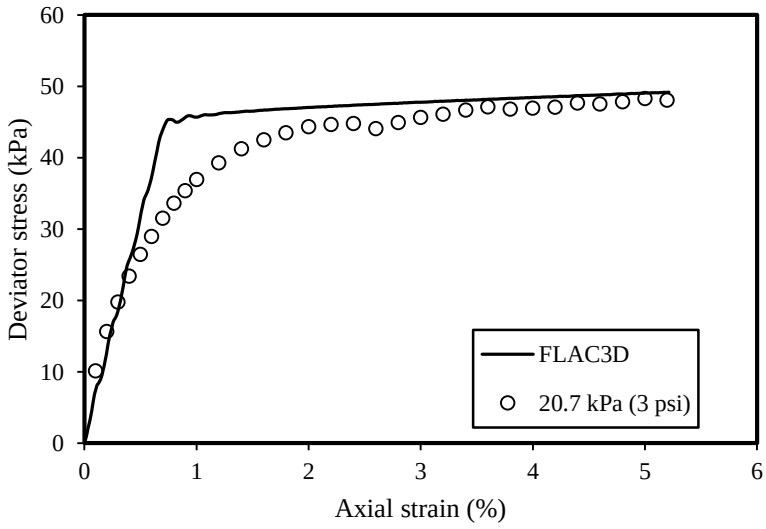

Figure 5.7 Triaxial test result of loose sand

Table 5.2 Loose sand material properties used in numerical analyses

Parameters	Value
friction angle (ϕ) (Deg.)	32
Elastic modulus (E) (MPa)	1
Poisson's ratio (ν)	0.3
Dilation angle (ψ) (Deg.)	0
Soil cohesion (c) (kPa)	0

Due to the fact that geotextile encasement is unable to carry compressive vertical loads, Khabbazian et al. (2010) suggested reducing the vertical stiffness (E_v) of geosynthetic encasement to a value of 1% of circumferential stiffness (i.e. $E_v = 0.01\ E_c$) to avoid any unfavorable effect on the numerical results. The vertical stiffness of the geotextile sleeve was changed from 300 kN/m (i.e. the stiffness provided by Strip-Tensile test) to 4 kN/m (i.e. 1% of circumferential stiffness) and no difference was observed on the numerical results. Therefore, the vertical stiffness was assumed to be 4 kN/m. Figure 5.8 depicts the calibration results of triaxial compression tests for three confining stresses: 34.47 kPa (5 psi), 69 kPa (10 psi), and 103.4 kPa (15 psi). FLAC3D results showed a reasonably good match with the experimental data. Table 5.3 summarizes the geotextile encasement properties used in the numerical modeling with FLAC3D.

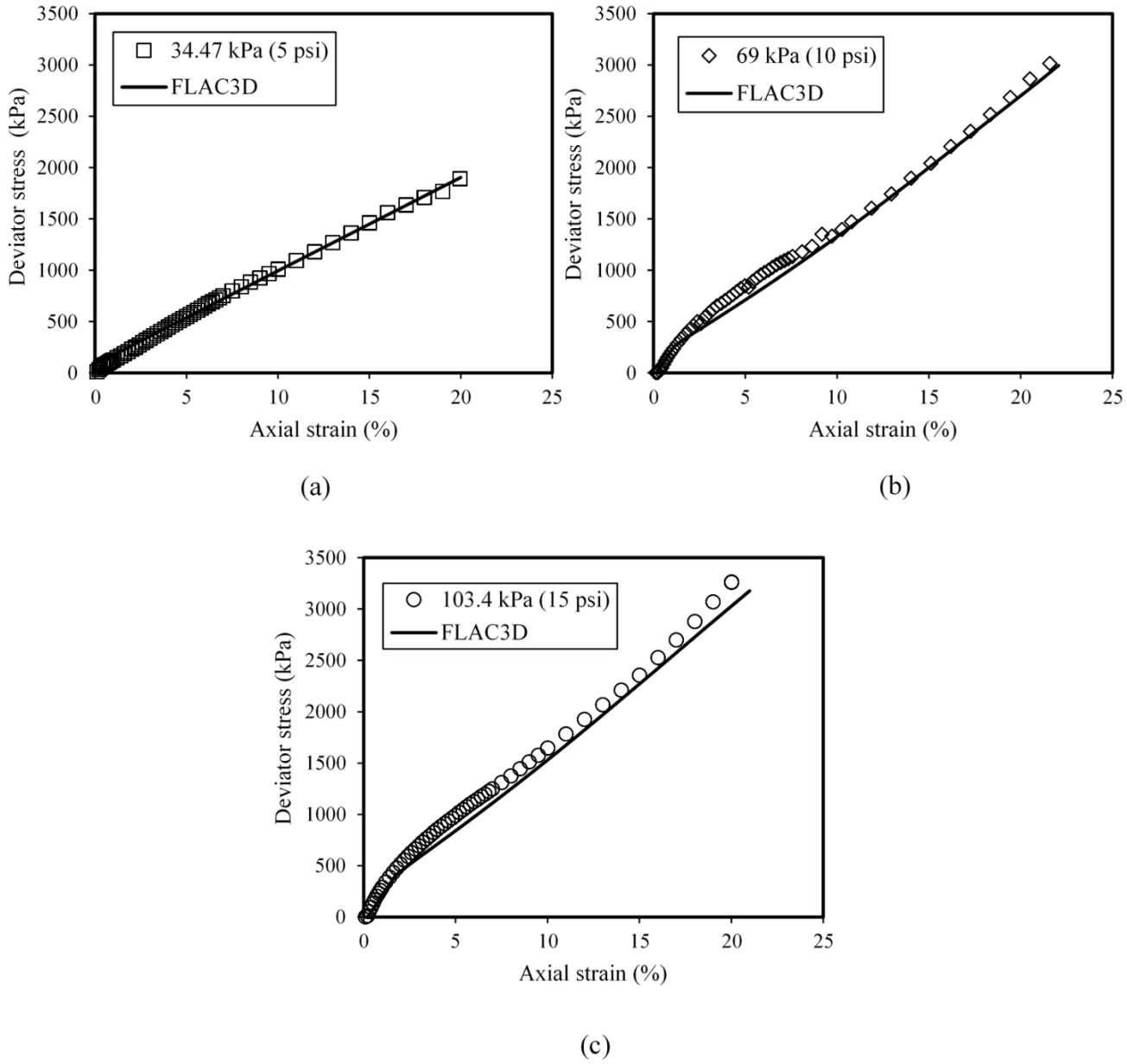

Figure 5.8 Triaxial test calibration for GESC at confining stresses: (a) 34.47 kPa; (b) 69 kPa; and (c) 103.4 kPa

Table 5.3 Geotextile encasement properties used in the numerical modeling

Parameters	Value
Circumferential stiffness (kN/m)	400
Vertical stiffness (kN/m)	4
Poisson's ratio (ν)	0.3
Geotextile thickness (mm)	1.5

5.4 Validation of FLAC3D Model

In order to simulate the experimental load tests conducted on GESC with surrounding weak soil, FLAC3D models were built using the material properties and constitutive models discussed in the previous sections. An embedded liner element was used to create two interfaces: one between the geotextile encasement and infill material and the other between the geotextile encasement and surrounding soil. The interface cohesion was assumed to be zero for both sides. The interface friction angles were determined by multiplying the friction angle by an interaction coefficient which was selected to be 0.7 based on the results of large direct shear test conducted by Abu-Farsakh et al. (2007) to investigate the geotextile-sand interface parameters. Therefore, the interface friction angle between the geotextile and infill sand was set at 29^{o}. Meanwhile, the interface friction angle between the geotextile and loose surrounding sand was set at 23^{o}. The GESC was loaded on its top area by applying equal load increments on the top of the loading plate. Figure 5.9 shows the finite difference mesh for a 15 cm GESC with loose surrounding soil and a L/D ratio of 6.

The numerical model was verified with the results of plate load tests for 15 cm diameter GESC with L/D ratios of 2, 4, and 6, as shown in figure 5.10. Numerical results matched reasonably well with the experimental data. Therefore, this model was adopted for this study.

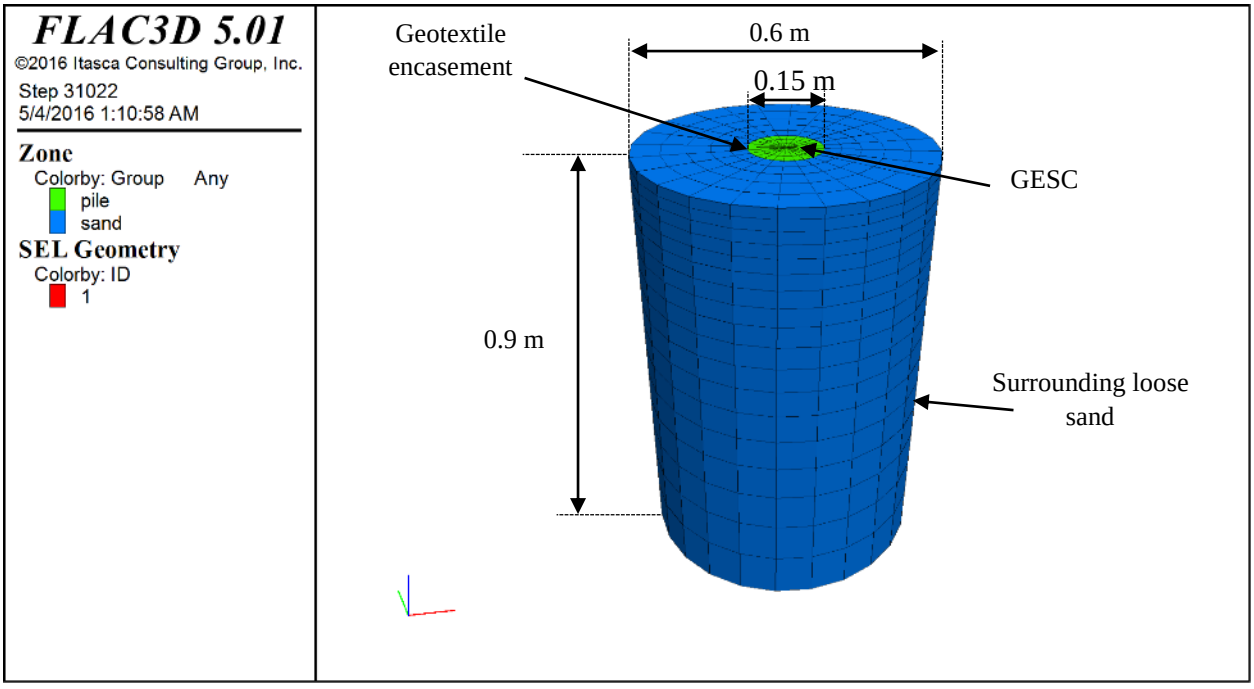

Figure 5.9 Finite difference mesh for a 15 cm GESC surrounded by loose sand with a L/D of 6

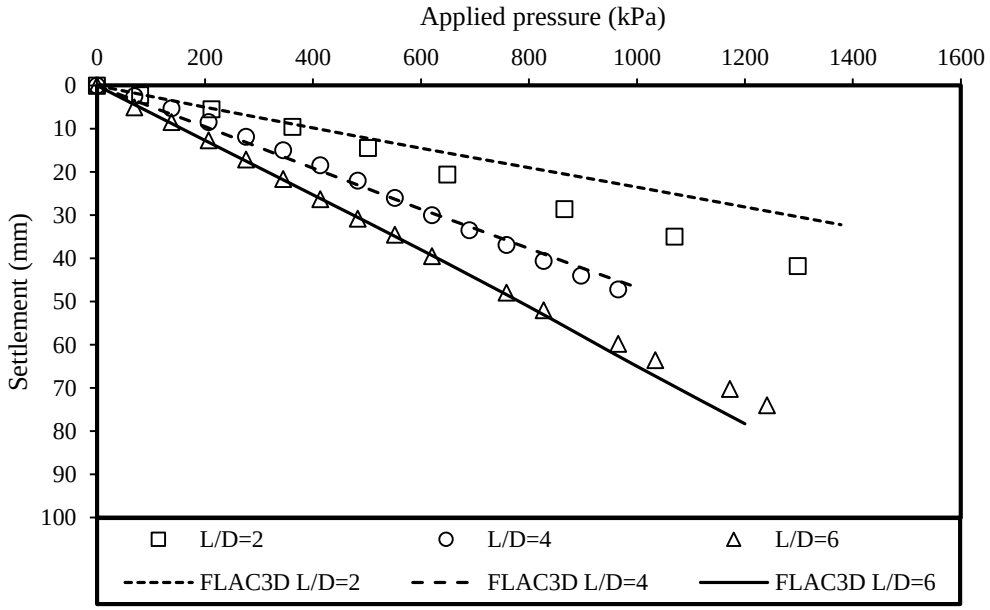

Figure 5.10 Validation of FLAC3D model with experimental results

5.5 Parametric Study

A finite difference program (FLAC 3D 5.01) was employed to perform the three dimensional numerical analysis of GESC with surrounding soil. For the baseline model, the length of the geotextile encased sand column and the thickness of the surrounding loose sand were taken as 3 m with a length to diameter ratio of 6. The diameter of geotextile encased column was chosen to be 0.5 m, which is the size commonly used in practice for GESC. The lateral extent of the surrounding loose sand was selected in a way that the influence of the boundary conditions on the model outputs was negligible. Meyerhof and Sastry (1978) pointed out that the failure region of a column is extended radially by 1.5 times the diameter of the column, when measured from the edge of the column. Therefore, the diameter of the outer cylinder surrounding the GESC was assumed to be 4 m. The displacements in z direction were restricted at the bottom boundary of the model. Meanwhile, at the circumferential boundary, the displacements in the x and y directions were restricted. The same properties of the interface (i.e. interface friction angles) that were explained in the previous section were used in this analysis. The load was applied only on the top plate (which had the same size as the GESC) by means of equal pressure increments to simulate the procedure used in experimental work. The finite difference mesh of the GESC with a surrounding loose sand is shown in figure 5.11. The mesh details for a GESC are shown separately in figure 5.12.

A series of parametric studies were conducted to investigate the parameters that may have a crucial influence on the performance of GESC. For example: GESC diameter, soil thickness, GESC length, encasement length, geotextile stiffness, and friction angle of infill material. The

parametric study was performed by changing one parameter while keeping all other parameters the same.

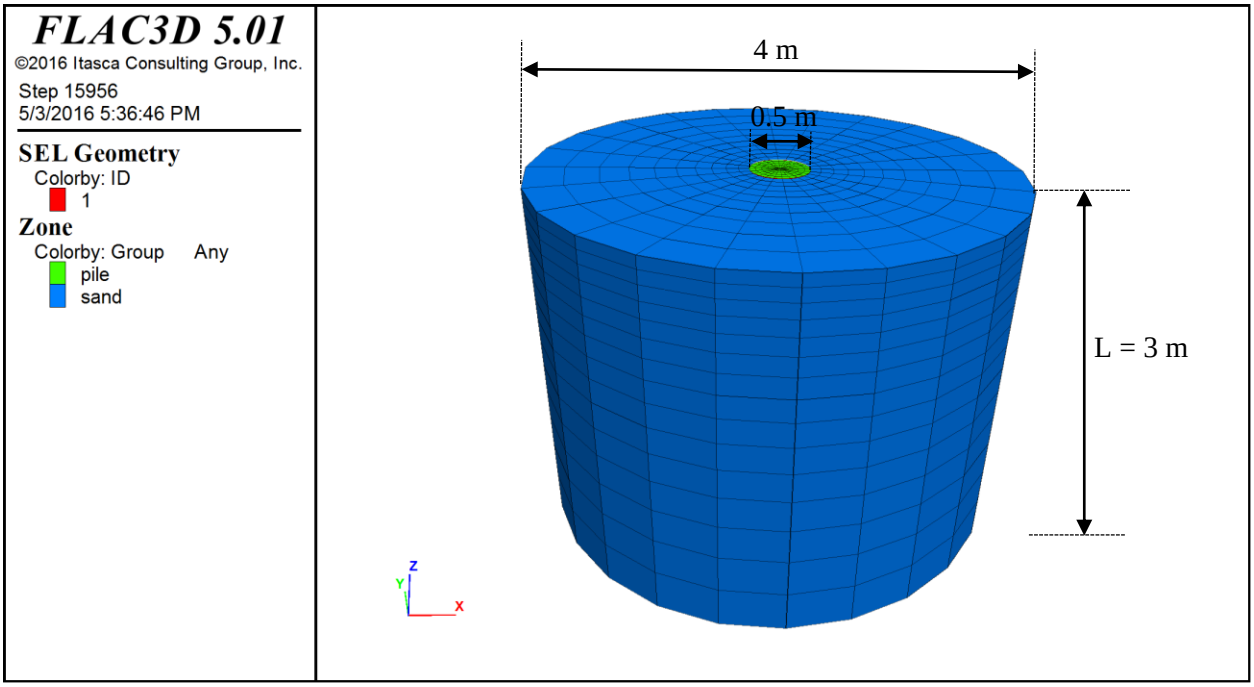

Figure 5.11 Finite difference mesh used in this study

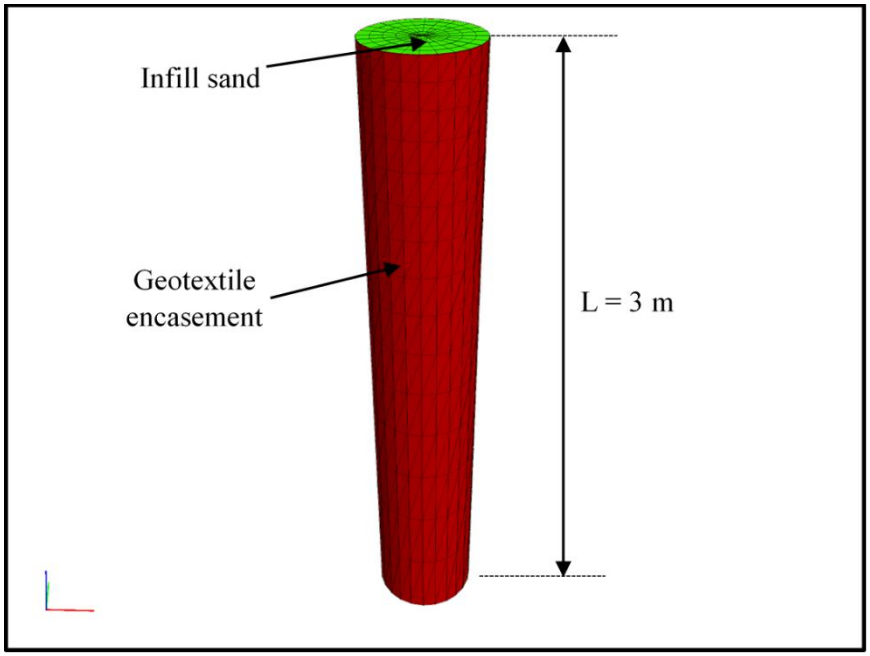

Figure 5.12 Geotextile encased sand column mesh details for this study

5.6.1 Effect of GESC Diameter

In order to investigate the effect of the column size on the performance of GESC on both the bearing capacity and lateral deformation (i.e. radial strain), the diameter of the GESC was varied from 0.25, 0.5, and 0.75 m, corresponding to a L/D of 12, 6, and 4, respectively. The radial extent of the zone of influence (i.e. diameter of the outer cylinder) was extended to 4 m as mentioned in the previous section to account for the largest size of the GESC used in this analysis (i.e. 0.75 m diameter), and to minimize the boundary effect on the performance of GESC. Increasing the size of GESC decreased its bearing capacity, as shown in Figure 5.13. This is consistent with the findings of Murugesan and Rajagopal (2009) and Castro and Sagaseta (2011), who found that increasing the diameter of GESC reduced the bearing capacity of GESC. This is mainly attributed to the reduced mobilized vertical pressure on the top of the GESC as the diameter of the column increased. In order to assess the influence of the GESC diameter on its performance, the size of GESC was plotted against the applied pressure on the top of the GESC for settlements of 50 and 100 mm, as shown in Fig. 5.14. Changing the diameter of GESC from 0.25 to 0.75 m decreased the bearing capacity by 60 and 53% for settlements of 50 and 100 mm, respectively.

The lateral deformation profile of various GESC diameters with depth for a vertical pressure of 300 kPa is shown in Fig. 5.15. Radial strain increased as the diameter of the column increased. For all curves, radial strains were higher near the surface and decreased with depth. Meanwhile, for the GESC of 0.75 m diameter, the radial strain curve peaked twice in a manner that was similar to the repeated pattern observed in the GESC in air. This strain pattern could be related to the lower confinement provided by the geotextile encasement for a column of large diameter.

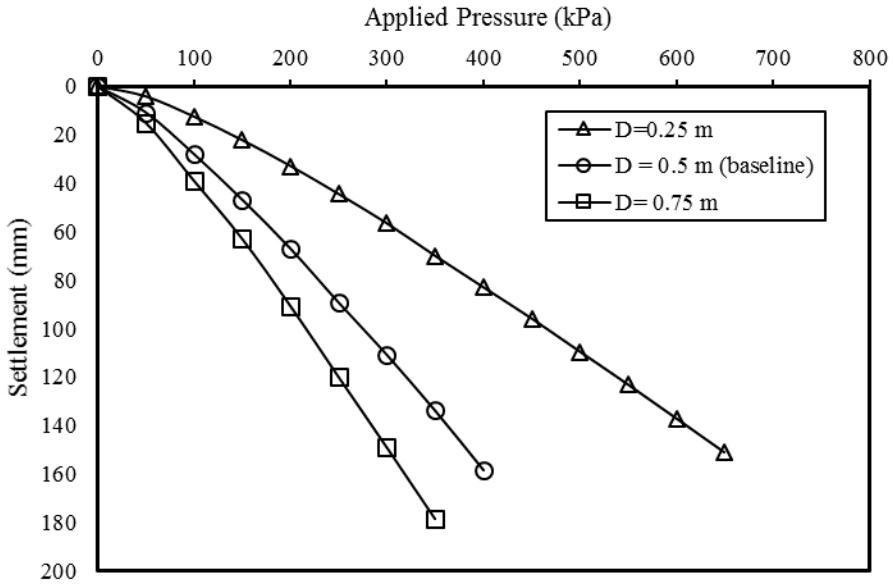

Figure 5.13 Effect of GESC diameter on the applied pressure-settlement behavior for L=3 m

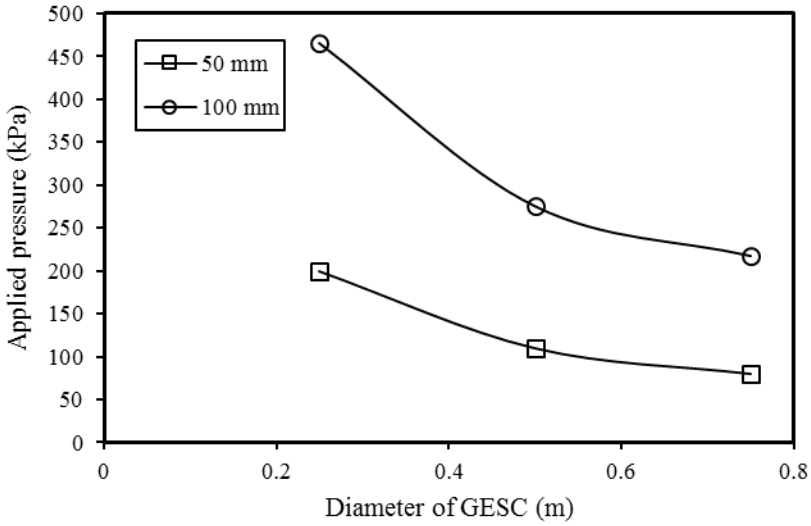

Figure 5.14 Applied pressure on the top of GESC corresponding to column diameter for L=3m

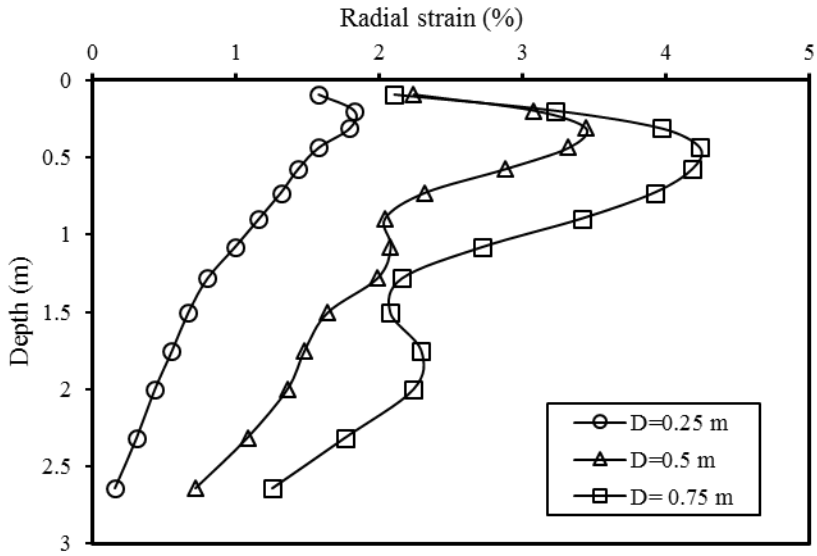

Figure 5.15 Radial strain of GESC with depth corresponding to GESC diameter for L=3m

5.6.2 Effect of Soil Thickness

The thickness of loose sand and length of the end-bearing GESC were varied in this section. Therefore, end-bearing GESC are GESC that have penetrated the whole thickness of soil and are in contact with a rigid bottom boundary as shown in figure 5.16. As mentioned earlier, the displacements in the bottom boundary were fixed in the z direction. The soil thickness was varied as 1, 2, 3, 4.5, and 6 m to represent L/D ratios of 2, 4, 6, 9, and 12, respectively. Fig. 5.17 depicts the applied pressure on the top of GESC versus settlement. It is evident that reducing the thickness of the soil to as little as 1 m increased the bearing capacity of GESC significantly due to the influence of the bottom rigid boundary. The effect of increasing the soil thickness beyond 3 m on the bearing capacity of GESC was found to be minimal. As a result, shorter end-bearing GESC exhibited higher bearing capacities than longer ones since GESC transmit the compressive load along the whole length and hence shorter end-bearing columns mobilize higher stresses compared with longer end-bearing columns at a given amount of settlement. The maximum lateral bulging

of the GESC occurred in the top portion of the column, and increasing the length of the end-bearing GESC did not improve the performance of GESC with regard to lateral expansion. The lateral bulging pattern of GESC was insensitive to changes in the end-bearing length under an applied pressure of 300 kPa, as shown in figure 5.18.

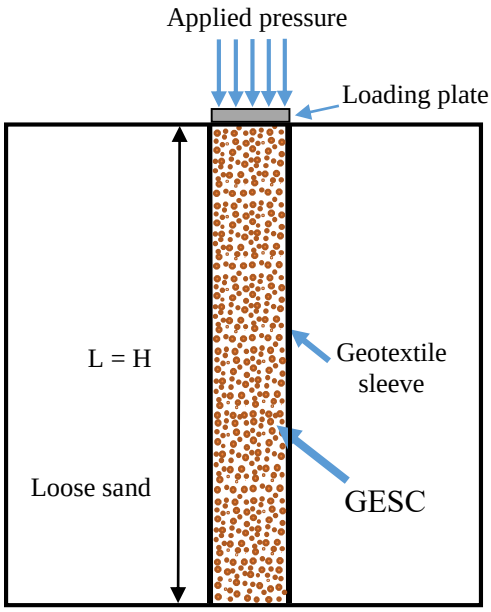

Figure 5.16 End-bearing GESC

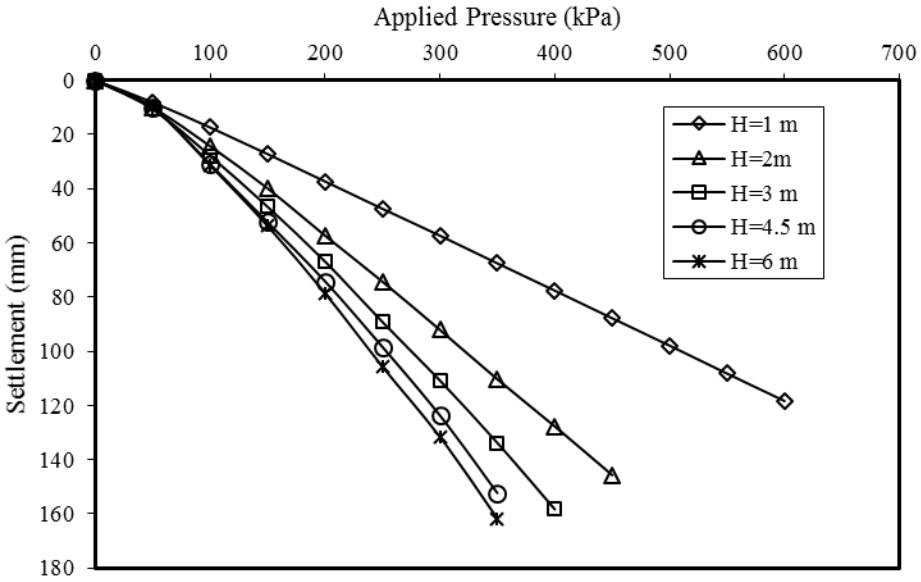

Figure 5.17 Effect of soil thickness on the applied pressure-settlement behavior

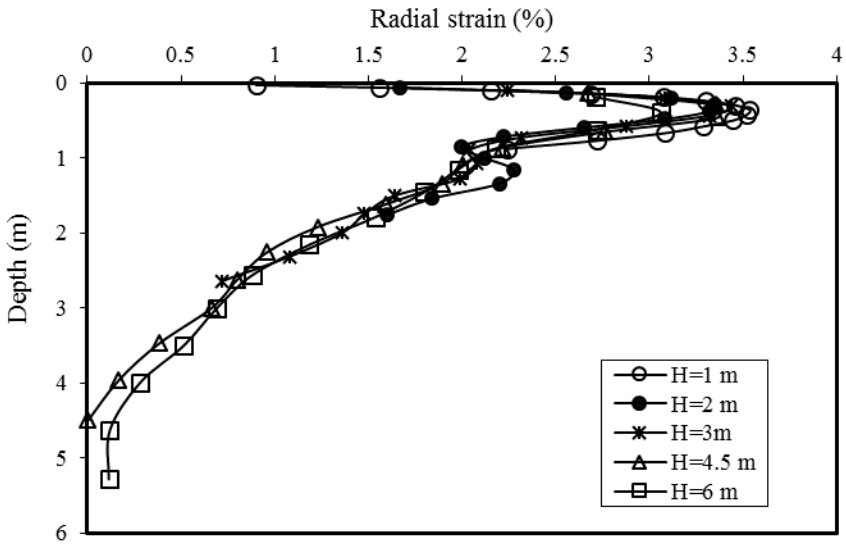

Figure 5.18 Radial strain of GESC with depth corresponding to soil thickness at 300 kPa applied pressure

Figure 5.19 shows the applied pressure on the top of GESC as a function of soil thickness for settlements of 50 and 100 mm. For instance, reducing the soil thickness from 2 to 1 m increased the bearing capacity of the GESC by 49 and 59%, corresponding to 50 and 100 mm settlements, respectively. Therefore, the influence of varying the soil thickness on GESC bearing capacity was more pronounced at higher settlements, as indicated by (Meehan et al., 2010). Meanwhile, the applied pressure on the top of the 3 m end-bearing GESC was 10 and 14.6% greater than that on the top of GESC of 6 m length for settlements of 50 and 100 mm, respectively.

5.6.3 Effect of GESC Length

All the above analyses were based on an end-bearing condition at which the bottom boundary of the GESC was assumed to be rigid. For this section the thickness of the surrounding soil was kept to 6 m, while the length of GESC was varied from 1 to 5 m to simulate the condition of partially penetrating GESC as shown in figure 5.20. An L/H ratio was used to refer to partially

penetrating GESC, where L= column length and H= surrounding soil thickness. Thus, the L/H was set to values of 0.17, 0.33, 0.5, 0.67, 0.83, and 1, and corresponds to the changed length of GESC from 1 to 6 m.

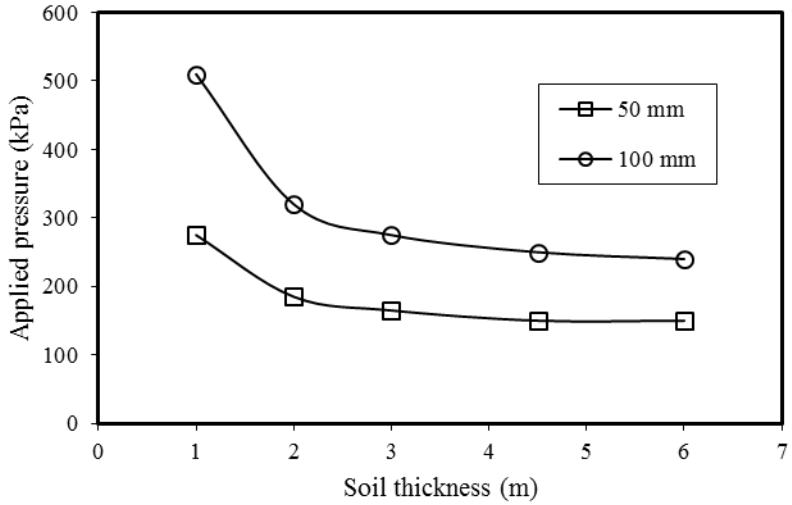

Figure 5.19 Applied pressure on the top of GESC corresponding to soil thickness

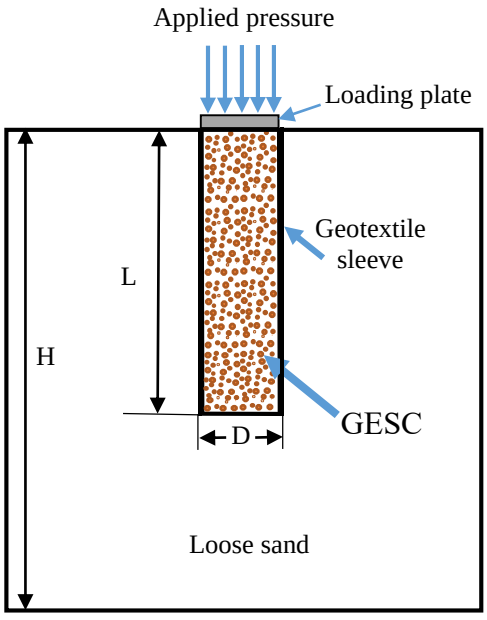

Figure 5.20 partially penetrating GESC embedded in loose sand

Loading test results of FLAC3D are shown in figure 5.21 that show the relationship between column length and the applied pressure and settlement. It is evident that increasing the L/H of the partially penetrating columns increased their bearing capacity. This finding is consistent with the findings of Sivakumar et al. (2004) on the effect of partially penetrating GESC on the performance of GESC. For shorter columns of L/H of 0.17 and 0.33, the ultimate bearing capacities were only 150 and 200 kPa, respectively. Increasing the L/H up to 0.5 enhanced the bearing capacity of GESC. Geotextile encasement transfers the applied pressure to greater depths and consequently increases the bearing capacities of GESC (Murugesan and Rajagopal, 2006), however increasing the L/H to a value greater than 0.5 had an insignificant effect on the bearing capacity and the behavior became similar to that of fully penetrating (i.e. end-bearing) GESC. Figure 5.22 presents the profile of radial strain for varying-length GESC at an applied pressure of 150 kPa. Shorter columns experienced lateral bulging along their entire length since the maximum bulging happened close to the surface. In addition, shorter columns bulged more at the base because of the lack of confinement.

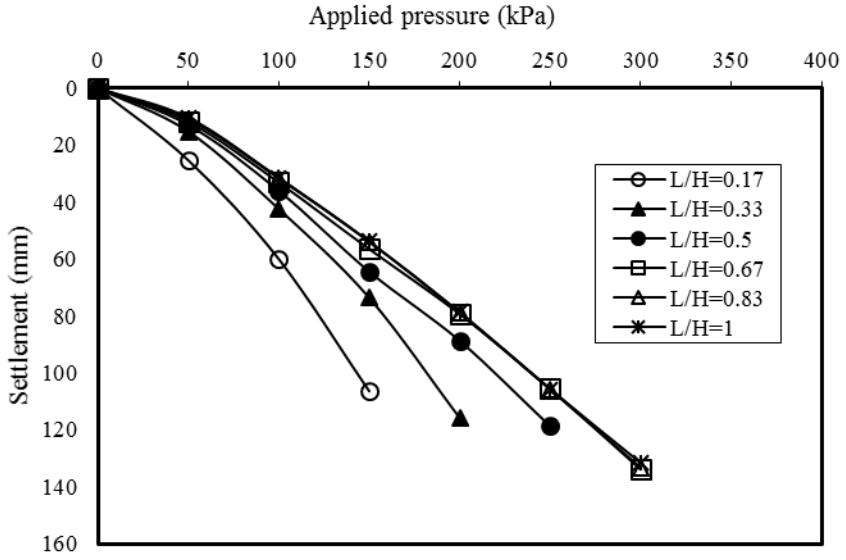

Figure 5.21 Effect of GESC length on the applied pressure-settlement behavior

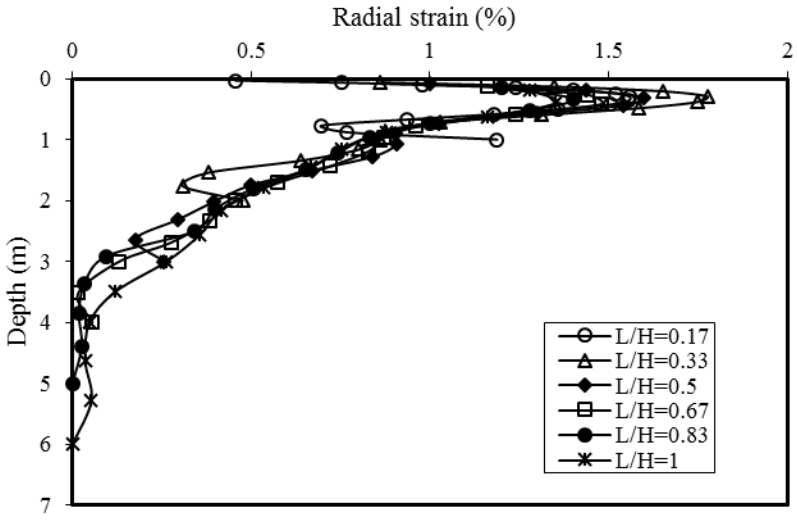

Figure 5.22 Radial strain profile of GESC with depth corresponding to GESC length at 150 kPa applied pressure

Figure 5.23 depicts the applied pressure on the top of GESC as a function of L/H. For example, increasing the L/H from 0.17 to 0.5 increased the bearing capacity of GESC by 42 and 52% for settlements of 50 and 100 mm, respectively. Similar to end-bearing GESC, the effect of increasing the column length was more pronounced at higher settlements.

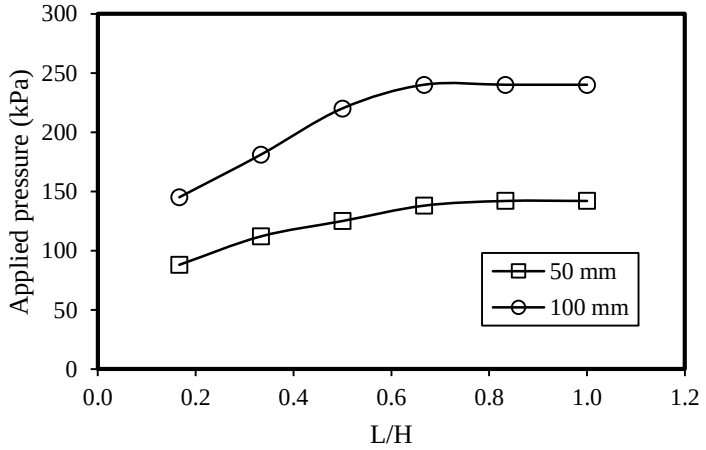

Figure 5.23 Applied pressure on the top of GESC corresponding to L/H

5.6.4 Effect of Geotextile Encasement Length

In order to determine the maximum effective length of geotextile encasement, the encasement length was changed to form a partially encased sand column. In this analysis, the thickness of soil and column length were 3 m to simulate the end-bearing condition. The encasement length was varied from 1D (i.e. 0.5 m) to 5D (2.5 m) in order to determine the influence of encasement length on the performance of GESC. Figure 5.24 shows the influence of geotextile encasement length on the bearing capacity of GESC. As the encasement length increases, the bearing capacity of a partially encased sand column increases until its behavior approached that of fully encased sand columns. The applied pressure on the top of partially encased columns as a function of encasement length to column diameter at 50 and 100 mm settlements is illustrated in figure 5.25. Changing the ratio of geotextile encasement length to column diameter from 1 to 4 caused the bearing capacity of GESC to increase by 39 and 43% at 50 and 100 mm settlement, respectively. Meanwhile, increasing the encasement length from 4D to 6D (i.e. fully encased column) increased the bearing capacity by only 8 and 14% for settlements of 50 and 100 mm, respectively. The benefit of increasing the geotextile encasement length beyond 5D on the bearing capacity of GESC was insignificant. This finding is consistent with Gu et al. (2015), who also found that the effective encasement length was three to four times the column diameter.

With regard to the column lateral deformation, the radial strain of a partially encased sand column compared to a fully encased column was plotted against the ratio of the height from the surface to column diameter for an applied pressure of 300 kPa as shown in figure 5.26. Increasing the length of encasement from 1D to 3D reduced the radial strain of GESC. The maximum bulging occurred just beneath the level of encasement.

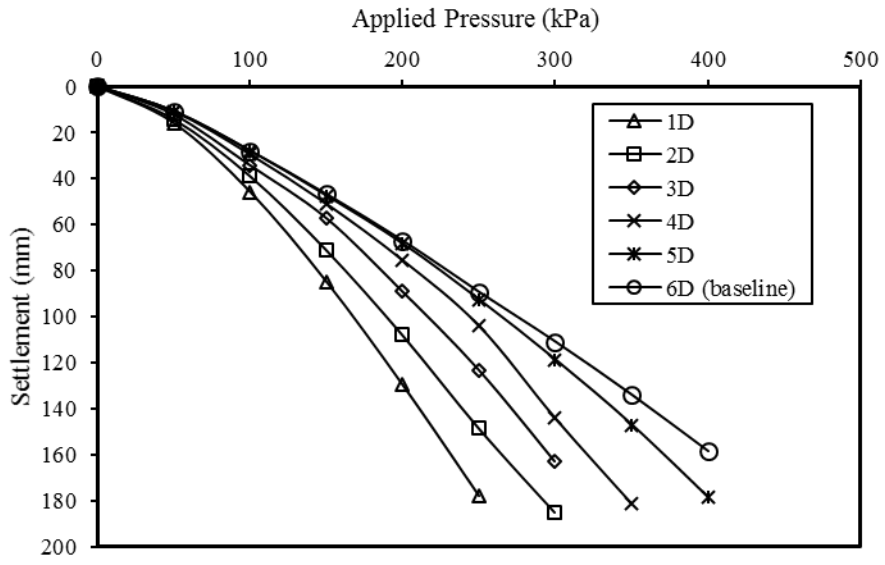

Figure 5.24 Effect of geotextile encasement length on the applied pressure-settlement behavior

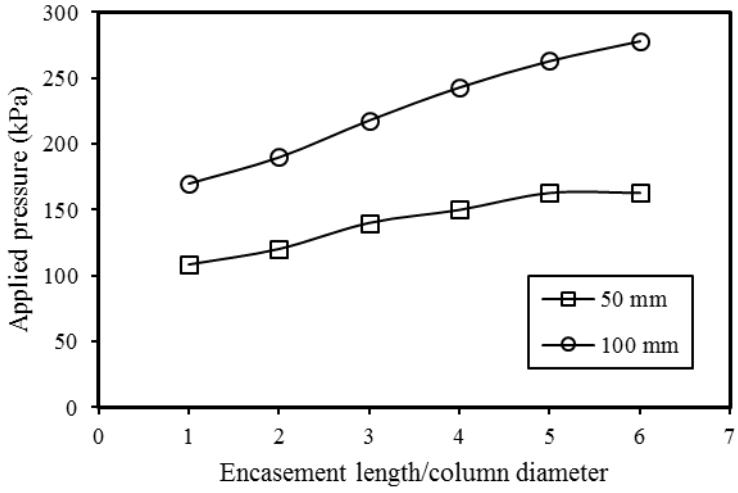

Figure 5.25 Applied pressure on the top of GESC corresponding to a ratio of encasement length to column diameter

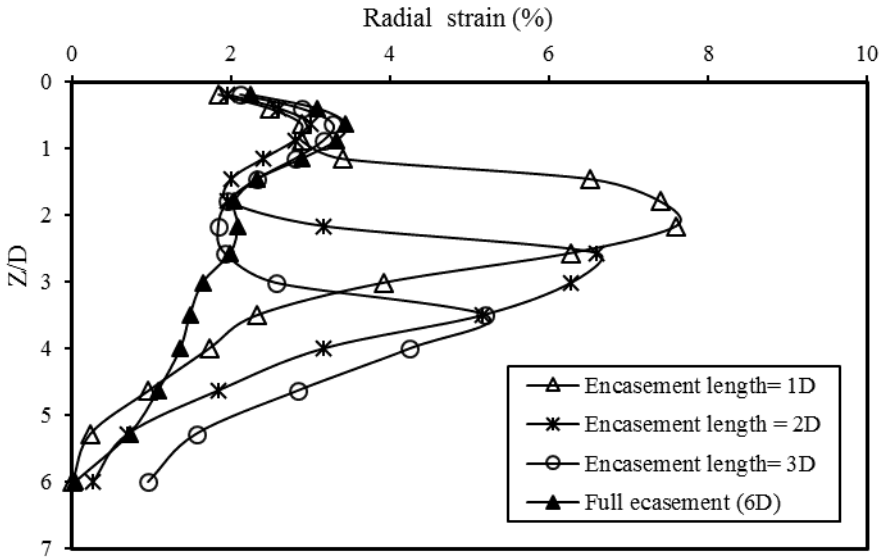

Figure 5.26 Radial strain of partially encased sand columns with Z/D at 300 kPa applied pressure

5.6.5 Effect of Geotextile Stiffness

In order to investigate the influence of geotextile stiffness on the performance of GESC, this parameter was changed from 400 kN/m (i.e. the baseline case) to 3000 kN/m. The applied pressure-settlement curves on the top of GESC for various values of geotextile stiffness are depicted in Fig. 5.27. This figures shows that the bearing capacity of the GESC was substantially increased as the stiffness of geotextile encasement increased. In order to assess the influence of geotextile stiffness on the performance of GESC, the applied pressure on the top of GESC as a function of geotextile stiffness was plotted for settlements of 50 and 100 mm as shown in Fig. 5.28. This figure shows that increasing geotextile stiffness from 1000 kN/m to 3000 kN/m increased the bearing capacity of GESC by 74 and 71% for settlements of 50 and 100 mm, respectively. Figure 5.29 shows the radial strain pattern of GESC with depth for an applied pressure of 300 kPa and for various values of geotextile stiffness. GESC exhibited higher lateral

deformations for geotextile sleeves with lower stiffness. Smaller changes of stiffness values, for instance from 400 to 1000 kN/m, reduced the maximum radial strain significantly, with a peak reduction of 55%. The benefit of increasing the stiffness beyond 2500 kN/m for the radial strain of GESC was insignificant.

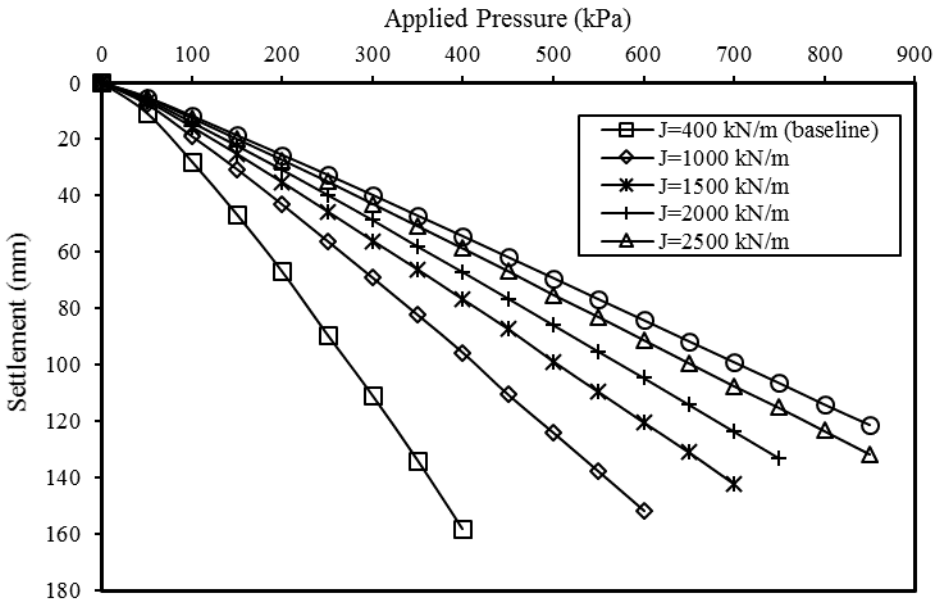

Figure 5.27 Effect of geotextile stiffness on the applied pressure-settlement behavior

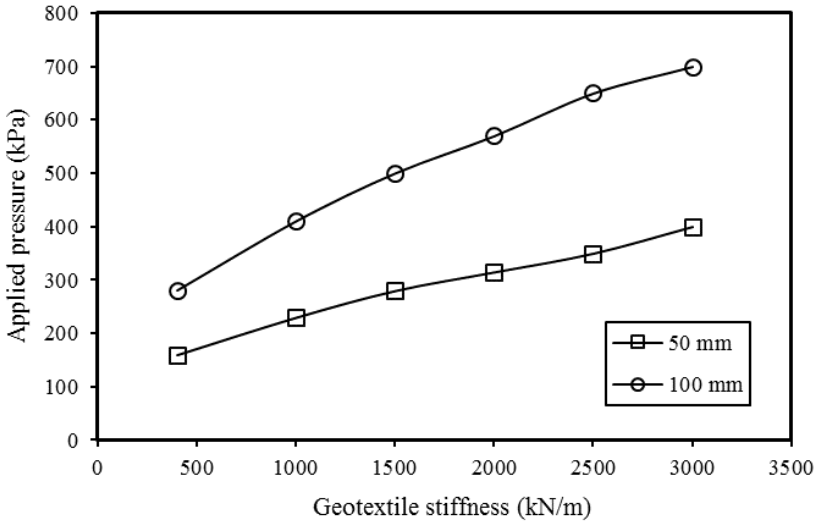

Figure 5.28 Applied pressure on the top of GESC corresponding to geotextile stiffness

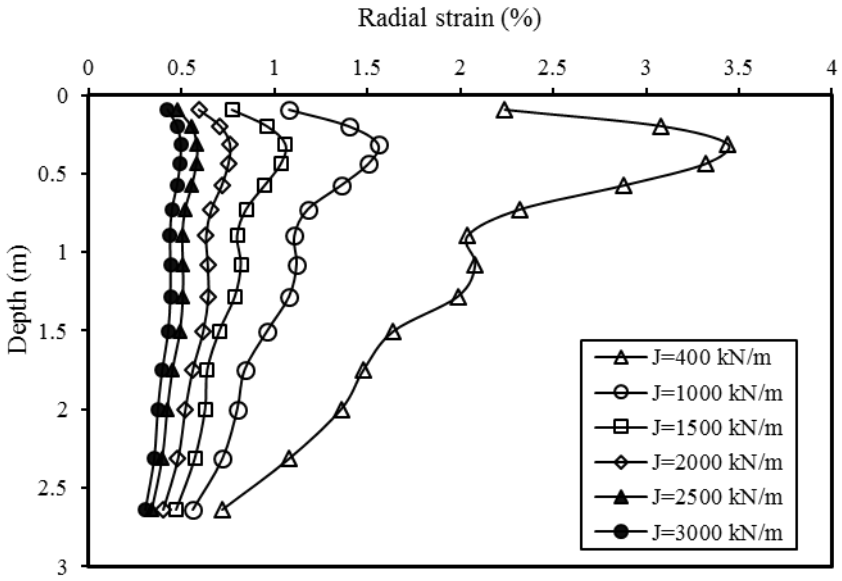

Figure 5.29 Radial strain profile of GESC with depth corresponding to geotextile stiffness at 300 kPa applied pressure

5.6.6 Effect of Friction Angle of Infill Material

The friction angle of infill material was set at three different values: 35^o, 38.6^o, and 45^o, to study the potential influence of this parameter on the performance of GESC. Figure 5.30 shows the applied pressure-settlement behavior of GESC for different friction angles of infill material. Increasing the friction angle enhanced the bearing capacity of GESC somewhat. In order to evaluate the degree of improvement relevant to this parameter on the bearing capacity of GESC, the applied pressure was plotted against the friction angle at 50 and 100 mm settlements as shown in figure 5.31. Increasing the friction angle of infill sand from 35^o to 45^o increased the bearing capacity of GESC by 33 and 36% for settlements of 50 and 100 mm, respectively. Thus the contribution of increasing the friction angle of infill material is substantial but not as significant as increasing the geotextile stiffness. The effect of friction angle on the lateral deformation profile is also shown in figure 5.32. As the friction angle increased, radial strains developed in GESC

decreased. The maximum radial strain dropped from 4% for a friction angle of 35º to 2.5% for a friction angle of 45º.

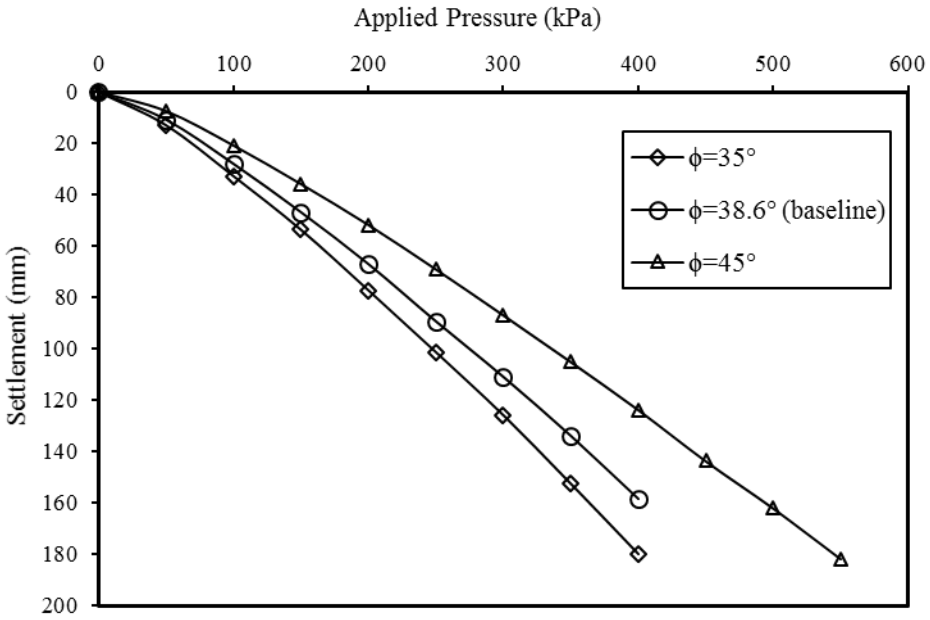

Figure 5.30 Effect of friction angle of infill sand on the applied pressure-settlement behavior

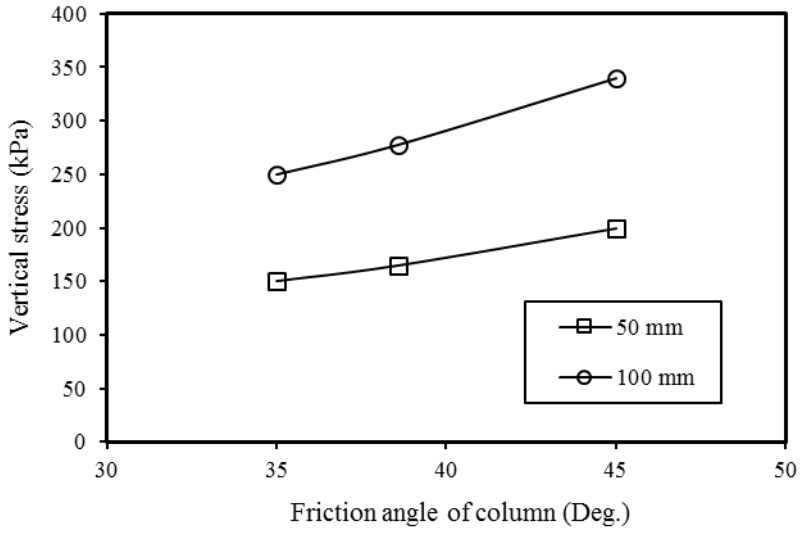

Figure 5.31 Applied pressure on the top of GESC corresponding to friction angle of infill sand

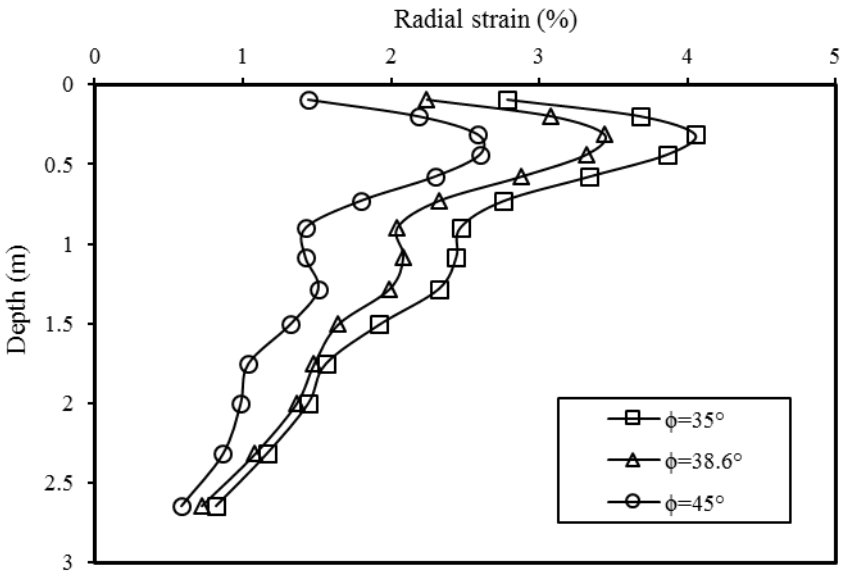

Figure 5.32 Radial strain profile of GESC with depth corresponding to friction angle of infill sand at 300 kPa applied pressure

5.6 Summary

In this chapter an individual GESC with surrounding weak soil was investigated using the finite difference method with the software package FLAC3D. Only the top area of the column was loaded to investigate the bearing capacity of GESC. Various parameters were investigated in this numerical study such as column diameter, soil thickness, column length, geotextile encasement length, geotextile stiffness, and friction angle of infill material. Increasing the size of GESC reduced its bearing capacity and increased the lateral bulging effect. Increasing the length of end-bearing GESC reduced their bearing capacity, while shorter, partially penetrating GESC had a lower bearing capacities as compared to longer ones. The maximum effective geotextile encasement length was found to be five times the column diameter. Geotextile stiffness had a substantial influence on the performance of GESC up to 2500 kN/m. The friction angle of infill

sand had a minor influence on the behavior of GESC when compared to the effect of geotextile stiffness.

CHAPTER 6

TWO DIMENSIONAL ANALYSIS OF GEOSYNTHETIC ENCASED SOIL COLUMN: NUMERICAL ANALYSIS

6.1 Introduction

Due to the complexity of 3D models, two equivalent 2D methods were used in this study; the column wall method and the equivalent area method. This chapter focuses on the degree of improvement achieved using geosynthetic encased stone columns as compared to ordinary stone columns on the stability of embankments constructed on soft soils under the short-term condition. The finite difference software FLAC/Slope 6.0 developed by Itasca Consulting Group was used to achieve this task. The effect of ground water table was not considered in this study.

6.2 Two Dimensional Finite Difference Analysis

In order to convert the 3D model of embankments supported by ordinary or geosynthetic encased stone columns into the plane strain condition (2D), two methods were adopted in this study: column wall and equivalent area methods.

6.2.1 Column Wall Method

The method of matching the geometry of stone columns was adopted in this study as illustrated in figure 6.1. In other words, the width of column wall was taken to be the same as column width (Tan et al., 2008). The properties of column wall can be summarized in the following equations (Zhang et al., 2014):

$$E_w = E_c a_r + E_s(1 - a_r) \quad (6.1)$$

$$c_w = c_s(1 - a_r) \quad (6.2)$$

$$\phi_w = \arctan(a_r \, tan\phi_c + (1 - a_r) tan\phi_s) \quad (6.3)$$

where E_w, E_c, and E_s = the elastic moduli of column wall, individual stone column, and soft soil, respectively; a_r = the area replacement ratio of column area (A_c) to that of the column wall (column width (d) * center-to-center spacing (s)), c_w and c_s = the cohesion of column wall and soft soil, respectively; and ϕ_w, ϕ_c and ϕ_s = the friction angles of column wall, individual stone column, and soft soil, respectively.

6.2.2 Equivalent Area Method

This method assumes the stone columns and surrounding soft soil work as a composite area. The equivalent properties of the composite ground can be computed as follows (Abusharar and Han, 2011):

$$E_{eq} = E_c a_s + E_s(1 - a_s) \quad (6.4)$$

$$c_{eq} = c_s(1 - a_s) \quad (6.5)$$

$$\phi_{eq} = \arctan(a_s \, tan\phi_c + (1 - a_s) tan\phi_s) \quad (6.6)$$

where E_{eq}, c_{eq} and ϕ_{eq} = the equivalent modulus, cohesion, and friction angle of the composite area; a_s = the overall area replacement ratio. In this study, the stone columns were arranged in a square pattern so that the overall area replacement ratio can be evaluated as follows:

$$a_s = \frac{\pi}{4}\left(\frac{d}{s}\right)^2 \quad (6.7)$$

6.3 Numerical Modeling

The dimensions and properties of the embankment, clay, sand and stone columns were chosen to match the Abusharar and Han (2011) study except for column width and spacing. Figure 6.2 shows the model meshes and dimensions solved by column wall and equivalent area methods.

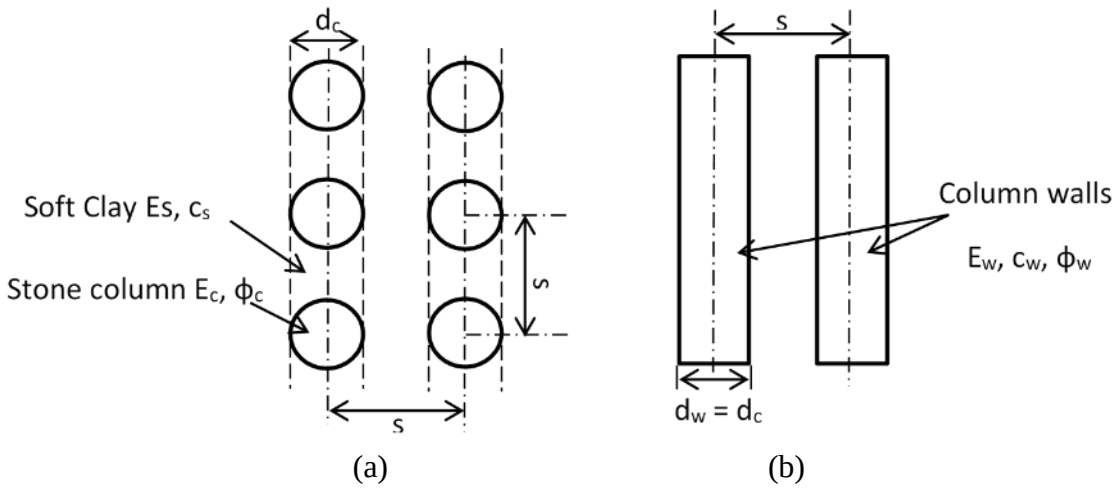

Figure 6.1 Top view of the stone columns and surrounding soft clay: (a) Individual columns (b) Column walls (not to scale), (Kadhim et al., 2015)

Due to symmetry, half of the problem was analyzed using FLAC/Slope 6.0 software. The foundation soil consists of 10 m thick soft clay overlying 2 m of sand. The column width (d=0.5 m) was selected to represent the typical geosynthetic encased column used in practice with a length of 10 m. The center-to-center spacing of columns was 2.5 m to achieve a diameter to spacing ratio of 20%. The embankment was 5 m in height with a 10 m crest width and a slope of 2H:1V. In order to avoid surficial failure, an excluded zone function available in FLAC/Slope 6.0 was implemented so the slip surface would not enter a 0.5 m thick zone at slope surface. The sand layer was underlain by firm layer like bedrock. Therefore, the bottom boundary was fixed in both the horizontal and vertical directions. Also, the two side boundaries were restricted in the horizontal direction but allowed to move freely in vertical direction.

The embankment fill, foundation soil and stone columns were modeled with Mohr-Coulomb failure criteria as linearly elastic-perfectly plastic. The elastic parameters are not required in FLAC/Slope 6.0 because they have no impact on the factor of safety computations. Only the

undrained, or short-term, condition for soft clay was analyzed for this paper. Table 6.1 shows the material properties of embankment fill, foundation soil, ordinary and encased stone columns.

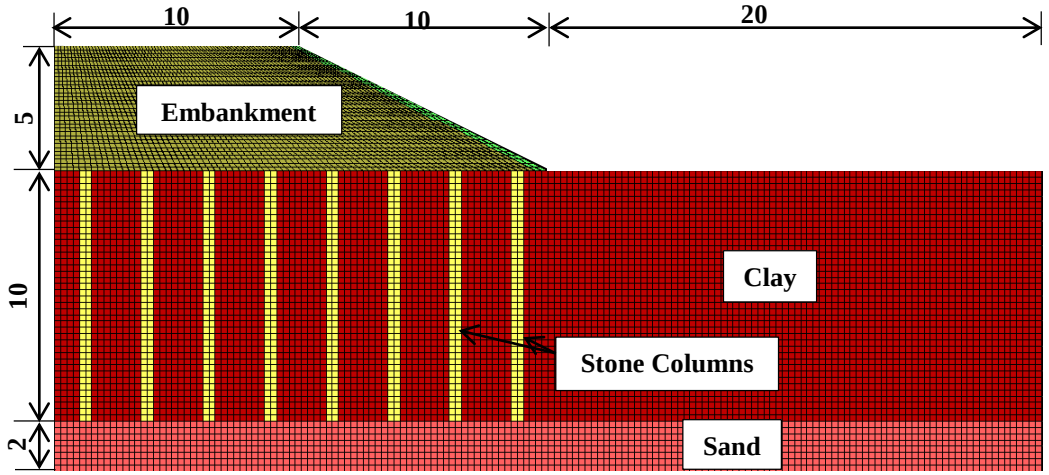

(a)

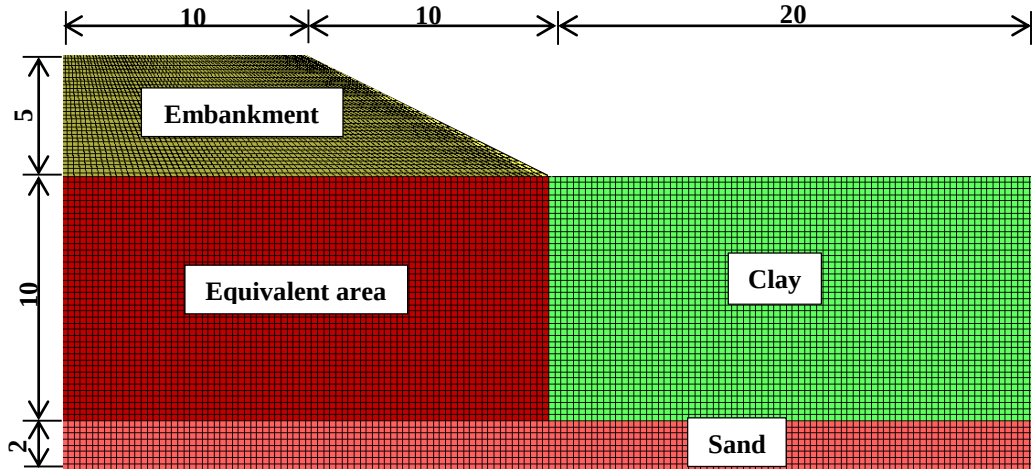

(b)

Figure 6.2 Numerical model: (a) Column wall method; and (b) Equivalent area method (unit: m) (Kadhim et al., 2015)

Table 6.1 Material properties of the embankment, foundation soil and ordinary and encased column wall for the diameter of column = 0.5 m and center-to-center spacing = 2.5 m

Item	Height (m)	Cohesion (kPa)	Friction Angle (Deg.)	Unit Weight (kN/m^3)
Embankment	5	0	32	18
Clay	10	20	0	16
Sand	2	0	30	18
Column	10	0	38	17
Encased column	10	565	38	17

6.4 Geosynthetic Encasement Modelling

As mentioned in chapter three, the effect of geosynthetic encasement was simulated as the degree of enhancement provided by the apparent cohesion of encased stone columns. The equation propped by Bathurst and Karpurapu (1993) was used to estimate the value of apparent cohesion. The circumferential strain was assumed to be mobilized at a value of 5% at failure.

6.5 Results and Discussion

A comparison was made between the stability factor of safety of ordinary columns (with no encasement) and encased columns using two methods: column walls and equivalent area. Several factors were involved in this study as follows:

6.5.1 Size of Stone Columns

Figure 6.3 depicts the influence of column width on the stability factor of safety. Three different diameters were investigated in this study: 0.25 m, 0.5 m and 0.75 m, to represent the diameter to spacing ratio of 10%, 20% and 30% respectively with constant center-to-center spacing of 2.5 m. For the ordinary case (no encasement), the factor of safety for both methods was increased when using larger diameters. The stability of the embankment was significantly enhanced after wrapping with the geosynthetic encasement. For the encased column wall and

equivalent area methods, the influence of increasing the column width greater than 0.5 m had a minimal effect on the stability of the embankment because the failure surface would not go through the strengthened foundation zone. Higher values of factor of safety were computed when using the equivalent area method for both the ordinary and encased columns. In other words, the equivalent area model developed a continuous slip surface so that all the points on this failure surface mobilized their shear strength. However, no continuous slip surface was noticed in the column wall model and the shear strength of the column walls was not fully mobilized at all locations at the same time (Zhang et al. 2014).

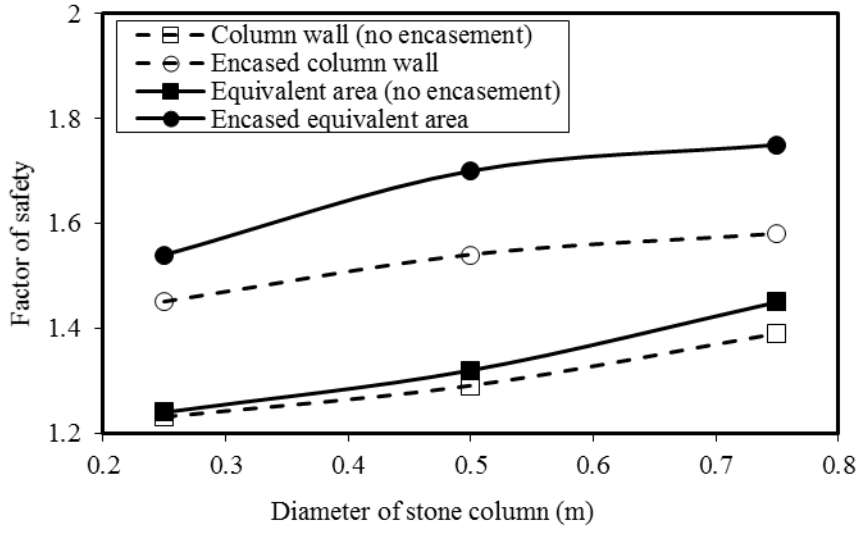

Figure 6.3 Effect of the size of stone columns

6.5.2 Spacing of Stone Columns

The effect of column spacing on the factor of safety is shown in figure 6.4. The selected values of center-to-center spacing ranged from 1.67 m to 5 m to achieve a diameter to spacing ratio of 30% to 10% respectively, which are common ratios used in practice (Abusharar and Han, 2011). The diameter of columns was fixed to 0.5 m for all cases. The factor of safety decreased when the column spacing increased for both methods. Including the geosynthetic encasement yielded higher

values of factor of safety for both methods. As discussed above in the previous section, the factors of safety for the equivalent area models were higher than for the column wall models for both the ordinary and encased columns.

6.5.3 Cohesion of Soft Soil

Figure 6.5 illustrates the effect of varying the soil cohesion of the surrounding soft clay on the factor of safety while fixing all other parameters. For both the ordinary and encased columns, a significant increase in the factor of safety was achieved when the soil cohesion was less than 25 kPa. The effect of increasing the soil cohesion beyond 25 kPa had a negligible effect on the factor of safety because the clay soil was strong enough that the failure surface was located above the foundation area. Furthermore, the factor of safety computed for the equivalent area model was higher than for column wall for ordinary and encased columns as explained previously.

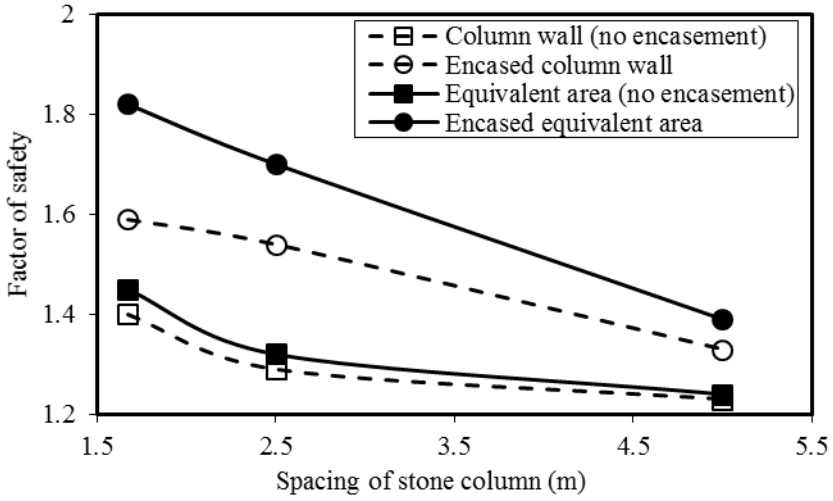

Figure 6.4 Effect of center-to-center spacing of stone column

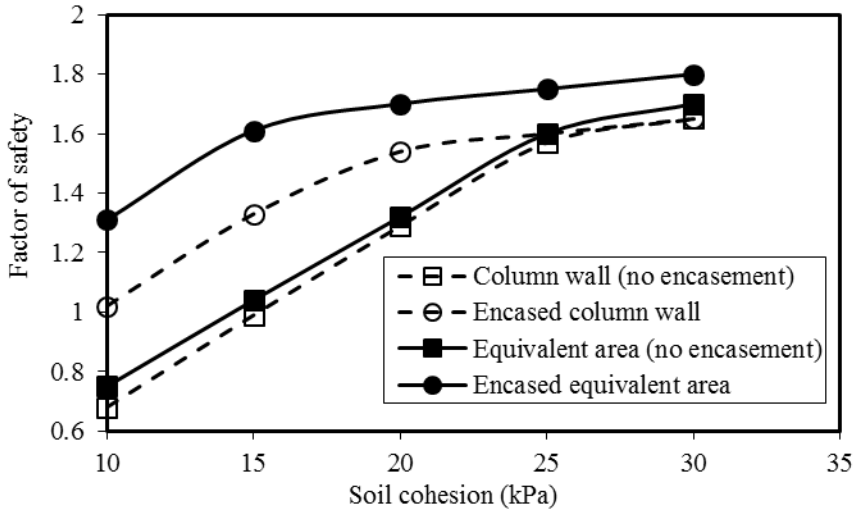

Figure 6.5 Effect of soil cohesion

6.5.4 Geosynthetic Stiffness

The geosynthetic stiffness was varied from 500 kN/m to 3000 kN/m to investigate the effect of strengthening the encasement on the stability factor of safety. Figure 6.6 shows a significant increase in the factor of safety as the stiffness of geosynthetic encasement increased. Furthermore, the equivalent area method yielded higher values of factor of safety than the column wall method. For geosynthetic stiffness values higher than 2000 kN/m, the values of factor of safety were not changed quite as much because the slip surface could not penetrate more deeply through the improved area.

6.6 Summary

A two dimensional finite difference analysis was conducted to quantify the factor of safety against the deep-seated failure of an embankment supported by ordinary or encased stone columns for the short-term condition. The impact of several parameters on the stability of embankments was investigated. Using geosynthetic encasement improved the stability of the constructed embankment on the soft soil. The equivalent area method yielded higher factors of safety than the

column wall method. The stability factor of safety decreased when the center-to-center spacing between columns was increased and increased when the soil cohesion was less than 25 kPa. Increasing the stiffness of geosynthetic encasement up to 2000 kN/m significantly increased the stability factor of safety.

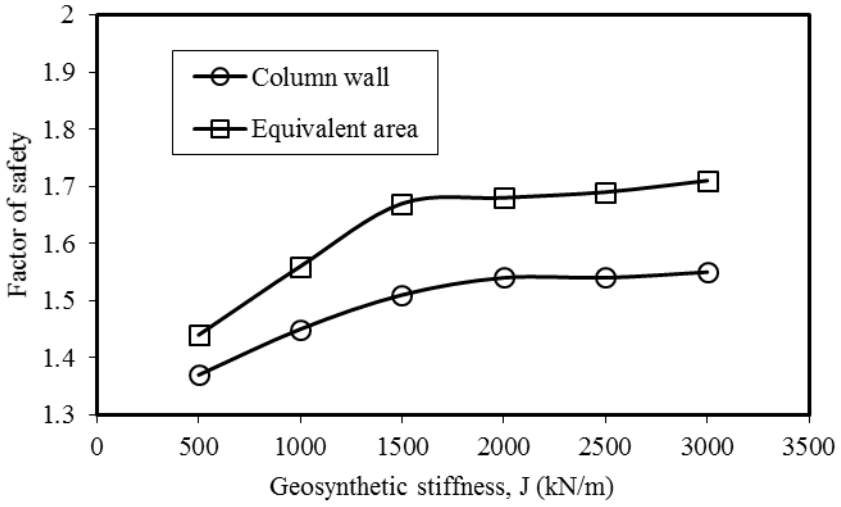

Figure 6.6 Effect of geosynthetic stiffness

CHAPTER 7

CONCLUSIONS AND RECOMMENDATIONS

7.1 Conclusions

The vertical stability of an individual geotextile encased sand column was investigated through a series of loading tests conducted in air and with surrounding loose sand to simulate the range of conditions that may lie in between those cases. Three dimensional numerical analyses using FLAC3D 5.01, were conducted to model an individual GESC with surrounding loose sand. Parametric studies were conducted to investigate the potential influence of different parameters on the performance of GESC. Lastly, a two dimensional finite difference analysis, using FLAC2D 6.0, was conducted to quantify the factor of safety against the deep-seated failure of an embankment supported by ordinary or encased stone columns for the short-term condition. The following conclusions can be drawn based on the results of this study:

1. Geotextile encased sand columns continued to yield higher shear strengths as the axial strains increased without failing, unlike the ordinary sand columns which approached steady state at relatively low axial strains.
2. The inclusion of geotextile encasement not only introduced an apparent cohesion to the shear strength parameters, but it also increased the friction angle of the column to a value greater than the peak friction angle of an ordinary sand column.
3. Loading tests performed on geotextile encased sand columns in both air and surrounded with weak soil showed that the geotextile sleeve typically failed at a seam. This finding supports the practice of using seamless encasements in real structures.

4. Loading tests conducted on GESC in air or with surrounding loose soil showed that columns of smaller diameters exhibited a higher bearing capacity compared with those of larger diameters.
5. Geotextile encased columns in air or with surrounding loose soil delivered higher bearing capacities at smaller length to diameter ratios.
6. Radial strains of geotextile encased sand columns in air increased with the increase in GESC diameter for the same length to diameter ratio due to the reduced confinement provided by the geotextile encasement for columns of larger diameters.
7. The trends of the radial and axial strains were relatively symmetrical for all encased sand columns installed in air and strains increased as the length to diameter ratios of the columns increased.
8. The inclusion of a 15 cm diameter GESC with a L/D of 4 increased the bearing capacity of the composite foundation by a factor of 10 compared with the unreinforced foundation represented by loose sand.
9. Encased sand columns with weak soil confinement delivered higher bearing capacities than those in air at the same diameters and length to diameter ratios.
10. Geotextile encased columns with surrounding loose sand exhibited lower radial and axial strains as compared with those in air when the same pressure was applied on the top area of the column.
11. The strength gain provided by the limited confinement from the weak surrounding soil was compared with the case of columns in air. Longer columns benefited more from soil confinement than did shorter columns, and GESC of larger diameters delivered higher strength gains compared to those with smaller column diameters.

12. The parameters of sand and geotextile encasement in the FLAC3D model were calibrated using the results from triaxial testing and the stress-strain output matched reasonably well.
13. Three dimensional numerical analyses showed that the geotextile encased sand columns of smaller diameter performed much better than those of larger diameters with regard to the applied stress-settlement behavior and the lateral expansion of the columns because of the higher confining stresses developed in smaller diameters of geotextile encased columns.
14. Shorter end-bearing GESC exhibited higher bearing capacities than longer ones since GESC transmit the compressive load along their entire length and hence shorter end-bearing columns mobilize higher stresses compared with longer end-bearing columns for a given amount of settlement.
15. When the bottom boundary of the GESC was not rigid, increasing the length of partially penetrating GESC increased the bearing capacity for the same amount of settlement.
16. Increasing the geotextile encasement length up to a value of five times the GESC diameter increased the bearing capacity and reduced the radial strain of the GESC.
17. Increasing the geotextile stiffness for values less than 2500 kN/m plays a substantial role in improving the bearing capacity of the GESC and reducing the lateral expansion of the column, while the influence of increasing the stiffness beyond 2500 kN/m was insignificant.
18. With regard to the infill material of the GESC, increasing the angle of internal friction of the infill sand increased the bearing capacity of the GESC, although the impact of using material with a higher friction angle was not as substantial as using a geosynthetic with a higher stiffness.
19. Encasing stone columns with geosynthetic enhanced the stability of the constructed embankment on weak (soft) soil by improving the factor of safety for slope stability.

20. The inclusion of the geosynthetic encasement was simulated in the two dimensional numerical analysis as equivalent or apparent cohesion (c_r).
21. The equivalent area method yielded higher factors of safety than the column wall method for both ordinary and encased columns because the equivalent area method developed a continuous slip surface and the column wall method did not.
22. The factor of safety decreased when the center-to-center spacing between columns increased and increased when column size increased.
23. The factor of safety was significantly increased when the unreinforced soil cohesion was less than 25 kPa.
24. The stability of the embankment can be greatly enhanced when increasing the stiffness of geosynthetic encasement up to 2000 kN/m due to the effect of apparent cohesion.

7.2 Recommendation for Future Work

In this study, experimental work and numerical analyses were employed to investigate the vertical stability of GESC. In addition, the stability of embankments supported by ordinary or encased stone columns was also investigated. The following topics are recommended for future study to understand the behavior of the geotextile encased sand columns with surrounding weak soils:

1. This study investigated the behavior of an individual geotextile encased sand column, which was only loaded on its top area, with surrounding loose sand. It is recommended for future studies to investigate the behavior of the GESC when the column and the surrounding soil are loaded together and behave as a unit cell to simulate an internal column within a grid of many columns subjected to embankment loading.

2. For the present study, the infill soil of the GESC was modeled as linearly elastic perfectly plastic using Mohr-Coulomb criterion. Further studies are recommended to model the infill sand using advanced soil constitutive models, such as the cap yield model or Duncan-Chang model, which can be employed to more accurately simulate the soil conditions. These advanced models update the tangent elastic modulus of the soil in accordance with the stress condition, while Mohr- Coulomb model depends only on the initial modulus that is kept constant throughout the analysis.
3. For this research, the soil surrounding the geotextile encased columns was assumed to be loose Kansas River Sand. It is recommended to conduct similar loading tests with a soft clay surrounding soil which simulates the more common real-life condition.
4. It is recommended to investigate the cost analysis of different material alternatives. The relative cost of various geosynthteic products and infill materials needs to be considered for an optimal and economic design of GESC for a particular project.

REFERENCES

Abu-Farsakh, Murad, Coronel, Julian, and Tao, Mingjiang. (2007). Effect of soil moisture content and dry density on cohesive soil–geosynthetic interactions using large direct shear tests. *Journal of Materials in Civil Engineering, 19*(7), 540-549.

Abusharar, Sari W, and Han, Jie. (2011). Two-dimensional deep-seated slope stability analysis of embankments over stone column-improved soft clay. *Engineering Geology, 120*(1), 103-110.

Ambily, AP, and Gandhi, Shailesh R. (2007). Behavior of stone columns based on experimental and FEM analysis. *Journal of Geotechnical and Geoenvironmental Engineering, 133*(4), 405-415.

Arvizhi, Mal, and Amparuthi, Il. (2007). Comparative study on the behavior of encased stone column and conventional stone column. *Soils and foundations, 47*(5), 873-885.

Bathurst, RJ, and Karpurapu, Rajagopal. (1993). Large-scale triaxial compression testing of geocell-reinforced granular soils. *Geotechnical Testing Journal, 16*, 296-296.

Cala, M, and Flisiak, J. (2001). *Slope stability analysis with FLAC and limit equilibrium methods.* Paper presented at the FLAC and Numerical Modeling in Geomechanics—2001 (Proceedings of the 2nd International FLAC Symposium on Numerical Modeling in Geomechanics, Ecully-Lyon, France, October 2001).

Castro, Jorge, and Sagaseta, César. (2011). Deformation and consolidation around encased stone columns. *Geotextiles and Geomembranes, 29*(3), 268-276.

Elsawy, Mohamed (2010). *Highway Embankment Constructed on Soft Soil Improved by Stone Columns with Geosynthetic Materials.* Universität Duisburg-Essen, Fakultät für Ingenieurwissenschaften» Bauwissenschaften» Bauingenieurwesen.

Gniel, Joel, and Bouazza, Abdelmalek. (2009). Improvement of soft soils using geogrid encased stone columns. *Geotextiles and Geomembranes, 27*(3), 167-175.

Gu, M, Zhao, M, Zhang, L, and Han, J. (2015). Effects of geogrid encasement on lateral and vertical deformations of stone columns in model tests. *Geosynthetics International*, 1-13.

Han , J., Parsons, R.L., Huang, J., and Sheth, A.R. (2005). *Factors of safety against deep-seated failure of embankments over deep mixed columns.* Paper presented at the Proc. of the Int. Conf. on Deep Mixing, Stockholm.

Han , J., and Ye , S.-L. (1991). *Analysis of characteristics to composite grounds.* Paper presented at the Proc. of First Young Asian Geotechnical Engineers Conference.

Han, Jie. (2012). *Recent Advances in Column Technologies to Improve Soft Foundations*. Paper presented at the International Conference on Ground Improvement and Ground Control, University of Wollongong, Australia.

Han, Jie. (2015). *Principles and Practice of Ground Improvement*: John Wiley & Sons.

Han, Jie, Chai, Jin-Chun, Leshchinsky, Dov, and Shen, Shui-Long. (2004). Evaluation of deep-seated slope stability of embankments over deep mixed foundations. *Geotechnical Special Publication* 945-954.

Han, Jie, Chen, Jianfeng, Hong, Zhenshun, and Shen, Shuilong. (2010). Mitigation of levee failures using deep mixed columns and geosynthetics. *Geomechanics and Geoengineering: An International Journal, 5*(1), 49-55.

Han, Jie, and Frost, J David. (1999). Buckling of vertically loaded fiber-reinforced polymer piles. *Journal of reinforced plastics and composites, 18*(4), 290-318.

Henkel, DJ, and Gilbert, GD. (1952). The effect measured of the rubber membrane on the triaxial compression strength of clay samples. *Geotechnique, 3*(1), 20-29.

Hong, Yung-Shan, Wu, Cho-Sen, and Yu, Yi-Sheng. (2016). Model tests on geotextile-encased granular columns under 1-g and undrained conditions. *Geotextiles and Geomembranes, 44*(1), 13-27.

Itasca. (2013). Fast Lagrangian Analysis of Continua in 3 Dimensional (Flac3D) Software Manual.

ITASCA, FLAC. (2008). Itasca Consulting Group, Inc., FLAC/SLOPE User's Guide Version 6.0: Licence.

Kadhim, Shaymaa, Parsons, Robert L, and Han, Jie. (2015). *Stability Analysis of Embankments Supported by Geosynthetic Encased Stone Columns.* Paper presented at the IFCEE 2015.

Khabbazian, Majid, Kaliakin, Victor N, and Meehan, Christopher L. (2009). *3D numerical analyses of geosynthetic encased stone columns.* Paper presented at the 2009 International Foundation Congress and Equipment Expo.

Khabbazian, Majid, Meehan, Christopher L, and Kaliakin, Victor N. (2010). *Numerical study of effect of encasement on stone column performance.* Paper presented at the GeoFlorida 2010@ sAdvances in Analysis, Modeling & Design.

Kumar, Rakesh, and Jain, PK. (2013). Expansive Soft Soil Improvement by Geogrid Encased Granular Pile.

Lo, SR, Zhang, R, and Mak, J. (2010). Geosynthetic-encased stone columns in soft clay: a numerical study. *Geotextiles and Geomembranes, 28*(3), 292-302.

Meehan, Christopher L, Khabbazian, M, and Kaliakin, Vladimir Nikolaevich. (2010). Numerical study of the effect of geosynthetic encasement on the behaviour of granular columns.

Meyerhof, GG, and Sastry, VVRN. (1978). Bearing capacity of piles in layered soils. Part 1. Clay overlying sand. *Canadian Geotechnical Journal, 15*(2), 171-182.

Mohapatra, S. R., Rajagopal, K. , and Sharma, J. S. . (2014). *Analysis of geotextile-reinforced stone columns subjected to lateral loading.* Paper presented at the 10ICG, Berlin.

Murugesan, S, and Rajagopal, K. (2006). Geosynthetic-encased stone columns: numerical evaluation. *Geotextiles and Geomembranes, 24*(6), 349-358.

Murugesan, S, and Rajagopal, K. (2009). Studies on the behavior of single and group of geosynthetic encased stone columns. *Journal of Geotechnical and Geoenvironmental Engineering, 136*(1), 129-139.

Raithel, M, Kirchner, A, Schade, C, and Leusink, E. (2005). Foundation of constructions on very soft soils with geotextile encased columns-State of the art. *Geotechnical special publication, 136*.

Sivakumar, V, McKelvey, D, Graham, J, and Hughes, D. (2004). Triaxial tests on model sand columns in clay. *Canadian Geotechnical Journal, 41*(2), 299-312.

Tallapragada, Kameshwar Rao, Y. S., Golait , and Zade, Ashwini S. (2011). Improvement of Bearing Capacity of Soft Soil Using Stone ColumnWith And Without Encasement of Geosynthetics. *International Journal of Science and Advanced Technology, 1*(7).

Tan, Siew Ann, Tjahyono, S, and Oo, KK. (2008). Simplified plane-strain modeling of stone-column reinforced ground. *Journal of Geotechnical and Geoenvironmental Engineering, 134*(2), 185-194.

Wu, Cho-Sen, Hong, Yung-Shan, and Lin, Hsien-Chin. (2009). Axial stress–strain relation of encapsulated granular column. *Computers and Geotechnics, 36*(1), 226-240.

Yoo, Chungsik. (2010). Performance of geosynthetic-encased stone columns in embankment construction: numerical investigation. *Journal of Geotechnical and Geoenvironmental Engineering, 136*(8), 1148-1160.

Zhang, Zhen, Han, Jie, and Ye, Guanbao. (2014). Numerical investigation on factors for deep-seated slope stability of stone column-supported embankments over soft clay. *Engineering Geology, 168*, 104-113.